Characterization of Cellulose Nanocrystals and Their Application in Polyethylene Composites

by

Gregory James Kaufman

A thesis submitted in partial fulfillment of the requirements for the degree of

Doctor of Philosophy

Department of Chemistry

University of Alberta

Abstract

Cellulose nanocrystals (CNC) are an emerging green nanomaterial with a unique property set that permits its use to enhance traditional materials in various ways. One of the main focuses has been to impart the incredible mechanical stiffness of these nano particles into conventional thermoplastic polymers. The scope of this thesis will investigate CNC using infrared reflection adsorption spectroscopy (IRRAS) to firstly assign the bands of the unique spectrum of this technique. The surface selection rule that is inherent in IRRAS combined with knowledge of the bond orientations within CNC to the incident IR beam permits the assignment of previously unassigned bands including assigning the 1205 and 1145 cm^{-1} to modes of the pyranose ring. Secondly, IRRAS will be used to monitor the adsorption of CNC to a variety of surface functional groups. Three variables were controlled; the CNC concentration, the functionality of the aqueous CNC suspension, and the ionic strength of the aqueous CNC suspension. The density of these layers was estimated by comparing IRRAS signal intensities with AFM thickness images giving insight into CNC-CNC as well as CNC-substrate interactions. This same method will be applied to CNC that were modified with diazonium derived aryl groups. A combination of infrared (IR) and X-ray photoelectron spectroscopy were used to confirm surface modification and IRRAS was used to study the interactions of the modified CNC with various surfaces. Lastly the incorporation of modified CNC into a melt extrusion of the common thermoplastic high density polyethylene (HDPE) was performed. The addition of modified CNC to HDPE was compared to virgin PE as well as a composite of unmodified CNC and PE. The elastic modulus was obtained for all

samples and a clear increase was observed only upon the addition of modified CNC where the elastic modulus increased by a factor of 2.7.

Preface

This thesis is an original work by Greg Kaufman under the supervision of Professor Mark McDermott. No part of this thesis has been previously published.

Dedication

The work detailed in the following thesis would not have been possible without the support and drive given to me by my family and friends; they are the people that make life worth working for and the body of work expressed herein is done with them and should be represented as such.

Acknowledgments

It takes a village to raise a child and it takes a community to train a chemist. The services available to a graduate student at the University of Alberta are essential to the work that is done. They leave time to focus all of ones energy on research by mitigating time consuming requirements. The boys in stores are always working for each and every group to streamline the work that can be accomplished. The machine shop and glass shop are essential to permit the breadth of ideas that require some of the oddest pieces of equipment – their expertise in bringing to reality some crazy ideas is second to none. It is necessary to give a big thanks to the local drinking holes where some of the best ideas are scribbled on napkins while enjoying a conclusion-less argument with some peers. The Chemistry Graduate Students' Society played a big role in getting to know fellow students in an environment outside of work as well as providing a whole new learning experience organizing and enjoying events, I hope this group grows long after I am gone. I have learned so much from the students that were before me and I hope I was as much help to those that follow. The entirety of the McDermott research group has been instrumental in the knowledge that I have gained, and especially the group's captain, Mark. He has helped me separate the meat from the fat in the projects that I have attempted and given me the chance to learn what is really important in a degree. My family and friends cannot go unmentioned for sharing parts of their lives with me both inside and outside this degree. The most profound of these is my wife, Yukiko. Meeting her halfway through my degree has changed my life in the most awesome way I could ever imagine and her support and honesty throughout this whole journey has been irreplaceable.

Table of Contents

List of Tables

List of Figures

Glossary of Terms

AUT	11-amino-1-undecanthiol
CUT	11-carboxyl-1-undecanethiol
HUT	11-hydroxyl-1-undecanethiol
CNC	Cellulose Nanocrystal
DODT	deuterated octadecanethiol
DDT	dodecanethiol
HDPE	High Density Polyethylene
IXS	inelastic X-ray scattering
IR	Infrared
IRRAS	Infrared Reflection Absorption Spectroscopy
LbL	Layer by layer
LLDPE	Linear Low Density Polyethylene
LDPE	Low Density Polyethylene
MCC	Microcrystalline Cellulose
MFC	Microfibrillated cellulose
Mya	Million years ago
NCC	Nano crystalline cellulose
NFC	Nanofibrillated cellulose
NMR	Nuclear magnetic resonance
PE	Polyethylene
SAXS	Small angle X-ray scattering
SAM(s)	Surface Adsorbed Monolayer(s)
SPR	Surface Plasmon Resonance
TFMB	Trifluoromethyl benzene
XRD	X-ray diffraction

Chapter 1
Introduction

Cellulose is currently the world's most abundant as well as most produced polymer. It exists as the main component of plant's cell walls and is responsible for the rigidity of plants as it provides strength and structure to their cellular networks. Photosynthesis is the source of energy that plants use to convert carbon dioxide and water into this fundamental building block, which is a showcase for the awesome potential of harnessing such an abundant source of energy. Wood and plant products have invariably been used by humans in many ways throughout history but as technology grows it is necessary and possible to demand more out of traditional materials. Understanding and utilizing cellulose to this end has been realized and is the focus of many researchers around the world.

It was not brought to researchers attention until recently that treating wood fibers with acid will hydrolyze sterically available ether linkages and if properly controlled will isolate nano-scaled, crystalline portions of the fibers.[1,2] These nano-scale fibers have gathered many names in the literature including nano whiskers, nanocrystalline cellulose and cellulose nanocrystals. Definitions are required for the different sizes, aspect ratios and morphologies but for the purpose of this work, the term cellulose nanocrystals (CNC) will be used to describe the isolated crystalline portion of cellulose that are a result of acid hydrolysis of a raw material.

To gain a full appreciation of cellulose it is humbling to take a look at it from its genesis. The story of cellulose starts some 440 million years ago (Mya) and is understood only through its fossilization. Through this record we can visualize not only the advent of cellulose as presented in plant matter fossils but also correlate these occurrences to drastic climatological changes. As algae made the move to land in favor of a less competitive but more inhospitable environment, aquatic luxuries such as relative buoyancy became obstacles. This occurred in this time period known as the Ordovician (488 to 443 Mya) and extended through the Silurian and into the Devonian (416 to 359 Mya). The first evidence of land plants is 473 to 471 Mya[3] with the first true plants (having seeds and roots) evolving later. In this time, terrestrial life was nothing like what we see today. Plants were less than one meter tall as their structure could not support taller growth and their primitive root network had no soil to anchor in. The forests that existed were fungal, with the tallest organisms reaching an impressive 8 meters. This would all change by the Carboniferous period (360 Mya to 300 Mya) where we can observe fossils of true plants that are capable of surviving thousands of kilometers from their ancestral ocean home. The evolutionary tendency towards the make-up of forests that we see today suggests that modern plants could out survive these funguses. This was possible due to a number of factors evolving in tandem, notably plant's root networks and the production of seeds. To gain an advantage from a stabilizing root system that could anchor in the increasing amount of terrestrial soil, great strength was demanded and it came in the form of lignin and cellulose. From the start to the end of the Devonian, plants heights increased from 30 cm to 30 m. It was the biosynthesis of these materials that allowed plants to dominate the terrestrial landscape. However, this

did have a catastrophic complication. This evolutionary weaponry was new to the stage of life on earth and was so successful that it locked up massive amounts of atmospheric carbon dioxide as cellulose and lignin in a geologically short amount of time. Once locked in dead plant matter it could not be recycled as there were not yet organisms to feed on it. This speaks to the difficulty in chemically and enzymatically dismantling cellulose.[4] This occurred to such a great extent that it changed the atmospheric conditions rapidly as the levels of CO_2, a greenhouse gas, dropped and is suspected to have played a major role in one of the five largest extinction events in earth's fossil history, the Late Devonian extinction.

This is an example of how cellulose has changed the world in the past. The changes that current research is aiming at are less catastrophic and more focused on the betterment of humans' materials but it is humbling to respect the forces of change that this unique polymer has left for us and how it has helped create the world in which we study it today. Several hundreds of millions years after these events, humans took to investigating this natural material and these endeavors will be the focus of the work presented in this thesis.

Anselme Payen, 1795 to 1878, isolated cellulose from green plants and first used the word "cellulose" to describe it.[5] From work done by Nickerson and Habrle in 1947 we see evidence of the isolation of portions of cellulose[1] with Ranby using X-ray diffraction to confirm observations that it contains crystalline regions.[6] These works would set the goals of many researchers for decades to follow, from understanding its complicated structure to employing it for specific purposes.

Three general areas can be assigned to this field; production, characterization and materialization. The main goal of employing CNC is and will likely be in the material area in large scale production used alone or in composite. To better facilitate the potential of CNC, its characterization and interactions on a saccharine level are essential. Much work has been conducted in this area including discerning its various crystal forms and understanding its inter and intra molecular chemical interactions. With this type of information, CNC materials can sooner lend themselves to industry.

Structure

The understanding of the polymeric structure of cellulose has been a world wide effort. As naturally produced, cellulose is arranged in plants in the cell walls in a layered mesh of microfibrils. These microfibrils are a kind of cable of many mostly-parallel crystalline cellulose strands, sometimes called elementary fibrils, which are held together by dispersive forces and range from 5-50nm in diameter and 1-5 μm in length. [7] The elementary fibrils are a more ordered chain than the microfibrils and consist of several dozen strands of cellulose which have, along their length, regions of crystalline and amorphous cellulose. Cellulose is a repeat polymer of cellobiose units where a cellobiose is simply two glucose rings attached through an ether linkage referred to as the glucosidic linkage, bond or bridge. The bonding along the chain is the same between glucose units and cellobiose units however due to the crystal nature of cellulose it is sometimes necessary to distinguish into cellobiose rather than simply a linear collection of glucose. This hierarchy is shown in Figure 1-1.

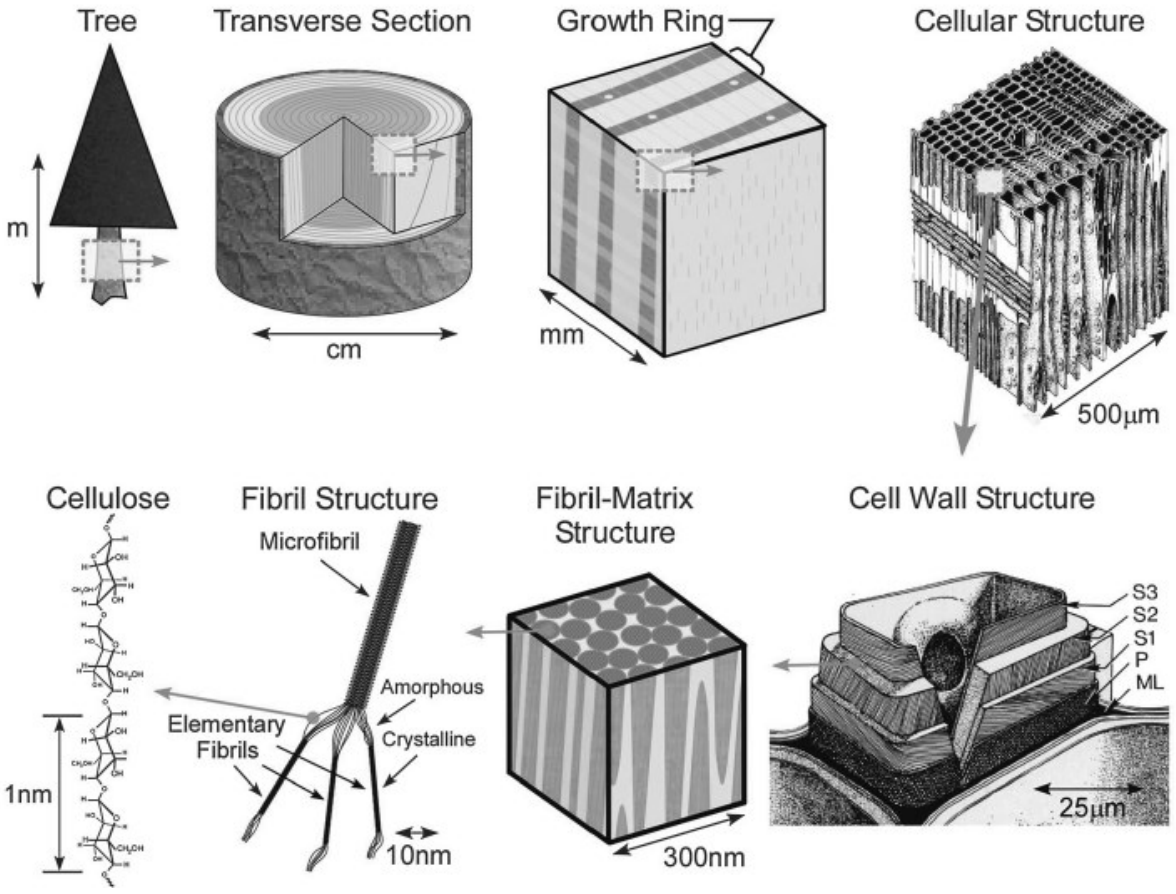

Figure 1-1. Hierarchical structure of cellulose. Reproduced from Ref. 7 with permission from The Royal Society of Chemistry.

Through light chemical treatment or mechanical shearing, long microfibrils composed of elementary fibrils containing both crystalline and amorphous regions can be isolated; these are referred to as microcrystalline cellulose (MCC) or microfibrillated cellulose (MFC). The elementary fibrils are commonly referred to as nanofibrillated cellulose (NFC). These names are analogous to nanocrystalline cellulose (NCC) which is a classic name of the particles left over after the amorphous regions of NFC have been removed. However the term CNC is a better description of this crystalline product. MFC and NFC are interesting forms of cellulose and have many commercial applications due to their fibril length and less intense isolation steps from raw materials. However, the main focus of this work will be on the further isolated product CNC.

The linkage between glucose/cellobiose is where the full name of cellulose starts, (1→4)-β-D-Glucan. The 1→4 explains what carbons on the two adjoining glucose rings engage in the glucosidic linkage. The beta describes the stereochemistry about the anomeric (C-1) of the glucose unit or the stereochemistry of the glucosidic bond. The "D" describes the configuration of the monosaccharide residues, in cellulose's case this corresponds to the equatorial position. The word "glucan" is the base glucose as that is the repeat unit of the polymer with the ending changed to "an" to indicate that it is a homopolysaccharide. Figure 1-2 shows 2 glucose units (cellobiose) in a polymer chain of cellulose with some of the possible intra-chain hydrogen bonding.

Crystal Structures and Allomorphs

CNC is as the name suggests, crystalline, but does not belong to a single crystal structure. There are many crystalline domains in natural cellulose and those domains

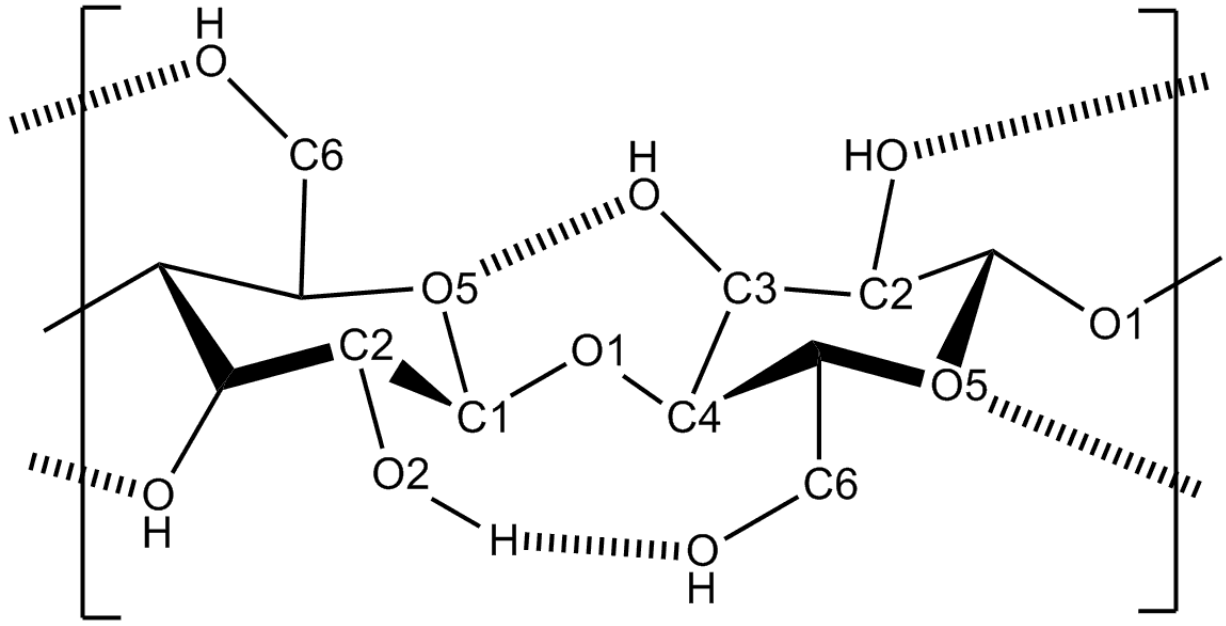

Figure 1-2. Structure of cellulose showing two glucose units with some of the atoms numbered.

can be any of a large number of crystal structures. The crystal structure of natural cellulose, that is as it exists in various plants and some bacteria, is called cellulose I. This form is metastable and can be converted to cellulose II through two methods; regeneration (solubilization and recrystallization) and mercerization (aqueous sodium hydroxide treatment).[8] These two forms, cellulose I and II, can be converted into cellulose III_I and III_{II} respectively. This is accomplished by treating with liquid ammonia or amines.[9–11] These two forms, cellulose III_I and III_{II}, can be converted into cellulose IV_I and IV_{II} respectively. This is accomplished by treating either of the cellulose III's with glycerol at 206^{O}C.[10] This interconversion of cellulose's polymorphs is detailed in Figure 1-3. The final crystallographic distinction was the one that posed the greatest confusion about this polymer, that is that the natural crystal form named cellulose I was produced in its living host in one of two crystal forms that would be named cellulose I_α and I_β.[12–17] It is important to realize the errors that this has introduced into the literature. Before this realization, the degree of crystallinity and the presence of amorphous regions were used to explain different spectroscopic results, namely x-ray diffraction and infrared. Different structures were proposed that fit the data and as such different structural elements were assigned to various infrared (IR) bands and bogus unit cells resulted from x-ray studies. With this in mind any assignments that were prior to 1984 should be carefully investigated with this understanding.

Before much was known about cellulose's structure, a difference in various infrared spectra was roughly correlated to "higher" and "lower" plants which would later be attributed to the allomorphs, alpha and beta.[15,18] The terms higher and lower with respect to plants was based on their evolution, lower plants are simpler and include

algae and bacteria whereas higher plants are vascular and have lignified tissue and include conifers and flowering plants. The two allomorphs of cellulose I, alpha and beta, occur in different ratios depending on the plant source and there is no simple rule as to where each can be found. Within a single microfibril both forms have been observed.[19] Cellulose I_β is a thermodynamically more favorable allomorph compared to I_α. This is apparent in that I_α can be irreversibly converted to I_β upon heating.[14,20] The most common sources of I_α are valonia, tunicate and ramie whereas the most common sources of I_β Include cotton and various conifer trees referred to as softwood as well as heat treating any source of I_α to convert it to its more stable allomorph. The ratios of the two allomorphs vary from source to source; this has been an issue in measuring pure alpha samples as they invariably contain some amounts of beta. Pure beta samples, one the other hand, are easier to achieve on account of their tending to convert to beta upon heating.[14,20–22] The ratio of crystal types as well as the degree of crystallinity depends on the plant source; some sources will yield greater amounts of CNC when isolated from raw material than others as there are more and/or larger crystalline regions to begin with.

With this in mind the plant sources that are used to isolate CNC make a big difference, not only for the nature of the crystal structure but also the size and shape of the crystalline regions. The cross sections of CNC from different sources vary in morphology and the assumption of a cylindrical CNC is not always correct as they frequently adopt a rectangular or parallelogram shape.[23,24]

The crystal phases of cellulose are well agreed upon in the literature and previous major discrepancies have been accounted for by the current unit cells that are proposed.

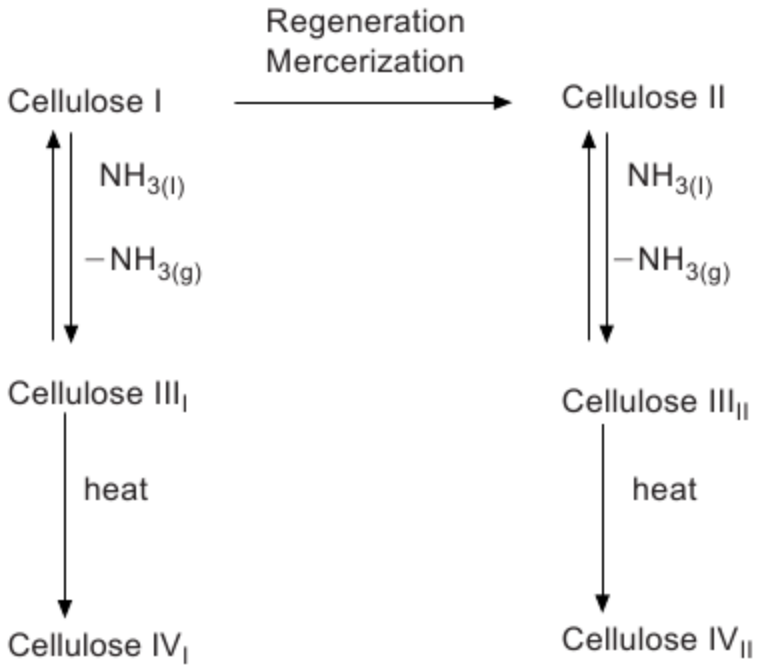

Figure 1-3. Interconversion of the polymorphs of cellulose. Reproduced from Ref. 5 with permission from Springer.

cellulose I_α is a triclinic single chain P1 unit cell where cellulose I_β is a monoclinic two chain $P2_1$ unit cell.

Hydrogen Bonding

The hydrogen bonding network in cellulose is ultimately responsible for the crystal structure. The covalent bonding and skeletal structure of all cellulose is identical; what changes the crystallinity is a rotation of single bonds that adopt different hydrogen bonding networks and thus change the crystal structure. For example, both allomorphs of cellulose I contain sheets of parallel hydrogen bonded chains. These sheets are stacked on top of each other and are connected via hydrophobic interactions.[19,25] The difference between alpha and beta are the staggering of these two sheets relative to the chain direction. Another example is when cellulose I is converted to cellulose III_I by ammonia treatment.[11] There is a rotation about the C_6-O_6 bond such that it is gauche to O_5-C_5 and trans to C_4-C_5 (gt) as opposed to cellulose I (tg). This breaks the intra-chain hydrogen bonding that occurred in cellulose I between the hydroxyl of the O_6 and the O_2 of a neighboring residue and replaces it with an inter-sheet hydrogen bond that did not exist in cellulose I.

Supermolecular Structure

Small angle X-ray scattering (SAXS) has been used to investigate the supramolecular structure of carboxymethyl cellulose.[26] This work was done with industrial applications in mind but points out the potential for cellulose to have a biological function in plants that is a result of some larger structural regularity; possibly in the same way that proteins gain their functionality from their 3D shape. The micro structure of native cellulose has also been investigated with 13C NMR.[17]

Isolation of CNC

Cellulose is the main strength component of plants and is found in all plants and some bacteria and animals. After nature does the energy intensive work of creating such a molecule it falls in human hands to isolate it. This is typically done with acids, the most common of which is sulphuric acid. [27,28] The acid will hydrolyze non-crystalline ether linkages and if properly controlled yield crystalline cellulose domains, also known as CNC. The source will ultimately dictate what the final dimensions of the isolated CNC will be. Other acids can be used and yield different surface functionality. Hydrochloric acid can be used and follows the same hydrolysis mechanism but uniquely yields a cellulose material that more resembles natural cellulose; the surface groups are hydroxyl.[29] Sulphuric acid is more common than hydrochloric on account of the resulting aqueous stability resulting from negatively charged sulphate groups on the CNC surface. Phosphoric acid has similarly been used with the proposed benefits of both previously mentioned acids.[30] This yields CNC with phosphate surface coverage. 2,2,6,6-tetramethyl-piperidinyl-1-oxyl (TEMPO) mediated oxidation is an isolation approach that is combined with mechanical methods and results in a carboxylic surface chemistry.[31,32] Other methods have been conducted but the ones mentioned here are the most common.

Strength of CNC

The nature of CNC gives it great mechanical strength with entangled lengths of covalently bonded chains that are connected along their lengths with multiple modes of dispersive attraction and hydrogen bonding. This hierarchy is what leads to the possible strength of plants from the tallest trees to the smallest algae. Some of the

reasons CNC have garnered so much attention is the unique combination of renewability from an abundant natural source along with immense potential strength.

Multiple experiments have been conducted on many cellulose materials with the intention of gaining values to represent its strength. The most common value, and one of the most useful in materials engineering is the modules of elasticity or Young's modules. This value is trivial to obtain when dealing with bulk materials; it is simply a matter of measuring the distance the material is deformed when a pressure is applied; commonly referred to as a stress-strain curve. An example of a stress strain curve is shown in Figure 1-4.

The strain is a ratio of the distance of deformation to the total length of the sample and is thus unitless. From this curve there are a number of regions of interest. In the early stress regions most materials will exhibit a linear response to strain, this is to say the material is behaving like a perfect spring and obeying Hook's Law. The slope of this region is the Young's Modules or elastic modulus. Beyond this region materials vary in the manner in which they eventually fail due to increasing pressure. Bulk materials are easily measured with machinery sensitive enough to large pressure changes over large distances. Attempting to make these same measurements on CNC, which is roughly cylindrical with a diameter of 4-12 nm and length 60-300 nm, can prove to be difficult. In addition CNC is anisotropic; its axial properties will be invariably different from it transverse. Furthermore, it has two transverse axes on account of having two planes that separate individual cellulose chains; the hydrogen bonding plane and its perpendicular dispersive plane (although in some crystal forms hydrogen bonding is present in both planes and the term dispersive

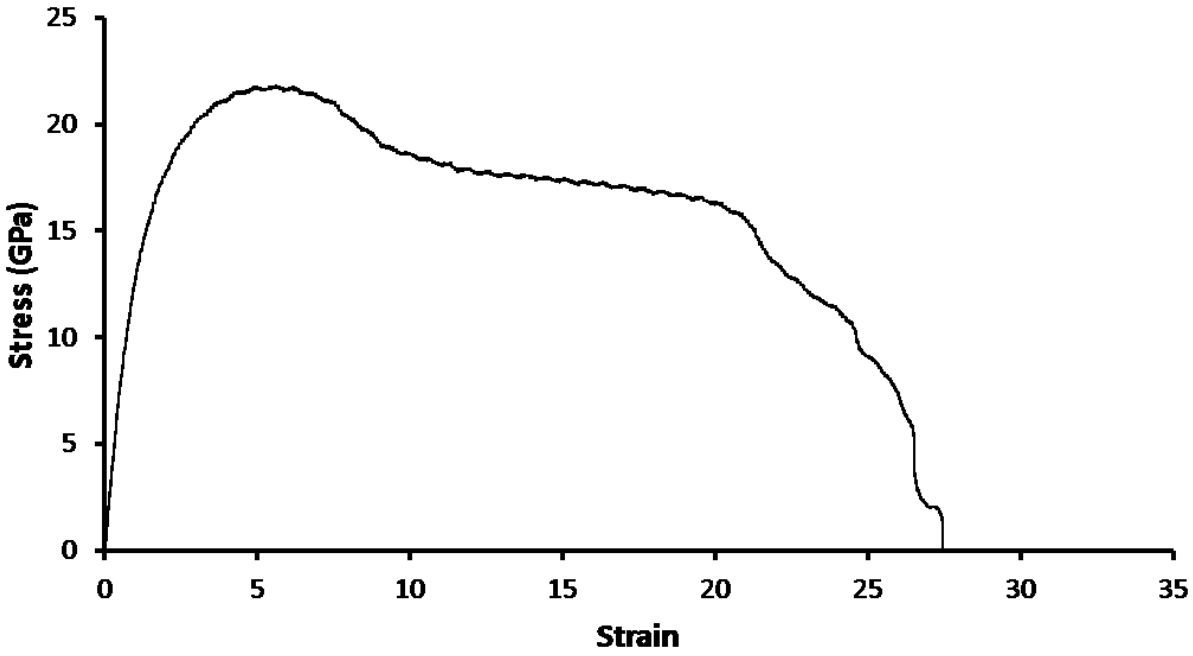

Figure 1-4. Example of a Stress Strain Curve.

plane or hydrophilic plane is not always correct). To solve this problem of scale and obtain reliable strength numbers many techniques imply results as opposed to directly measuring them.

The main approaches to measure the elastic moduli in the axial and transverse directions are computer modeling which will not be discussed in this work. Empirical tests include applying a mechanical stress while monitoring a bulk sample with X-ray or Raman spectroscopy. Techniques that focus on a single CNC include AFM 3-point bending tests and indentation. There is considerable variability in the results obtained from these different methods and is somewhat to be expected as there is bound to be variability in different CNC even if they are sourced from the same parent material and isolated in the same manner. As a result, their relative standard deviations are in the range of 20 to 30%. This is understandable in that each method involves a number of assumptions about the samples orientation, degree of crystallinity, ratio of allomorphs and others specific to each measurement type.

X-ray diffraction (XRD) gives values for the axial elastic modulus to be 120–138 GPa[33–35] but it has been noted that this is likely an underestimate as the results assume prefect orientation of the crystals and perfect load transfer between crystals. Inelastic X-ray scattering (IXS) of microfibrils has been compared to XRD and ideally would not be affected by the same load transfer issues as its sensitivity to crystal properties discriminates the contribution of disordered material.[33] This technique gives an axial elastic modulus of 220 ± 50 GPa. It was also able to estimate the transverse elastic modulus to be 15 ± 1 GPa.

Raman spectroscopy has been evaluated to represent physical properties of cellulose materials under stress by assuming knowledge of the load bearing bonds that have Raman active vibrational bands. The sample is mixed with an epoxy to restrain the fibers and the entire material is stressed causing individual celluloses to be stressed. The shift in the 1095 cm^{-1} band along with calculations has found the axial elastic modulus to be between 57–105 GPa in plant CNC, 114 GPa in bacterial CNC and 143 in tunicate sourced CNC.[36–38] Similarly, MCC was analyzed to have an axial elastic modulus of 25 ± 4 GPa.[39]

AFM 3 point bending tests have been performed on cellulose samples. CNC was adsorbed to a surface containing regular grooves 227 nm apart. AFM imaging could then eventually locate a single CNC that crossed these grooves perpendicularly. This method is far more experimental than the others but relies on adequate characterization of the cantilever being used. Axial elastic moduli of tunicate sourced CNC from acid hydrolysis and TEMPO mediated oxidation were found to be 151 ± 29 and 145 ± 31 respectively.[40] Similarly, Bacterial derived cellulose was measured to be 78 ± 17 GPa. Direct measurements of the less studied transverse elastic modulus have been studied by nano-indentation. Values of 18–50 and 9 ± 3 GPa have been reported.[41,42]

Despite the variability in these measurements the values are not immediately useful for material production. That is to say that creating a bulk material that comes close to these values would be very difficult, save a single crystal that is on the scale of meters. The same discrepancy is noticed with carbon nanotubes; despite the highest Young's modulus ever measured, no bulk material has been produced with comparable strength. These figures have been glorified to state that cellulose is "stronger than steel" which is

an unfair comparison considering the relative scale of measure; steel being on the cm or larger and CNC being on the nano-scale. However, they are promising values. This is not to say these figures are of no use. There is great use for them in modeling calculations for CNC when it is used as an additive in composite materials.

Cellulose is a mechanically strong polymer. This strength arises from the rigidity of its crystalline regions which are held together by a combination of covalent and hydrogen bonding as well as dispersive forces. Each polymer chain is covalently linked allowing for a high elastic modulus in the axial direction and a lower modulus in the transverse direction. This difference is due to the inter chain hydrogen bonding and van der Waals interactions. This strength is one of the aspects of CNC that makes it such an attractive material for modern, high preforming materials.

Imaging CNC

Due to the size of CNC, direct imaging of individual particles is relegated to either electron microscopy (EM) or atomic force microscopy (AFM). Both have been used to study CNC and each has its own advantages and disadvantages.[43] For each technique sample preparation steps are necessary and introduce their own difficulty. For AFM, the CNC need to be immobilized on a preferably flat surface, mica is the most common and well suited for this. A sample preparation issue for EM includes sample staining or immobilizing on a grid. EM offers a more complete view of both height and width of fibers as AFM suffers from tip effects which will exaggerate the width. However, AFM offers more accurate height figure and can give an accurate measure of the surface roughness.[44,45] Since various sources of CNC have various cross-section measurements such as square, rectangular, and parallelogram [7] it is important to not

treat all fibers as if they have equal heights and widths. For softwood and cotton samples, cotton being the source used in these experiments, the cross-section is square with dimensions of 6.1 nm and 6.0 nm giving a hypotenuse of distance 7.5 nm.[46] Choosing an imaging method will depend on the information required and one technique will not be superior in all aspects.

Optical Properties of CNC

CNC satisfy their delegation to the realm of nano materials in that they behave differently on the nano scale than they do on the bulk. Early indications of this uniqueness were the observation of birefringent regions in dried-down films of cellulose crystallites viewed through a polarizing microscope by Marchessault in 1959.[47] The asymmetrical rod-like nature of CNCs permits the formation of chiral nematic (cholesteric) liquid crystal phases when the concentration in aqueous solution is sufficiently high.[47,48] The pitch of these phases can be in the range of visible light which makes CNC relevant to optical applications. Furthermore, the pitch can be controlled by the addition of salts to the aqueous solution permitting control over the observed birefringence.[49] Other factors affect the chiral nematic pitch including size, shape, dispersity, counter ion, and charge.[7,50,51]

Infrared Spectroscopy

The concept of infrared radiation and its association to heat was first realized by Sir William Herschel in the 1800's when he was expanding on the concept of the spectrum of light that was first realized by Isaac Newton in the 1660's.[52] This famous experiment was observing the temperatures of different colors of light. The colours of a spectrum

were incident upon different thermometers with a control thermometer out of the visible and beyond the red light and, as it would turn out, in the IR region. This is illustrated in Figure 1-5.

The result of the intended control was that it showed a higher temperature than any of the visible colours. This realization would pave the way for the broad field of infrared spectroscopy. It would be realized that the energy involved in the vibration of many common bonds is in this frequency region and would allow a detailed IR spectra. This in turn offers insight into the presence or absence of specific bonds and functional groups. The combination of the Michelson interferometer, Fourier transform mathematics and computers fast enough to calculate the transform in a practical time frame furthered the potential of IR spectroscopy.

Infrared radiation (IR) can be defined as light with a wavelength longer than the visible radiation and shorter than radio waves, which is between 0.7 μm and 1 mm. Most qualitative IR spectroscopy covers the range from about 2.5 to 25 μm, the so-called mid-infrared range. This range is more commonly expressed in wavenumbers (400 to 4000 cm^{-1}). It is within this frequency range that chemical bonds in most organic molecules vibrate. A vibrating dipole will absorb radiation provided they are both of the same frequency. This offers the potential to gain an absorbance spectrum of a material with bands specific to chemical bonds. However, not all bonds will absorb incident IR radiation. Radiation will only interact with chemical bonds with a change in a permanent dipole on account of a vibration of that dipole. For this reason, symmetrical molecules such as diatomic molecules are not active in IR spectroscopy. Examples of

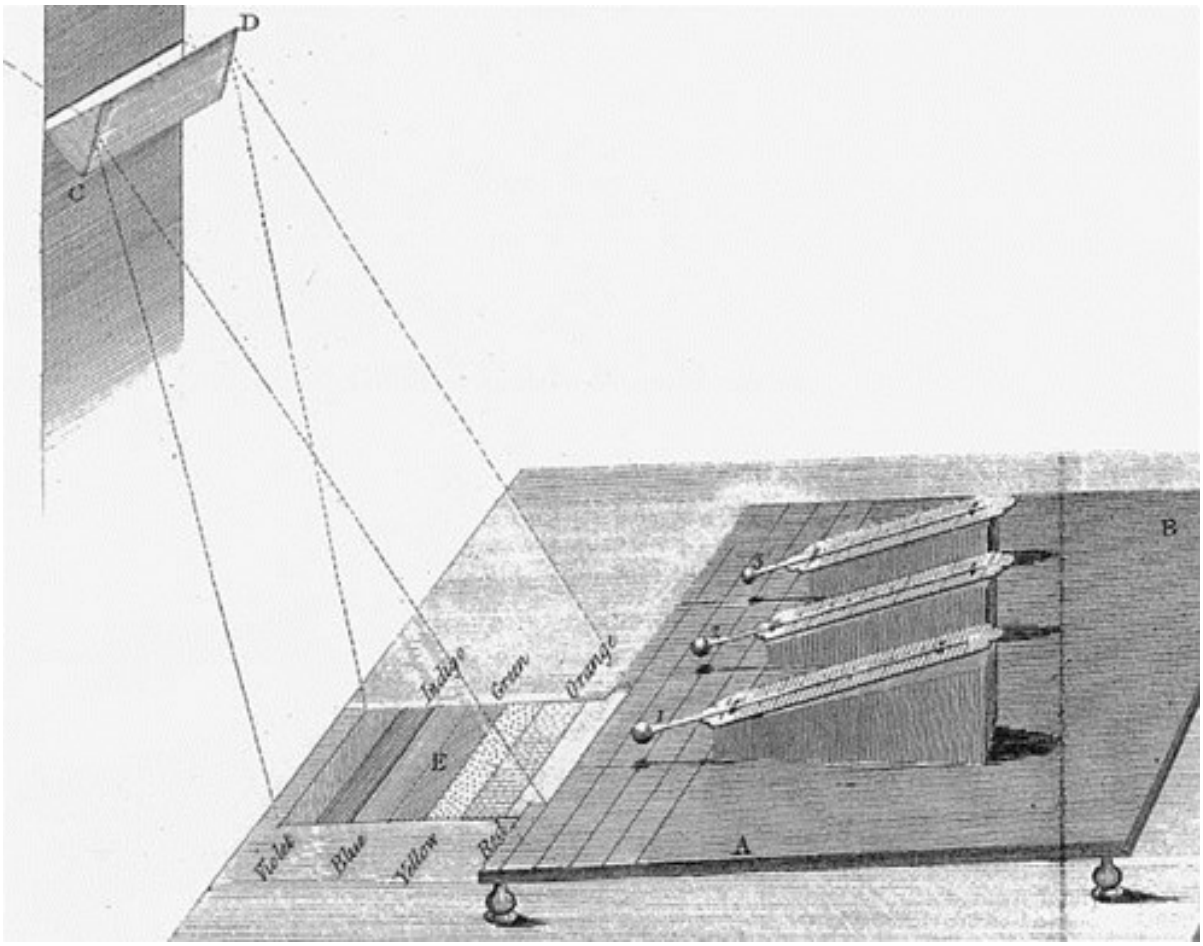

Figure 1-5. Illustration of William Herschel's IR experiment.

common bonds that absorb in the IR region (have permanent dipoles) are those formed between any two of carbon, nitrogen, oxygen, or hydrogen. The strength of IR spectroscopy is that the nature of the bond produces a distinct absorbance band position. Tables of group frequencies are available and give common ranges for various bonds. For example, alkane C-H stretching occurs between 2850 and 3000 cm^{-1} while alkene C-H stretching occurs between 3200 and 3100 cm^{-1}. Also, single bonds will appear at lower frequencies than double bonds, which will appear at lower frequencies than triple bonds. Another factor in IR spectroscopy is the mode of vibration of the dipole. Depending on the symmetry and complexity of the molecule certain bonds can stretch in multiple ways (symmetrically or asymmetrically) and some can bend in multiple ways (scissoring, wagging, twisting or rocking). For these modes to be IR active their motion needs to cause a change in the dipole of the molecule. An example of this is that an alkane C-H will stretch between 2850 and 3000 cm^{-1} while the same bonds bending region is much lower in wavenumber, between 1350 and 1470 cm^{-1}. As long as the stretch or bend occurs at a regular frequency and the vibration results in a change in the permanent dipole, infrared radiation of that frequency can interact and those bonds will be IR active.

Within the IR spectrum there is a region where many vibrational modes of common bonds overlap. The level of detail in this region of an IR spectrum is typically very high and for this reason has become known as the fingerprint region. It is roughly between 500 and 1500 cm^{-1}. The consequence of the complexity is that for larger molecules this region will appear to have a series of bands that will be the culmination of many modes and lesser absorbing bonds that will be difficult or impossible to identify. The difference

in local chemical environments will cause similar bonds to yield a broad absorption band. For this reason an instrumental wavenumber resolution of 2 cm^{-1} is commonly used and sufficient.

IR spectroscopy is extremely sensitivity to water. OH groups in water adopt a myriad of local environments on account of water's high degree of hydrogen bonding. This combined with a strong dipole and resulting high molar absorptivity values makes water a broad and highly influencing sample or contaminant and it can easily dominate a spectrum. Steps have to be taken to adequately dry any sample before a spectrum is collected if one is looking for peaks where water absorbs.

IR spectroscopy has the advantage of being both a qualitative and quantitative tool. IR finds use mostly in confirming the presence or absence of certain functional groups and is complimented by other analytical techniques. There are many very detailed IR spectra libraries that are useful to compare spectra for identification.

Transmittance Infrared

As the potential of IR spectroscopy began to be realized, different methods of obtaining spectra were implemented. The most common is simple transmittance IR where a beam of radiation is passed through a sample. The presence of bonds absorbs certain wavelengths which results in an adsorption spectrum. This method ideally follows Beer's Law, yielding the potential for quantitative measurements.

Attenuated Total Reflectance (ATR)

Another common IR technique is attenuated total reflectance (ATR). With this approach, the IR signal is internally reflected through a crystal with a high refractive

index, the sample is pressed against the crystal. As the signal internally reflects within the crystal, an evanescent wave is produced at the surface of the crystal, which will interact with the sample and attenuate the signal. This attenuation is compared to a blank sample and an IR absorption spectrum results. A result of this setup is that the penetration into the sample is on the order of a few wavelengths or less, so bulk analysis is not possible and the sample needs to be very close to the crystal.

Infrared Reflection Adsorption Spectroscopy (IRRAS)

This technique is the primary tool of this thesis and will be discussed in more detail than the others. Infrared reflection absorption spectroscopy (IRRAS) is also broadly referred to as glancing or grazing angle IR spectroscopy. IRRAS is effective for observing samples that are close to a smooth metal or glassy carbon surface. As radiation transits the sample, certain frequencies will be absorbed and will give the user a spectrum that is a result of the nature of the layer at the metal surface. IRRAS was first observed in 1959.[53] The so called "surface selection rule" was defined in 1976.[54] The understanding of the science behind the surface selection rules offered a method to organize experiments to take advantage of such an effect.

IRRAS has some requirements. Firstly, the surface must be reflective and smooth. Smooth being relative to the incident IR light which covers a wavelength range from 2.5 to 25 μm, any surface feature should be much smaller than 2.5μm to avoid diffuse reflections. This smooth surface must also be reflective to the incident radiation as transmitted or totally absorbed light will not give a signal. Secondly, the substrate must be a material with an abundance of conduction electrons. Thin films of Au, Ag or Pt are often used. This situation synergizes with a third requirement; the dipole must have a

component perpendicular to the surface. This is required because the dipole of the analyte will interact with an induced electric field in the metal and create a virtual dipole within the metal that will enhance the signal. Fourthly, the incident radiation should be p-polarized, that is in a plane perpendicular to the surface. Light of this nature will interact with the analyte's dipole, a dipole that is enhanced more when it itself is perpendicular to the surface as mentioned above. Any s-polarized light will show little to no absorbance as dipoles in the analyte that are parallel to the surface will be effectively cancelled due to the same enhancing effects of surface-perpendicular dipoles. A diagram of this "perfect metal" effect is shown in Figure 1-6. The ratio of the signal from p-polarized light to s-polarized can be as high as 100,000.[55] With these four requirements met, the IRRAS technique can be very powerful.

The effect of the angle of incidence is not simply a matter of having the electric vector of the incident light perpendicular to the surface, i.e. 90 degrees will not give the highest signal. This has been explained by Porter et. al and involves solutions to Maxwell's equations at a surface when considering the refractive indices of the air, the film and the substrate.[56] The effect of the angle of incidence on the mean square electric field is show in Figure 1-7. The consequence of the selection rule is that the maximum signal will ultimately depend on the substrate material. In the case of the experiments described in this thesis the substrate is gold and an angle of incidence of 80 degrees was used.

The spectra of IRRAS differ from conventional transmission on account of the surface selection rule which affects the magnitudes of bands but not their positions. In IRRAS, like in transmission, IR bands are affected by the nature of the bond providing the dipole

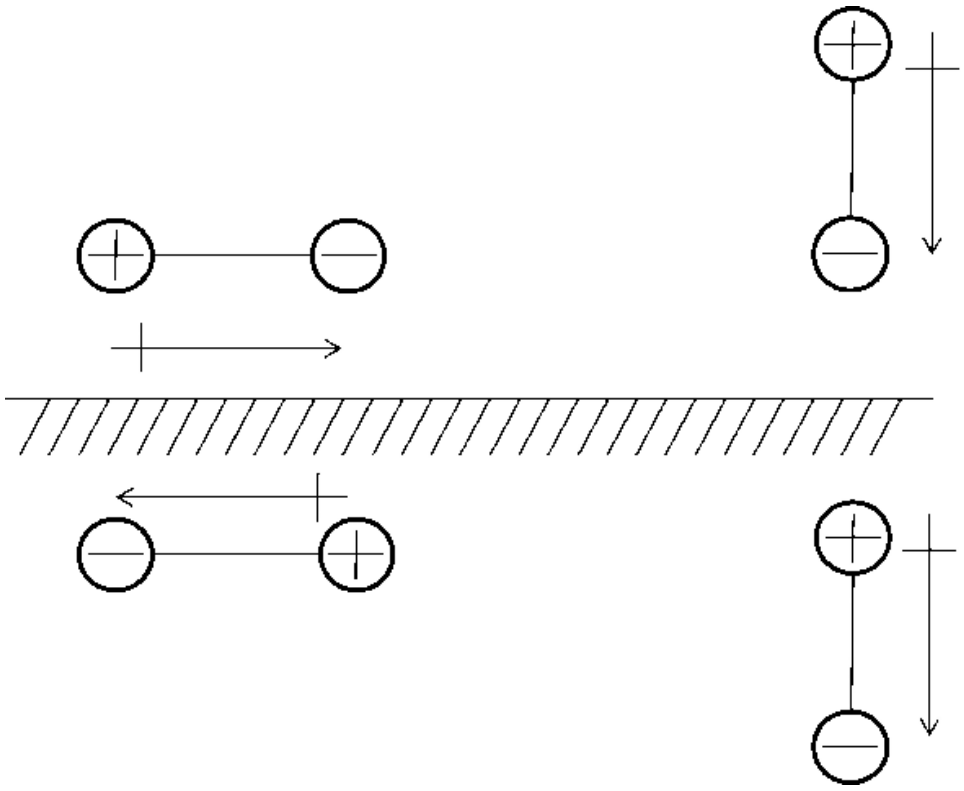

Figure 1-6. Visualization of dipoles close to a conductive surface

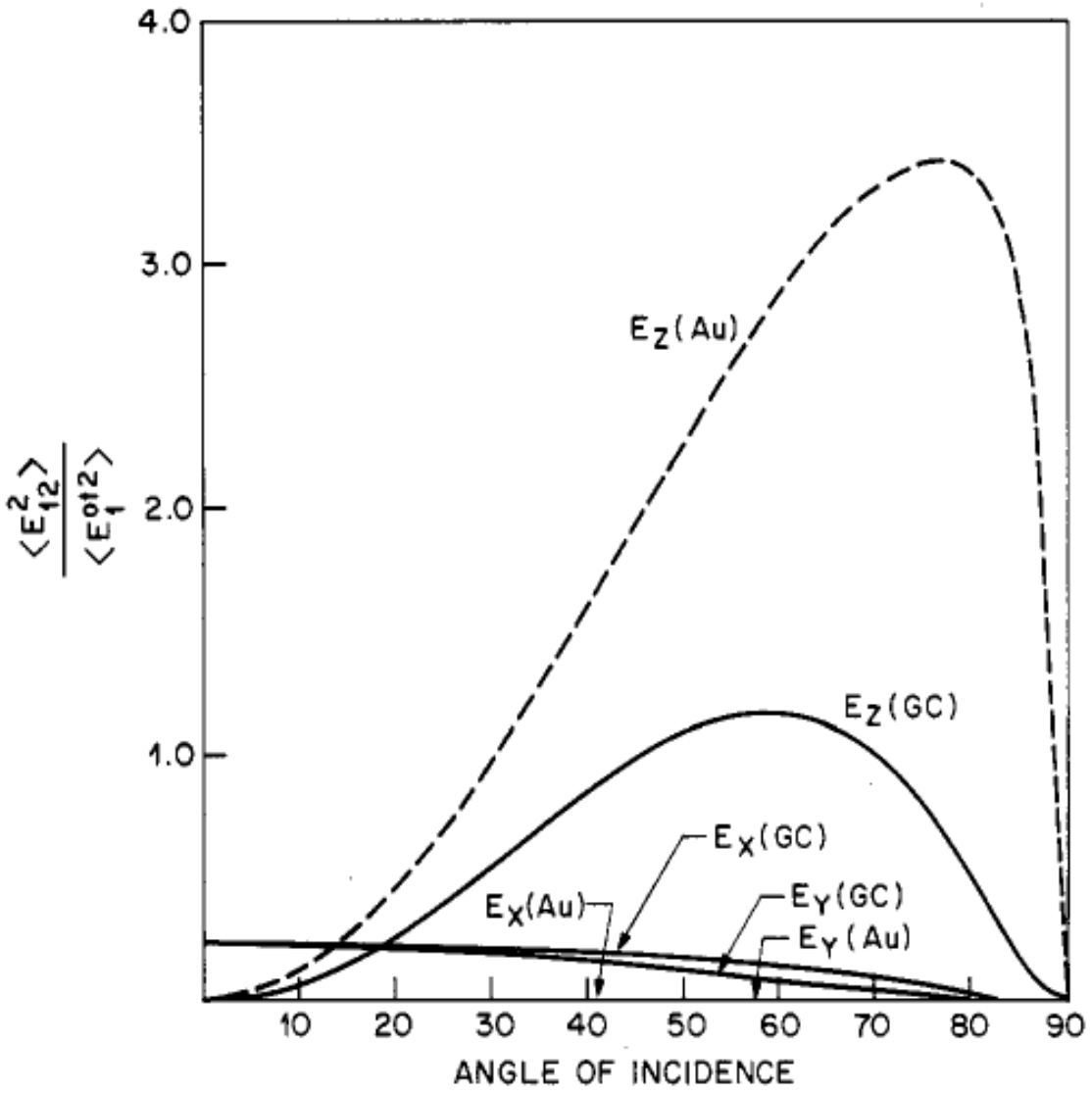

Figure 1-7. The mean-square electric field at 2000 cm^{-1} as a function of angle of incidence and polarization at the surface/air interface. Reprinted with permission from Reference 57. Copyright (1986) American Chemical Society.

and these factors are lumped together in the molar absorptivity or epsilon as written in Beer's law and are specific to each frequency. These factors affect both transmission and IRRAS signals as the source of these bands are the same. However, in IRRAS there is another consideration, the angle of the dipole relative to the surface. Since this dipole is amplified by a virtual dipole present in the metal, its absorption is proportional to the square of the angle between the surface and the dipole. This means that bonds parallel to the surface will be invisible to IRRAS and bonds that are closer to perpendicular will be increasingly enhanced. This has led to applications of IRRAS in discerning the orientation of surface adsorbed monolayers.[55,57–61]

Advantages

The advantages of IRRAS include monolayer sensitivity on surfaces, which would not be possible with transmission techniques. Sensitivity is due to the amplification of the surface perpendicular dipoles as well as the angle of incidence. With an angle of 80 degrees to a gold substrate for example, the radiations path through a monolayer transits significantly more sample than if the radiation were normal to the surface. These two factors allow for incredible surface detail with absorption values 25 times greater than conventional transmission.[55]

Disadvantages

Disadvantages of IRRAS include the requirement that the sample to be close to a smooth metal surface. Some bonding information will be omitted; if such a bond of interest is desired to be investigated the only solution is to re-orient that bond relative to the surface. Surface adsorption or surface bonding is popular to tether the sample close to the surface but this will intrinsically alter the structure near the surface and

might introduce different abortion band positions. To be responsive to such small absorption signals, liquid nitrogen cooled mercury cadmium telluride (MCT) detectors are generally used. Traditional thermocouple or pyroelectric detector exhibit too much thermal noise. Obtaining background spectra is not as trivial as is in transmittance modes. Ideally, the background should be identical to the sample with the sample removed which in the case of species adsorbed to a gold metal slide would be a bare gold slide. Achieving a clean gold surface is difficult because airborne contaminants readily adsorb to such a surface. When the sample is as thin as a monolayer, even a small amount of surface contaminant can be significant. To prevent contamination it is common to use a gold slide with a protective layer on it such as a long alkane chain attached to the surface by a thiol group. The stability offered by the chain stacking of long alkanes provides the required protection. However this introduces into the background an abundant source of C-H vibration, both bending and stretching, that will affect the final sample spectra. To deal with this inconvenience a deuterated alkane chain can be used which will shift the position of these bands into regions that are likely outside the region of interest.

Spectroscopy of CNC

The study of cellulose has been under investigation for decades and within that elucidating its various structures has been perused. Spectroscopy has been at the heart of this work with main contributions coming from nuclear magnetic resonance, (NMR)[62,63] X-ray and neutron diffraction,[11,19,64–66] infrared spectroscopy,[67–69] and Raman spectroscopy.[69–73]

Vibrational Spectroscopy of CNC

The complimentary pair of vibrational spectroscopies, IR and Raman, has been applied to the study of plant substances. A major limitation of IR is its inherent water sensitivity, and so IR studies have been limited to dry material. Raman spectroscopic signals for water are weak so this technique offers an advantage of monitoring wet samples. Although IR has been generally more common than Raman due mainly to instrumental issues, advances in lasers, filters and detectors have made Raman a capable candidate. This is due even more so when considering the ability to measure aqueous samples and uses a highly focused microscope.[70] With the combined use of these techniques a wealth of information has been gathered about cellulose and more specific to this thesis, CNC.

Infrared Spectroscopy

IR spectroscopy has been widely used for the study of cellulose. Bands due to –OH, -CH, and C-O stretching are readably observed and interpreted. The level of detail observed in IR spectra is subject to peak broadening with the main sample source being the degree of crystallinity (presence of non-crystalline regions) of the material and the ratios of various allomorphs. The most studied allomorphs are invariably natural cellulose or cellulose I with its two crystal structures cellulose I_α and I_β. These two are very similar in that the heavy atoms are in very similar environments but the network of hydrogen bonding is vastly different.[63]

IR spectroscopy has been used to differentiate the alpha and beta components in cellulose I.[21] IR spectroscopy has been used to determine the degree of crystallinity by calibrating peak ratios to known crystallinity. Namely the ratios of the 1429 to 893 cm^{-1}

[74] and 1372 to 2900 cm^{-1}.[75] IR spectroscopy has been used to determine the surface sulphate coverage by interpreting the asymmetric S=O at 1250 cm^{-1} and the symmetric C-O-S at 833 cm^{-1}.[68] The sensitivity of this approach is inadequate to gain a coverage value but it can confirm the presence of these groups. When the surface sulphate coverage was determined with XPS it was calculated to be one third to one half of the surface hydroxyls[68] and in another report between 10 and 25%.[76] This range of sulphate was detectable by IR but not quantitatively.

IRRAS of CNC

The IRRAS spectra of CNC have not been reported in the literature. IRRAS has been used with cellulose to determine the orientation of long alkyl side chains in a Langmuir-Blodgett film.[61] As well, IRRAS combined with ATR has been employed by E Gilli et al to measure the amount of carboxymethyl cellulose attached to cellulosic films.[59] IRRAS offers several differences when compared to other IR spectroscopy methods. Possibly the greatest difference is the inclusion of the surface selection rules which will change the nature of collected spectra. As a result of this, established IR spectral interpretations which rely on peak magnitude, such as peak ratios, will not be applicable without reassessing the origins of the signals and establishing a new ratio with correcting factors. However, for this same reason IRRAS does present spectral features that are not interpretable from traditional spectra.

A method that gives comparable results to IRRAS has been applied to Iβ cellulose films. Polarized spectra of these not-completely-disoriented systems allowed for the difference spectrum of two perpendicular polarizations spectra.[77] After subtraction, the result was a spectrum that would reveal peaks that were preferentially oriented along a unit cell

axis. The result is a view of the c-axis perpendicular dipoles (as in IRRAS) but without the enhancement due to the surface selection rules. Some peak heights and band positions from the work in this thesis disagree with this but most agree and the assignments that resulted from that work are applicable as a basis for peak assignments of IRRAS spectrum.

Raman Spectroscopy

Raman spectroscopy has been employed to the study of cellulose. Similarly to the work done in the late 50's and early 60's with IR ratios relating to crystallinity, Agarwal et al has found a relation between Raman signals and crystallinity.[71] It involves the ratios of the shifts at 380 to 1096 cm^{-1} with some mathematical constants to correlate with percent crystallinity. In addition to this he proposed a better fitting multivariate method obtained from partial least squares (PLS) regression based on the same principals but involving different shifts.

The spectral contributions of lignin and other carbohydrate polymers found in natural wood sources observed by Raman spectroscopy have been investigated.[78] This study highlights the potential of Raman spectroscopy to be used to differentiate cellulose from hemicellulose and lignin which could be useful to determine the quality of manufacturing of CNC from raw materials.

Total internal reflection Raman spectroscopy (TIR) has been used to monitor the adsorption, with time resolution, of two molecules (CTAB and TX-100) to a cellulose film.[79] These surfactants exhibit adsorption isotherms as different concentrations of each as well as mixed solutions are flowed across a cellulose surface. This could be

comparable to the present work as a method to monitor adsorption to a surface over time.

The Raman stretching band at 1095 cm^{-1} has been correlated to strain on the glycosidic linkage. This information has been used to back-calculate strength properties such as axial elastic modulus.[36,38]

Spontaneously-Adsorbed Monolayers

Self-adsorbed monolayers (SAMs) have been used across a broad spectrum of chemical applications. This is in part due to their ease of preparation and consistent formation. The ability to create a substrate with well-defined surface topology and chemistry is at the heart of a SAMs usefulness. Specific to this research, two types of SAMs will be mentioned, those derived from diazonium salts and those derived from alkane thiols.

Diazonium Salt Derived Films

Diazonium salts are known for their radical activity to spontaneously or electrochemically form covalent bonds to certain substrates through a radical intermediate and can result in multilayer films.[80–83] This reactivity and the variety of functional groups that can be para to the N_2 make this reaction desirable as a means to modify surfaces to yield a desired chemistry. An example of the formation of a spontaneously adsorbed monolayer from an aryl diazonium salt terminated with a functional group “R” is show in Figure 1-8.

Specific to the work presented here, the novel use of a diazonium radical surface reaction has been employed to modify a CNC surface with a variety of functional

groups. This work was pioneered by Dr. Rongbing Du and used NO_2 and CF_3 functionalized diazonium salts to create the corresponding modified CNC surfaces that were investigated for their ability to facilitate the addition of modified CNC into high density polyethylene (HDPE).

Thiolate Derived Monolayers

It has long been known that alkane thiols form SAMs on certain metals.[84–89] This chemistry has been thoroughly researched and is well understood making it a powerful candidate for applications related to the work presented here. Early work includes the observation of layer formation of disulphides on gold by Allara and Nuzzo. [90] Furthering this work were several groups who saw this stable surface as a candidate for uses such as protein adsorption and detection.[84,85,87–89,91–94] The combination of a controllable, organically terminated monolayer and a reflective metal surface lends itself directly to applications of IRRAS. These conditions satisfy the mandatory condition of a reflective metal surface (gold) and allow a variety of surface chemistries via choosing different functional groups to terminate the non-thiol end of the alkane chain. An example of the formation of a self assembled monolayer from an eleven carbon alkane thiol terminated with a functional group “R” is show in Figure 1-9.

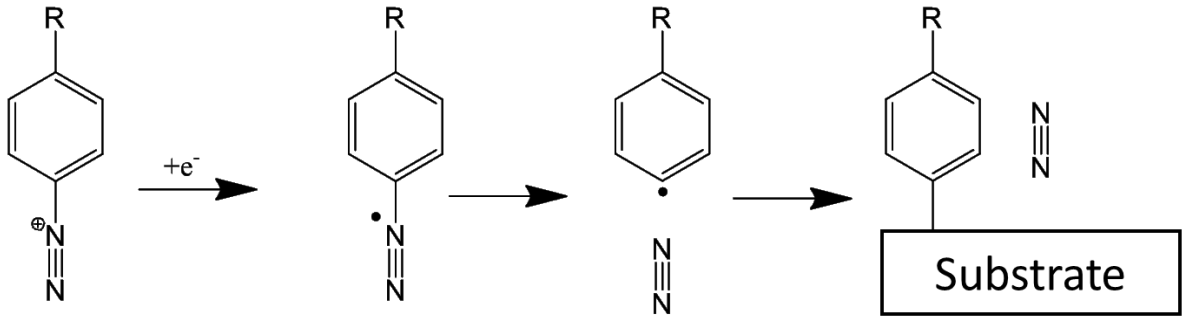

Figure 1-8. Formation of a spontaneously adsorbed monolayer on a substrate. The electron can be produced chemically or by applying an electric potential.

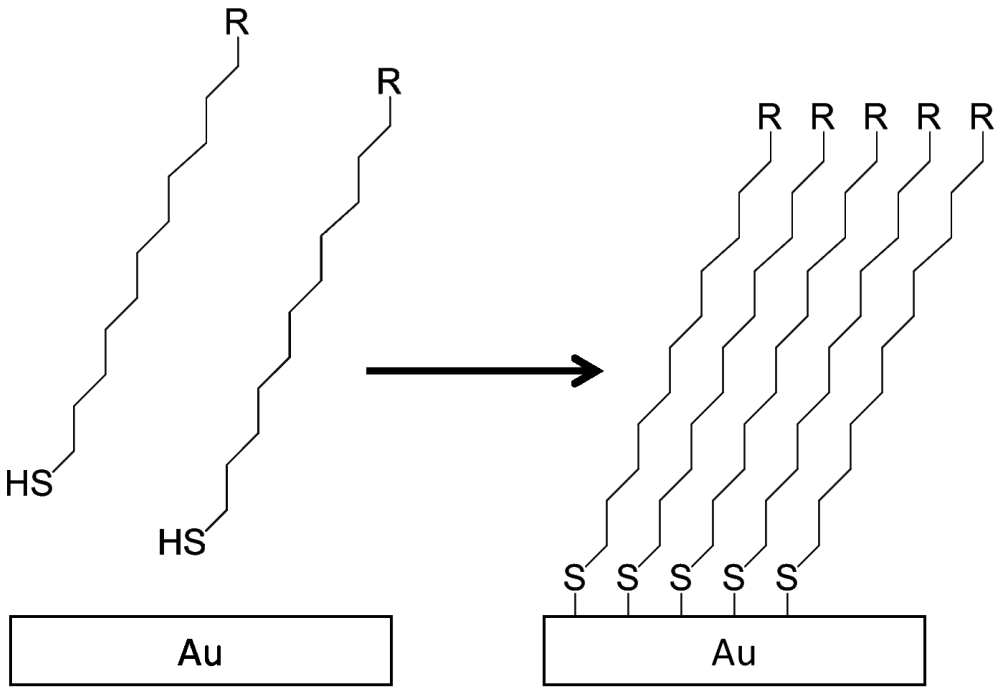

Figure 1-9. Formation of a self assembled monolayer (SAM) on a gold (111) surface.

Surface Functionality and Grafting of CNC

Two main categories can be defined in the surface modification of CNCs, chemical functionalization and polymer grafting.[95,96] Polymer grafting is defined as the bonding of a polymer to or polymerizing it from a CNC surface. Chemical functionalization is defined as changing the surface chemistry of a CNC with small molecules. The two are obviously related with the main difference being the size of the group that is chemically bonded, or in some cases adsorbed, to the CNC.

The surface chemistry of any material will play major roles in its use. Cellulose is no different. When compared to other materials, such as carbon nanotubes, cellulose is somewhat unique in that its production is a matter of isolation from existing raw material rather than construction from smaller parts; sometimes called building from the top down rather than the bottom up. This is one reason why cellulose is so attractive; nature has done the energy intensive work of organizing atoms in such a crystalline manner. As cellulose exists in its biological host, the surface is patterned with hydroxyl groups which vary in levels of hydrogen bonding and dispersive attraction to ultimately yield a larger structure. During a surface modification, these hydroxyl groups are manipulated to result in a different functional group. Invariably, the first modification will arise when crystalline portions of cellulose are isolated from some biological host.

Mechanically treating a raw material containing cellulose will separate it into a fibrillar form containing regions of crystalline and amorphous structure. The surface groups are hydroxyl, like that of natural cellulose. Crystalline cellulose is isolated from amorphous regions by chemical removal of the less ordered portions on account of their higher reactivity due to lack of crystalline steric protection. The resulting surface chemistry and

functionality are affected by the type of treatment. The most common approach is sulphuric acid hydrolysis which leaves varying degrees of sulphate groups on the remaining cellulose surface, the degree of which depends on the acid concentration and reaction time.[27,28] Already we can see a method to control the surface chemistry of an isolated cellulose material by means of choosing a technique to liberate it from its amorphous regions.

The dominant reason to modify the surface of a cellulose material is to control the surface interactions to allow its incorporation into a host material. Another reasons is to control the chiral nematic nature of CNC suspensions. CNC being dispersible in water is exploited for isolating it from natural plant material. However being dispersible only in polar solvents limits their possible use significantly when considering CNC's tremendous mechanical strength and trying to incorporate them as additives or fillers in various materials. Polymer additives are a promising use for this material. After the isolation step, many methods have been developed to further modify the CNC surface and they can be divided into two approaches; adsorption of surfactants and covalent bond formation.

Surfactant Adsorption

Surface adsorption relies on the electrostatic attraction of some surfactant to a charged CNC surface. For this reason a CNC surface with sulphate or carboxylic acid is preferred. Examples include cetyltetramethylammonium-bromide (CTAB) which is also used in metal nanoparticle creation [97] and atactic polypropylene (aPP).[98] The nature of surfactant adsorption to modify CNC works well with layer-by-layer deposition (LbL) where a surface is alternately immersed in solutions of opposite surface charged

molecules.[99–101] This provides a mechanism to create macroscopic films. For LbL technique, the surface charge of the cellulose material is important and can also be done after a covalent modification to alter the nature of the surface.

Covalent Modification

A far more popular approach to CNC modification is the formation of a chemical bond. This involves reactivity with the surface available hydroxyl groups or whatever those groups have been converted to in previous reactions. The polarity, which can imply reactivity, of the surface hydroxyl groups can be ordered: C2-OH > C6-OH > C3-OH.[102] The polarity can be useful to consider when attempting to modify cellulose and to gain insight into what degree of surface hydroxyl modification to expect. Also, in the common case of sulphuric acid isolation 10 - 25% of surface hydroxyl groups are replaced with a sulphate.[76] This can have implications when considering surface chemistry on CNCs. Some of the more common surface modifications are shown in Figure 1-10.

When starting with natural cellulose, any reaction that involves a hydroxyl group can be performed. Depending on the desired nature of the final cellulose surface, appropriate reactions can be selected, and once modified, the product can be used for its application. For polymer mixing, there is still the challenge of dispersing the modified CNC throughout the matrix. Various approaches can overcome this problem and some will be discussed below.

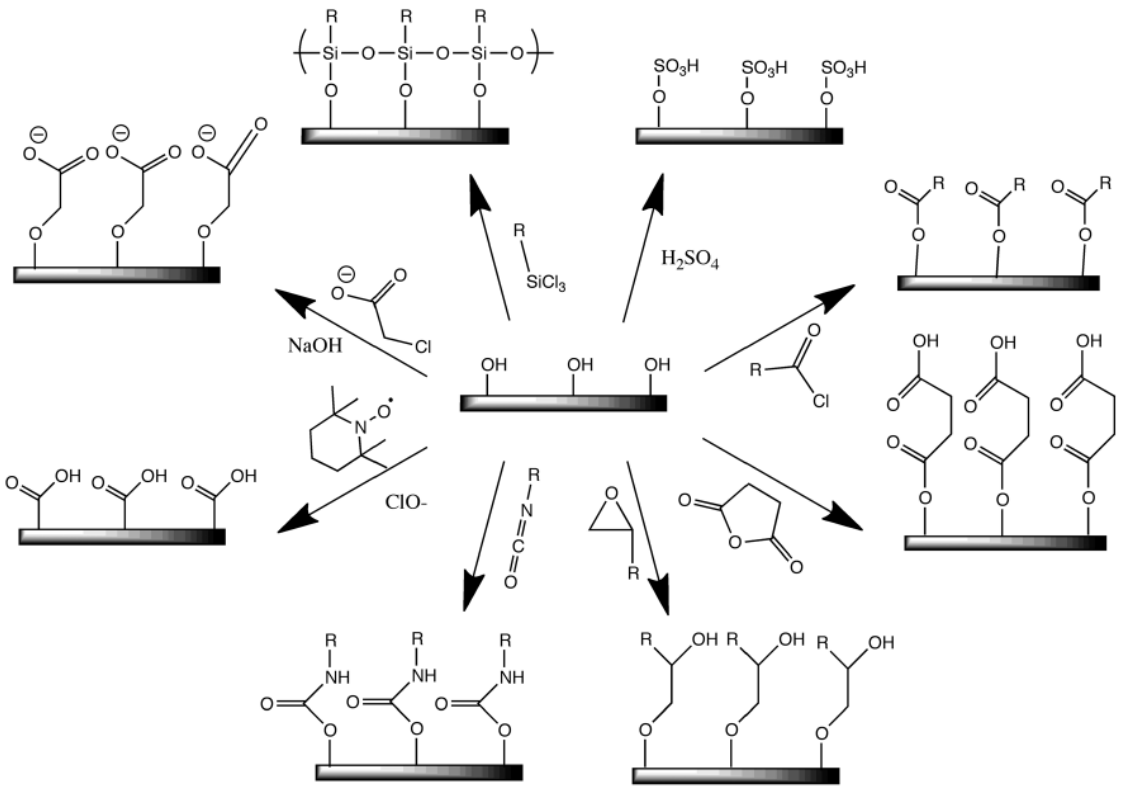

Figure 1-10. Modification of CNC Surfaces. Reproduced from Ref. 7 with permission from The Royal Society of Chemistry.

Incorporating CNC as a Matrix Additive

A common end goal with CNC or other cellulose materials is to gain a property advantage by incorporating them in an existing material. This is usually facilitated by modifying the surface as discussed in the previous section. Specifically to mechanical advantages, which cellulose holds much promise, dispersing the CNC about a matrix is crucial. To accomplish this, several methods that are common to polymer engineering have been applied to cellulose.

Melt Mixing or Extrusion

Melt-mixing quite simply mixes an additive to a thermoplastic polymer by raising the temperature above the melting point of the polymer; solvents can be used to facilitate the integration of the additive to the matrix. The melt is continually stirred, often by a twin screw device. This agitation permits the dispersion of the additive via shear mixing, provided they are miscible. From this mixed melt, an extrusion is pulled and cooled and formed into any desired mold or geometry.

Melt mixing has been applied to cellulose materials including a method to mix cellulose fibers with a notoriously hydrophobic low density polyethylene (LDPE).[103] Another study used polyoxyethylene as a surfactant to facilitate the mixing of LDPE with CNC.[104] A major challenge aside from adequate mixing when combining this technique with cellulose materials is thermal degradation. Only polymers that melt at low enough temperatures are suitable.

Solvent Casting

Solvent casting involves dissolving both the polymer and an additive in a suitable solvent. After sufficient mixing, the solution is cast and the solvent is removed by evaporation or freeze-drying. Solvent casting allows the precipitating mixture to remain mixed provided they are compatible in the first place.[95,105] Solvent casting is similar to melt mixing but requires less heat. However, it does require solubility of CNC in the solvent and polymer.

The solvent casting approach to cellulose composites mainly involves water soluble host materials as cellulose benefits from great aqueous suspension. Commonly used solvents are THF and DMF and combine cellulose with polymers that are stable in water.[106,107]

One aspect of the work presented in this thesis is incorporating CNC into polyethylene (PE). PE can be solvent cast from decaline or xylene using an antioxidant 2,6-di-tert-butyl-p-cresol (BHT), high temperatures are required as the PE is basically melted in the solvent more so than dissolved.[108,109] For this reason solvent casting of CNC in PE is not suitable.

Electrospinning

Electrospinning allows the manufacturing of fibers with diameters from micrometers to hundreds of nanometers by applying a voltage between a conductive tip that contains a polymer/additive blend and a collection plate. The electrostatic forces force a thin cord of material to be “spun” onto the collection plate. Electrospinning does suffer from the same difficulty as mentioned before of dispersing CNC in the polymer.

The issue of CNC dispensability has not hindered the use of electrospinning to create cellulose composite materials. Habibi and co-workers have used surfactants and polymer grafting to improve the compatibility of CNC's in organic media such as THF and DMF to mix with polymers such as polystyrene and polycaprolactone.[110–112]

Co-polymerizing

In the previous CNC modification methods, CNC or modified CNC were mixed with another material with the main obstacle being dispersing the CNC. In those methods, modifying the surface chemistry is usually a preliminary step followed by the mixing. However, modification and mixing can be combined if the graft is also in-situ polymer. Combing these steps involves attaching a polymer directly to the surface to make the whole cellulose nanoparticle compatible with that polymer.[96,113,114] This can be carried out in a mixture of the same polymer which effectively combines the steps. This is referred to as "grafting-to". Alternatively, polymers can be manufactured from an active site attached to the CNC.[96] This is referred to as "grafting-from". "Grafting to" suffers from steric problems as higher degrees of polymerization will prevent further graft-able polymers from reaching the cellulose surface. Comparatively, the "grafting-from" approach allows the growing polymerization more freedom from the bulky CNC and can lead to longer polymer chains and higher degrees of cross-linking.[96]

World Production of Cellulose Nanomaterials

Across the world 1.5×10^{12} tons of annual biomass in the form of cellulose is produced.[8] For comparison the most produced polymer by human industry is polyethylene with an annual amount of 7.5×10^{7} tones as estimated by the ICIS for the 2012 year. The interest in CNC for a variety of purposes has been growing throughout the world as higher

performing materials become expected and even demanded for businesses in competition in this area. Currently there are several pilot plants worldwide that have started turning out multi kilograms per day or higher. There is anticipation with all the interest and buzz that when an application demanding isolated CNC or MFC material on an industrially large scale is implemented that these plants will be able to facilitate and take advantage of an up and running operation. These plants can be divided into ones with a primary aim of CNC or MFC. Most of these are assisted by government sponsorship from a variety of scientific initiatives.

CNC

- Celluforce Inc, Windsor, Canada
- Alberta Innovates Technology Futures, Canada
- FPInnovations, Canada
- US Forest Products Laboratory, United States
- Melodea, Israel
- Bio Vision Technology Inc., Canada

MFC

- University of Maine, United States
- Innventia, Sweden
- Daicel and Nippon Paper, Japan
- J. Rettenmaier & Söhne, Germany
- Borregaard, Norway
- UMP, Finland

Research Objectives

The issue of understanding the molecular structure of cellulose has proven to be convoluted. The structural repetitiveness resulting when forming a crystal brings hope of a discernable and calculable three-dimensional atomic arrangement. With this information, accurate predictions can be made for individual particles as well as systems that include such particles. This useful information varies from figures regarding reactivity to mechanical strength. Regarding cellulose, a great body of research has been directed towards these goals from the time cellulose was discovered. Cellulose's molecular structure will manifest itself in many ways within many techniques that aim to monitor this polymer. Spectroscopy, including X-ray and IR, will provide this information with proper interpretation of the results. Despite concerted efforts by multiple researchers, there are still unanswered questions about the specific atomic arrangements of this ubiquitous polymer. Its complex multi-crystal phase composition and transitions between allomorphs lends itself to structural disagreements within the literature. The work within this thesis partially aims at using IRASS to monitor CNC and interpret the resulting signals. This work will expand on the knowledge base of IR band assignments.

Making economically responsible use of CNC has been a struggle. CNC holds promise in composite materials as an additive to increase strength properties. The gap between science and industry is difficult to bridge, with the current availability for high performance materials that plastic engineering can offer and the advantage that cellulose has of being environmentally produced does not factor into a profitable advantage. This has not stopped research towards this goal and pilot plants are

operating to sooner bring the advantages of cellulose to industry. This thesis offers a method to monitor and compare the molecular interactions between cellulose and functional groups that are common to many polymers. Functionalizing cellulose is a means to permit its incorporation into polymer systems. A novel method of CNC surface modification has been investigated with IRRAS. Furthermore, the incorporation of this modified CNC into polyethylene was investigated with regards to mechanical strength enhancement.

Chapter Overviews

Chapter 2

A method to obtain a detailed IRRAS spectrum of CNC is presented. The observed IR bands are assigned using a combination of factors, namely the surface selection rule that arises from the IRRAS technique and comparing spectra with those of other glucose dimers and polymers as well as a comparison with the wealth of existing infrared studies of cellulose.

Chapter 3

A method to control the experiments presented in Chapter 1 allows observations of the propensity of CNC to adsorb to controlled organic substrates. Several experimental conditions were tested; the CNC concentration, the functionality of the substrate to which the CNC adsorbs, and the ionic strength of the aqueous CNC suspension. All these factors were observed over time as the CNC were allowed to adsorb to the substrate. From this insight into the strength of interactions and the density of adsorbed layers was gained.

Chapter 4

A novel method using diazonium radical modification to control the CNC surface chemistry was investigated using the methods developed in the previous Chapters. NO_2 and CF_3 functionalities were imparted to a CNC surface. IR and XPS were used to confirm the modification. The interactions of these modified CNC were monitored as they adsorb to controlled organic substrates.

Chapter 5

The modified CNC presented in Chapter 4 were incorporated into a melt extrusion of polyethylene (PE). The mechanical properties, with focus on elastic modulus, were investigated. Virgin PE was compared with PE CNC and PE modified-CNC nanocomposites. An increase in elastic modulus was only observed with modified CNC as a nanocomposite additive which reveals the beneficial effects of the novel CNC surface functionalization.

Chapter 2
Infrared Reflection Adsorption Spectroscopy (IRRAS) of Cellulose Nanocrystals (CNC)

Introduction

Cellulose nanocrystals (CNC) are a promising nano material with potential applications across many fields. Their strategic implementation within other materials has been used to influence properties such as rheology, mechanical strength, and optics. The bulk properties of a material created with the incorporation of nano particles can be greatly affected by subtle structural changes within the nano particles. The general hierarchy from trees and plants to single cellulose chains is well established. In this hierarchy there are a number of crystal phases which ultimately exist on account of specific bonding that are subject to change during stresses such as surface modifications or thermal treatment. These changes are unavoidable when incorporating CNC as a material additive. Understanding the specific chemical bonding environments of CNC during such processes can facilitate the directed use of CNC towards these goals.

Infrared (IR) spectroscopy has been used to study of cellulose since the early 1940's.[115,116] The sensitivity to hydrogen-oxygen bonds and detailed fingerprint region make IR applicable to the study of this crystalline polymer. These observed bands in the IR spectrum have been assigned with an understanding that bands are invariably a sum of many sources with indistinguishable overlap.[75,77,117–122] Infrared spectroscopy

has been integral, in combination with other spectroscopic techniques such as X-ray diffraction (XRD) and nuclear magnetic resonance (NMR), in elucidating the structure of the celluloses. Most notably, it has offered the suggestion of two crystal allomorphs within cellulose I[18] that were later confirmed by cross-polarization magic angle spinning (CPMAS) ^{13}C solid state NMR[12]. IR spectra have been interpreted to estimate the crystallinity of cellulose from peak ratios.[75,123,124] Similar approaches have been carried out using Raman spectroscopy.[71] The ratio of cellulose I allomorphs have been related to various band ratios.[12,18,68,118] Sulphate groups remain on the CNC surface after the common step of sulphuric acid hydrolysis is used to isolate CNC from its natural amorphous regions. These groups have been detected by IR spectroscopy.[68] Many different modification schemes have been exercised with the interest of controlling the surface chemistry of CNC with the goal of increasing dispensability in various mediums. The specificity of IR to confirm the presence of functional groups in a sample makes it an inexpensive spectroscopic candidate to confirm the success of such a modification.

Infrared reflection adsorption spectroscopy (IRRAS) is a technique with specific sample requirements that offers unique and complimentary information to traditional IR spectroscopy. IRRAS mandates that the sample be thin enough to avoid diffuse reflection and close to a reflective conductive surface. IRRAS offers a unique response that is due to the surface selection rule; the magnitude of adsorption bands is a function of the angle of the dipole moment relative to the surface. If the orientation of specific bonds within a sample can be determined, band assignments to specific bonds can be assisted by this understanding. The crystal structures of CNC have been established relative to the nanocrystal orientation.[25,125] Atomic force microscopy (AFM) has been

used to study all types of celluloses. For the application to IRRAS, AFM can be used to image the reflective surface with adsorbed CNC to learn the orientation that individual crystals have relative to the surface. The combination of orientation and the crystal structure will prove useful in the IRRAS study of CNC. IRRAS has been employed indirectly to CNC in determining the arrangement of long alkyl side chains on a Lamgmuir-Blodgette film of alkylated 2,3-di-octadecylcellulose[61] and to monitor the amount of carboxymethyl cellulose (CMC) attached to cellulosic films.[59]

In Chapter 1 we present a well-resolved IRRAS spectrum of CNC and MFC which are compared with literature infrared band assignments. Unique information is revealed by IRASS which elucidates previous IR band assignment ambiguities. The surface adsorption of CNC from aqueous suspensions to a controlled functional surface has been demonstrated. Furthermore, second derivative data analysis predicts the positions of possible under-lying bands within the complex fingerprint region.

Experimental

Reagents and Materials

CNC were obtained from Alberta Innovates Technology Futures (AITF) as dried powder samples from a cotton source. MFC were obtained from Dr. Yaman Boluk at the University of Alberta as partly dried samples from a softwood source. The CNC and was isolated using sulfuric acid hydrolysis and the MFC was isolated using mechanical refinement and enzymatic treatment.

Deuterated octadecanethiol [$HS(CD_2)_{17}CD_3$] (DODT) 98% was purchased from Aldrich (Milwaukee, WI). 11-amino-1-undecanethiol [$HS(CH_2)_{11}NH_2$] HCl (AUT) was from

ProChimea (Sopot, Poland). All thiols were used as received. Millimolar thiol solutions were prepared in anhydrous ethanol (Commercial Alcohols, Brampton Ontario).

Substrate Preparation

The glass substrates were pre-cleaned in piranha solution (1:3 H_2O_2:H_2SO_4) at 90ºC for 15 minutes, rinsed thoroughly with deionized water and dried under Argon. Glass slides were immediately introduced into the vacuum chamber of a thermal evaporation system (Torr International Inc.). A 10 nm adhesive under-layer of chromium was evaporated followed by 300 nm of gold (4n purity).

Monolayer Formation

Self-assembled monolayers (SAMs) of DODT and AUT were prepared on gold substrates. One mM ethanolic solutions of each thiol were prepared and the gold substrate was immersed for 48 hours to ensure stable SAM formation. Slides were then removed and rinsed thoroughly with ethanol to remove unbound thiols. AUT-derived monolayers were immediately used for experiments to avoid contamination. DODT were stored in a nitrogen purged environment and cleaned with ethanol before each use as a background signal.

Infrared Spectra Measurements

IRRAS spectra were collected with both a Mattson Infinity FT-IR spectrometer (Madison, WI) and a Bruker Vertex 70 FT-IR spectrometer equipped with low-noise mercury-cadmium-tellurium (MCT) detectors cooled with liquid nitrogen. In both instruments, the incident radiation was reflected from the sample at 80º. One thousand scans were collected with a wavenumber resolution of 2 cm^{-1}. The sample chamber

was purged with nitrogen for 8 minutes prior to each measurement to limit interfering atmosphere signals. A spectrum of the atmosphere of the purged chamber was subtracted from all spectra to reduce remaining unwanted signal. A background signal was collected using the DODT substrate. OPUS v. 5.5, Winfirst and Essential FTIR v. 3.00.040 software was used to collect and handle the data. All spectra were manually and linearly baselined at like wavenumbers: 4000, 3633, 3134, 3013, 2779, 1818, 1406, 1178, 949 and 821 cm^{-1}. All samples were subject to mild mechanical stirring via a magnetic Teflon stir bar at minimal RPM to promote consistent liquid-substrate interactions.

Transmission IR spectra were collected using a Thermo Nicolet 8700 with attached Continuum FTIR microscope with 2 cm^{-1} resolution. Data was collected with OMNIC v. 8.3 software and handled with Essential FTIR v. 3.00.040 software.

The second derivative of the IRRAS spectra of CNC was calculated using Essential FTIR v. 3.00.040 software. For the CO region, a value of 19 was used for the smoothing window, and for the OH region a value of 37.

Raman Spectra Measurements

Raman spectra were collected with a Renishaw inVia Raman Microscope equipped with a high performance near IR (HPNIR) diode (785 nm with a 40 x 2 μm spot size, 1200 l/mm) laser and a charged coupled device (CCD) detector. Laser power was 300 mW, a 50 x microscope objective was used, and the sample integration time was 30 seconds with 6 acquisitions.

XRD Calculations

Synchrotron X-ray crystallographic data of cellulose I_β was copied from the supplementary portion of a paper published by Nishiyama et al.[25] ATOMS v. 6.3 software was used to exact the position of each atom. The angles that bonds made with the unit cell's c-axis were calculated in Excel 2010 using the Pythagorean Theorem.

Procedure

A method was developed to observe IRRAS spectra of CNC and is dipicted in Figure 2-1.

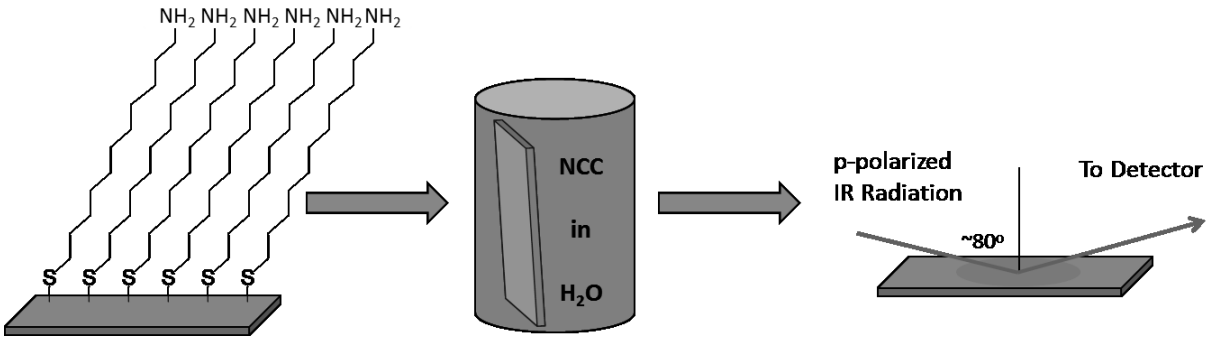

Figure 2-1. Diagram of method to obtain IRRAS of CNC

IRRAS requires a metal surface. Gold was chosen as it offered the freedom to create a surface adsorbed monolayer (SAM) with different chemical functionalities. For this project an 11-amino-1-undecanthiol (AUT) SAM with a terminal NH_2/NH_3^+ group was chosen as it offered electrostatic attraction with the negatively surface charged CNC. One mM AUT was dissolved in ethanol and fresh gold evaporated slides were introduced to the solution for 48 hours to ensure a well oriented surface was created.[87] SAMs form within hours of immersion but if a longer time is permitted better stacking of

the alkane chains ensues and a more stable layer is created. The gold coated slide with this AUT derived monolayer was then rinsed and immersed in an aqueous solution of CNC. At a desired time the slide was removed, rinsed in 18 MΩ water, dried with argon and an IRRAS spectrum was collected.

Results and Discussion

IRRAS of CNC

This chapter focuses on interpreting the IRRAS spectrum of CNC adsorbed on a substrate. We employ IRRAS to characterize the adsorption of CNC to well defined monolayer substrates in Chapter 3. Chapter 3 shows that monolayers formed from 11-amino undecanethiol (AUT) adsorb the highest coverage of CNC particles. Amine terminated monolayers are partially protonated at pH 7 and thus produce a net positively charged surface.[86] The negatively charged CNC interacts electrostatically with this layer to form a complete layer. Thus, for the results described below, we chose the AUT-derived monolayer as the substrate to support CNC particles for IRRAS characterization.

Figure 2-2 contains a 2 x 2 μm AFM image of a CNC layer adsorbed to an AUT derived monolayer from a 0.0015% aqueous solution. The CNC film contains individual particles that are 7 ± 3 nm in diameter and 130 ± 50 nm in length. The thickness of this film as measured by AFM scratching is roughly 7 nm indicating monolayer coverage of the CNC. The thickness measurements will be described in more detail in Chapter 3. The long axes (c-axes) of the CNC particles are mainly oriented parallel to the surface, which will be important to the spectral interpretation described below.

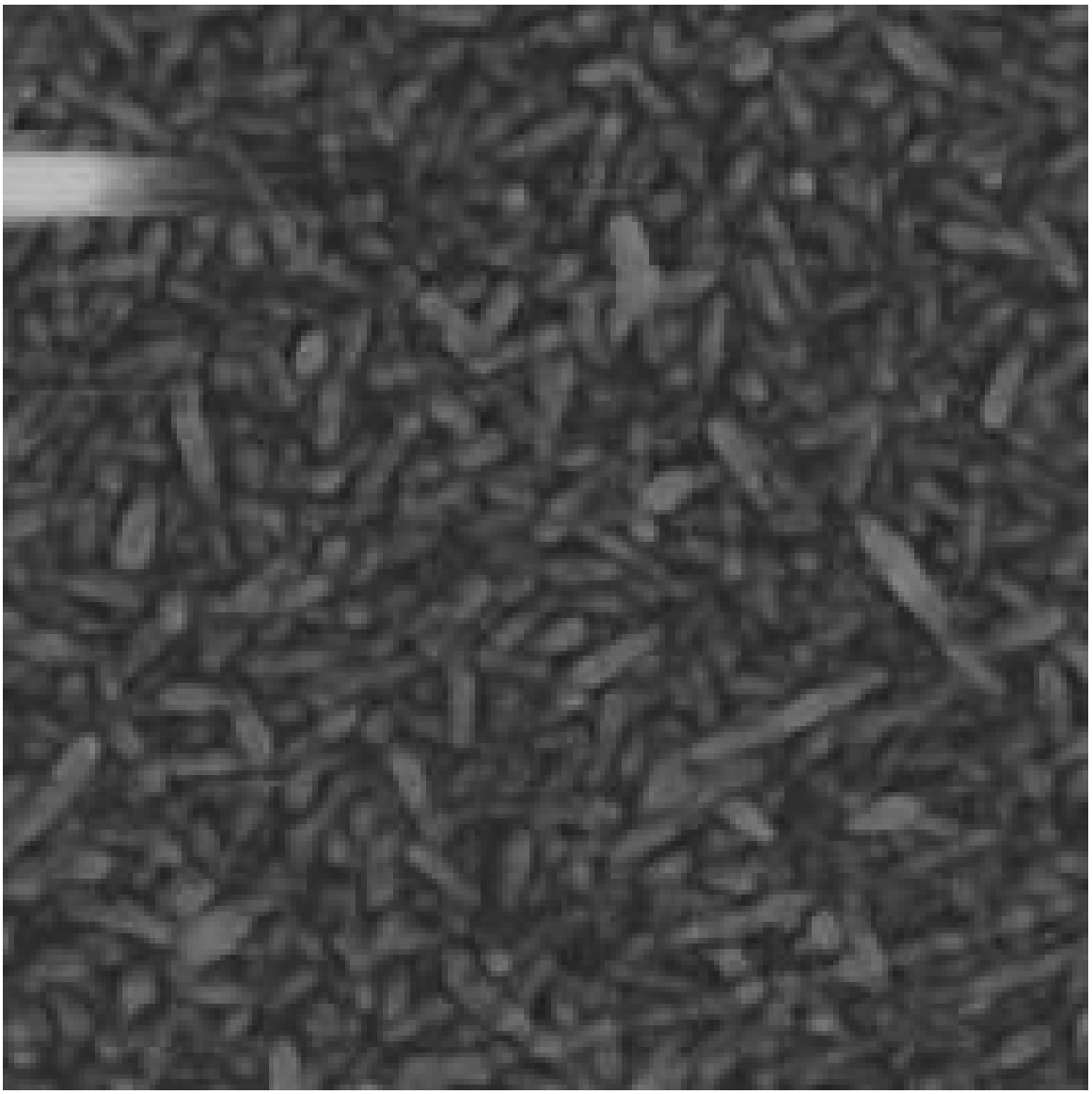

Figure 2-2. 2 μm x 2 μm AFM height image of CNC adsorbed to an AUT derived SAM.

Figure 2-3 contains IRRAS spectra of the AUT derived monolayer substrate and of a CNC film adsorbed from a 0.0015% solution. The spectrum of the AUT monolayer is similar to those reported previously.[86] Bands in the region around 2900 cm^{-1} correspond to C-H stretches. The most intense band in this region is the asymmetric CH_2 stretch and is located at 2922 cm^{-1} indicating that the alkyl chains in the monolayer are densely packed but not perfectly crystalline.[87] Low absorbance bands at 1465 cm^{-1} are attributed to the CH_2 bending deformation, and 1550 cm^{-1} which has been assigned to the bending deformation of the protonated amine group (i.e., $-NH_3^+$ deformation).[86] Importantly, this spectrum is consistent with a well-ordered monolayer terminated in $–NH_2$ and $–NH_3^+$ groups.

The spectrum of the adsorbed CNC layer in Figure 2-3 exhibits most of the characteristic bands reported in IR spectra of CNC.[77,119,126–128] Three relatively well-resolved bands are observed in the O-H stretching region between 3100 and 3550 cm^{-1}. The intensity of the bands in the C-H stretching region around 2900 cm^{-1} increases relative to the AUT substrate. The contribution of C-H stretching absorbance from both the substrate and CNC complicate interpretation of these modes. The fingerprint region contains a variety of C-O stretching modes as well as C-H bending modes. The bands with negative absorbance in the 2200 cm^{-1} region are C-D stretches from the deuterated reference sample. The bands in the IRRAS spectrum of adsorbed CNC will be assigned and compared to those in a transmission spectrum of randomly oriented CNC particles. As a starting point, we expect the intensity of the bands in the IRRAS spectrum to be governed by the IRRAS surface selection rule. That is, modes with a dipole moment with a large component

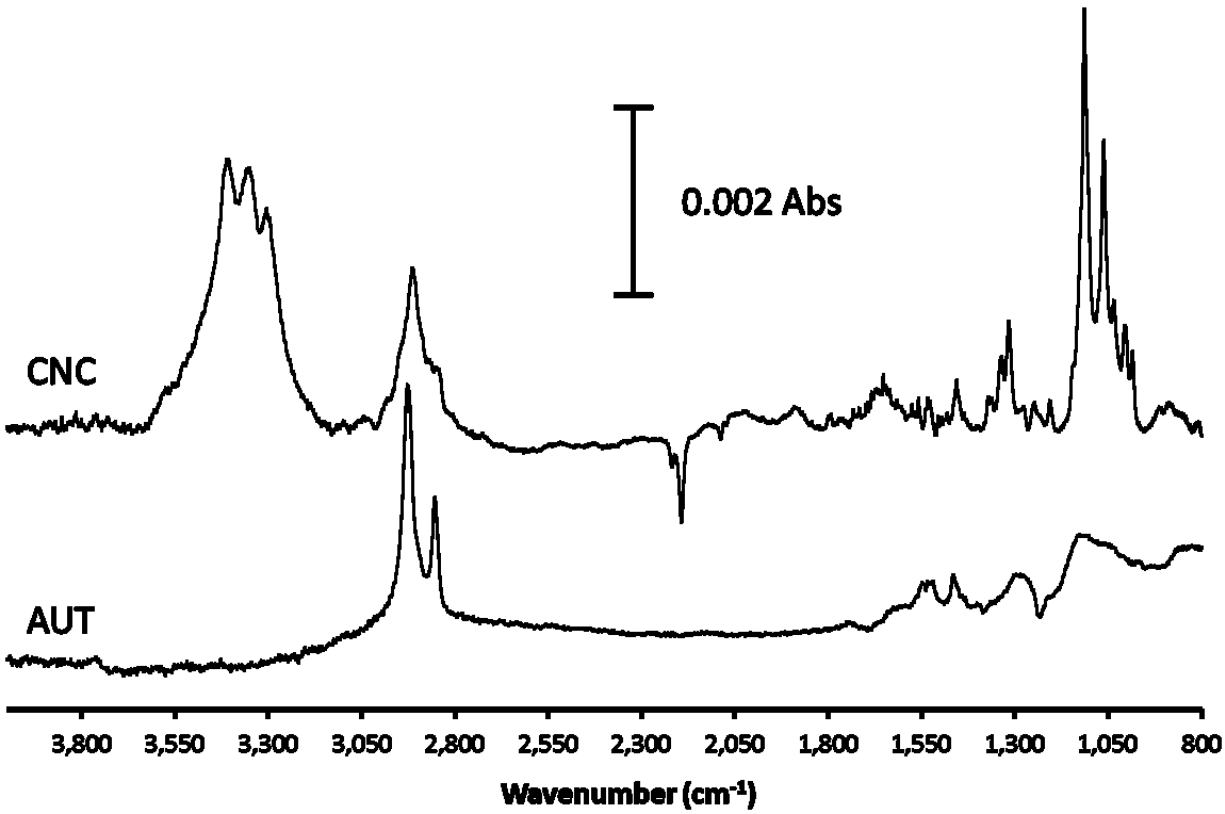

Figure 2-3. IRRAS spectra of CNC adsorbed to and AUT derived SAM and the spectra of just an AUT derived SAM. Both are baseline corrected.

perpendicular to the surface will exhibit greater absorbance relative to those with a smaller perpendicular component. The finger print region is a culmination of the apparent, strongly absorbing C-O bonds and the weaker absorbing C-C stretching, C-H bending and C-O bending. Thus, assignments based on intensities predicted by bond angles contain some uncertainties. To help guide us in understanding the various bond angles and in the spectral interpretation we consider the crystal structure of CNC reported by Nishiyama et al.[25]

The crystal structure of cellulose was interpreted and the orientation of the most common configurations of the C-O bonds in cellulose I β relative to the c-axis were calculated as described in the Experimental section. Figure 2-4 shows the structure of part of a single chain of cellulose identifying the c-axis and labeling the various carbons and oxygens. Table 2-1 contains the various C-O bonds for cellulose and their calculated angle relative to the c-axis. Also listed are the predicted IRRAS relative intensities based on the surface selection rule and suggested bands corresponding to each bond. The structure of cellulose Iβ is characterized by 2 parallel chains with slightly different conformations that organize into sheets and ultimately form a monoclinic unit cell. Accordingly, Table 2-1 contains bond angles for each chain.

Based on the AFM image in Figure 2-2, the CNC particles are arranged on the AUT substrate such that the c-axes are more-or-less parallel to the metal film. It is known that different edges of a CNC particle possess different chemistries arising from the crystal edges parallel or perpendicular to the plane separating the hydrogen bonded chains – sometimes called the dispersive plane. The AFM image does not have the

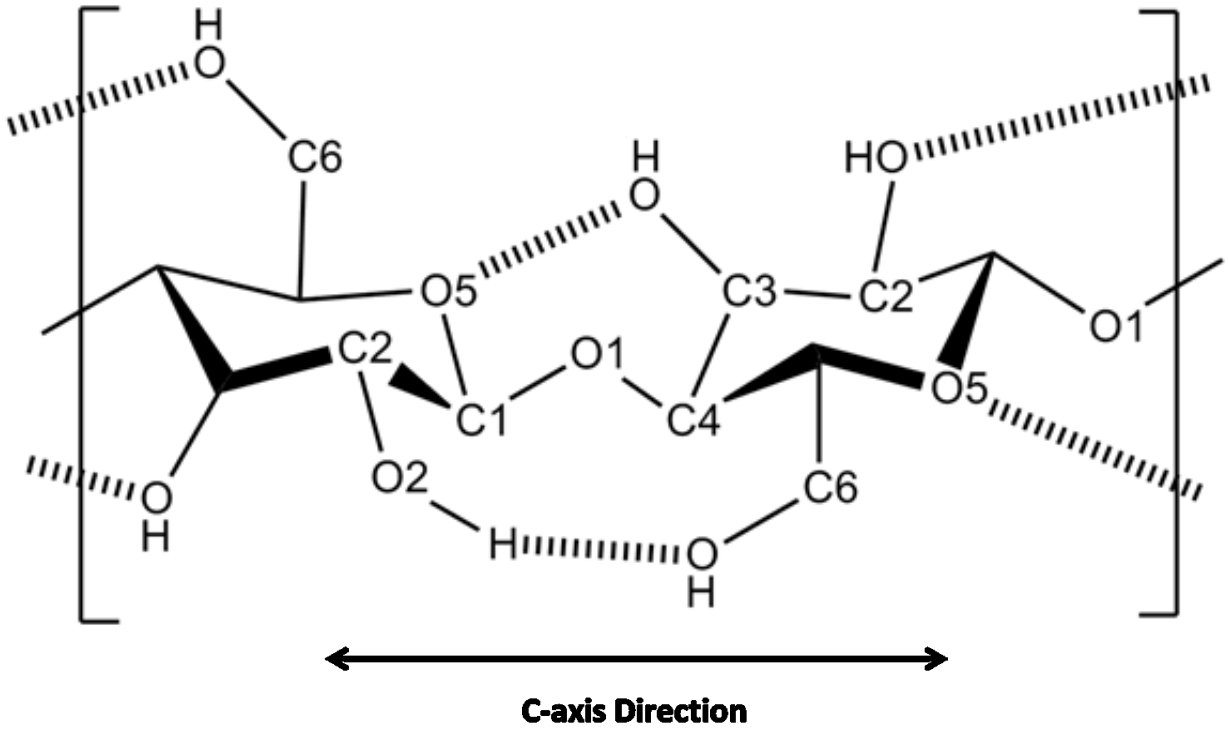

Figure 2-4. Example chain of cellulose showing the direction of the c-axis and the numbering system.

capability to determine if there is a preferential radial orientation to adsorb to the surface and we assume that the CNC particles adsorb with random radial orientation. Thus the sample is oriented relative to the electric field of the incident IR radiation. The sample for the transmission measurement was solid CNC powder sandwiched between KBr plates and is randomly oriented relative to the incident radiation. Comparing the IRRAS spectrum to the transmission spectrum provides further positive support in the identification of certain bands as we know their c-axis projection magnitudes. The IRRAS and transmission spectra of CNC samples are compared. For clarity, the plots are separated into the OH stretching region (Figure 2-5) and the CO stretching region (Figure 2-6). The transmission spectrum had to be divided by 300 to bring it to the same scale as the IRRAS.

Table 2-1. Bond angles to the c-axis calculated from crystal data collected by Nishiyama et. al.[25] of cellulose 1β using Atom Software.

Bond	Angle to c-axis		IRRAS band assignment (cm^{-1})	IRRAS intensity
	Chain 1	Chain 2		
C4-O1	32°	32°	N/A	N/A
C1-O1	33°	33°	N/A	N/A
C2-O2	68°	72°	1115	Most intense
C3-O3	49°	52°	1061	2nd most intense
C6-O6 (dominant)	42°	46°	1035	3rd most intense (adopts multiple configurations)

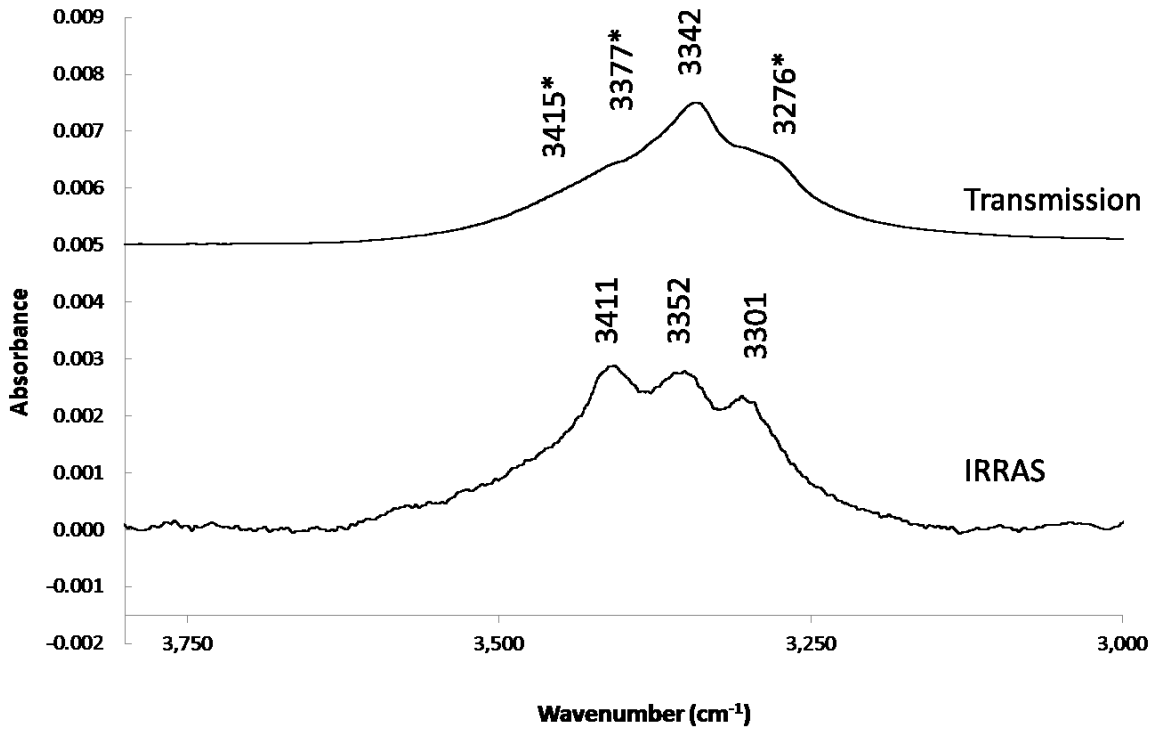

Figure 2-5. IRRAS and transmission IR of CNC in the OH region. * indicates peak positions determined by 2nd derivative analysis using Savitsky-Golay Quadratic/Cubic. The manipulation was done with Essential FTIR v3.00040 and used a software Smoothing Window value of 21. The transmission spectrum was divided by 300 and then shifted upwards 0.005, the IRRAS spectrum was unchanged on these axes.

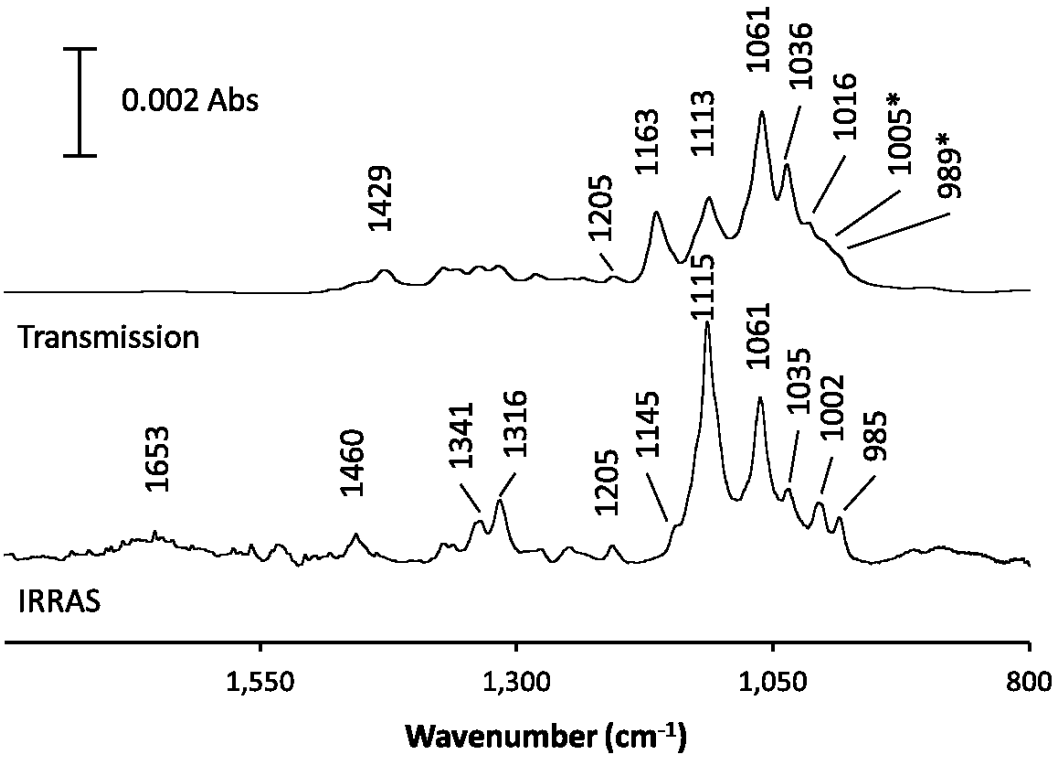

Figure 2-6. IRRAS and transmission IR of CNC in the CO region. * indicates peak positions determined by 2nd derivative analysis using Savitsky-Golay Quadratic/Cubic. The manipulation was done with Essential FTIR v3.00040 and used a software Smoothing Window value of 21. The transmission spectrum was divided by 300 and then shifted upwards 0.005, the IRRAS spectrum was unchanged on these axes.

1163 cm^{-1}

The assignment of this band is well established as the glycosidic asymmetric stretch, C1-O1-C4. [77,102,117,119,126–128] The presence of this band in the powder spectrum and its absence in the IRRAS spectrum in Figure 2-6 is the key example of the influence of the surface section rule on IRRAS intensities in this sample. This bridging ether forms a dipole that is parallel to the c-axis as the crystal structure shows the C4-O1 and C1-O1 bond angles relative to the c-axis at 32.0 and 32.1 degrees respectively. Hence, we expect only a minor component of the dipole moment of this mode to be perpendicular to the metal film resulting in low IRRAS absorbance. Here, the absence of this band in the IRRAS spectrum is a positive assignment on account of its presence in transmission IR spectrum.

1115 cm^{-1}

This band has been assigned to the C2-O2 stretch.[77] The absorbance of the C2-O2 stretch in the transmission spectrum (1113 cm^{-1}) is of medium intensity consistent with a moderate molar absorptivity relative to the other bands. However, this band exhibits the largest absorbance in the IRRAS spectrum. The C2-O2 is the most perpendicular of all the C-O's with an angle of 68^{o} relative to the c-axis as listed in Table 2-1. We would thus expect this band to exhibit the highest absorbance in the IRRAS spectrum, which agrees with the observation in Figure 2-6.

1060 cm^{-1}

This band has been assigned to the C3-O3 stretch and exhibits the highest absorbance in the transmission spectrum. Table 2-1 shows the absorbance of the C3-O3 mode is

expected to be less enhanced than the C2-O2 band in the IRRAS spectrum due to its angle of 49^{O} relative to the c-axis. This is consistent with the observation in Figure 2-6.

1035 cm^{-1} – 1005 cm^{-1} – 985 cm^{-1}

Bands in this region are generally assigned to C6-O6 stretch of the primary alcohol. Band positions of primary C-O stretches are generally of lower wavenumber than secondary. The powder spectrum contains only one discernable band in this region at 1036 cm^{-1}, while the IRRAS spectrum reveals 3 well-resolved bands. Maréchal and Chanzy preformed polarization resolved IR spectroscopy on cellulose films and have suggested that variations in hydrogen bonding at O6 results in slightly varied conformations of the cellulose Iβ crystal by a rotation about the C5-C6 bond.[77] Two of these possible conformations have the O6 inter- and intra-chain hydrogen bonded. These environments were assigned to the 1035 cm^{-1} and 1002 cm^{-1} bands. Hydrogen bonding within the same chain has been reported as the least probable configuration and the weakest H bond. Thus, the 1035 cm^{-1} band is assigned to the inter-chain conformation and the 1002 cm^{-1} band is assigned to the C6-O6 of the interchain H-bond. Certain conformations within the cellulose Iβ crystal should contain some O6 that are involved weakly or not at all in H bonding. The C-O stretch of such a weak-hydrogen bonded group would appear at a lower wavenumber relative to groups involved in stronger H-bonding. We thus tentatively assign the 985 cm^{-1} band to non/weakly-H bonded C6-O6. The transmission spectrum shows a weak band at 1016 cm^{-1}. This band is unique to the transmission spectrum and has been tentatively assigned to a minor conformation of the C6-O6.[77] The absence of this band from the IRRAS suggests this mode adopting an angle parallel to the c-axis.

1145 cm^{-1}

This band is observed as a shoulder in the IRRAS spectrum. This band has been made visible due to the absence of the overwhelming glycosidic asymmetric band centred at 1160 cm^{-1}. A band at 1145 cm^{-1} has not been reported in cellulose spectra but is present in the powder spectrum of maltose available from the NIST database.[129] The structure of maltose is characterized by a α(1→4) glycosidic bond and thus a strong 1160 cm^{-1} band is absent and bands at 1204 cm^{-1} and 1145 cm^{-1} are present. The bands at 1145 cm^{-1} and 1205 cm^{-1} in both cellulose and maltose suggests their origin of a mode that is common to both. We assign the band at 1145 cm^{-1} to a ring ether vibration.

1205 cm^{-1}

There is disagreement in the literature about assigning the 1205 cm^{-1} band to either the C-O-C glycosidic stretch or the C-O-C stretching mode of the pyranose ring. The spectrum of polymer hyaluronan makes it clear that this band is due to one of these two modes. [130] Hyaluronan is an alternating β(1→3)/β(1→4) linked polysaccharide that is similar to cellulose in that it contains a pyranose ring and glycosidic ether. The environments about these two modes are similar due to equivalent hydrogen bonding in these two polymers. From the spectrum of hyaluronan, bands at 1160 cm^{-1}, 1205 cm^{-1} and 1145 cm^{-1} are observed.[130] All other bands are different from cellulose as they arise from different C-O and carbonyl groups. The commonality of bonds and bands supports their correlation. To assign the 1205 cm^{-1} to one of these modes we will look at the spectrum of maltose from the NIST database with similar logic to that of assigning the 1145 cm^{-1}. By changing the nature of the glycosidic bond we see the

disappearance of the 1160 cm^{-1} band but the persistence of the 1205 cm^{-1} and 1145 cm^{-1} which brings us to conclude the 1205 cm^{-1} being of a pyranose ring origin. The spectrum of cellobiose from the NIST database shows bands at 1206 cm^{-1}, 1147 cm^{-1} and 1168 cm^{-1}, which are consistent with our previous band assignments.

3301 cm^{-1} – 3352 cm^{-1} – 3411 cm^{-1}

The OH stretching region of the IRRAS and transmission spectra of CNC are compared in Figure 2-5. The OH region of the spectra shows resolved bands despite the broad nature of OH infrared vibrations. Three bands are present with obvious components from other OH modes contributing to the broad background. Two bands at 3411 and 3301 cm^{--1} present in the IRRAS spectrum are identical to what is seen by Maréchal and Chanzy[77] in position but differ in relative magnitudes due to the nature of the surface selection rules in IRRAS. The third peak at 3352 cm^{-1} is unique to the IRRAS spectrum. We adopt these assignments of 3411 and 3301 cm^{-1} being of the O6H6 dominant and minor configurations respectively. Free or weakly hydrogen bonded hydroxyl groups absorb at higher wavenumbers than their hydrogen bonded counterparts and as such the weakly hydrogen bonded dominant O6H6 configuration will exhibit bands at the highest wavenumbers of all the of primary alcohol configurations. This is the dominant C6O6H6 configuration and shows an OH with weak hydrogen bonding and a stretch at 3411 cm^{-1} and a CO with strong hydrogen bonding and a stretch at 1035 cm^{-1}. The IRRAS band at 3352 cm^{-1} is close to a band presented by Marechal and Chanzy and results from the combination of multiple modes that sum to a band at 3345 cm^{-1} in transmission IR. When subject to the surface

selection rule this band shift to 3352 cm^{-1}. The largest contributing mode to this band is the C3O3 and we assign it accordingly.

Comparing CNC to MFC

The adsorption of monolayers of CNC on an AUT-derived monolayer allowed spectral interpretation of CNC with appropriate band assignments. The same method was applied to a sample of MFC prepared from softwood. The AFM image in Figure 2-7 shows the orientation of both MFC and CNC prepared for analysis with the main difference being the much longer length of MFC. The orientation of both celluloses is important for the spectral characterization of specific bonds.

Figure 2-8 and Figure 2-9 contains IRRAS spectra of CNC and MFC adsorbed from a 0.0015% solution in the OH and CO stretching regions respectively. Bands in both samples show expected similarity in band position with the largest shifts of 5 cm^{-1}. The MFC spectrum exhibits poorer resolution of bands on account of the ratio of crystalline to amorphous content.

The appearance of the glycosidic asymmetric peak at 1163 cm^{-1} in the MFC spectrum is an indicator that not all the MFC are positioned parallel to the surface. The bonds giving rise to this band are occasionally oriented more perpendicular to the surface allowing them to absorb incident radiation. Even this weak presence is enough to overshadow the small peak at 1145 cm^{-1}.

Aside from broadening, we see a change in the apparent magnitude of some peaks. This is due to variable angles between the bonds of the MFC particles and the surface that does not occur in samples of CNC. This can be attributed to amorphous content

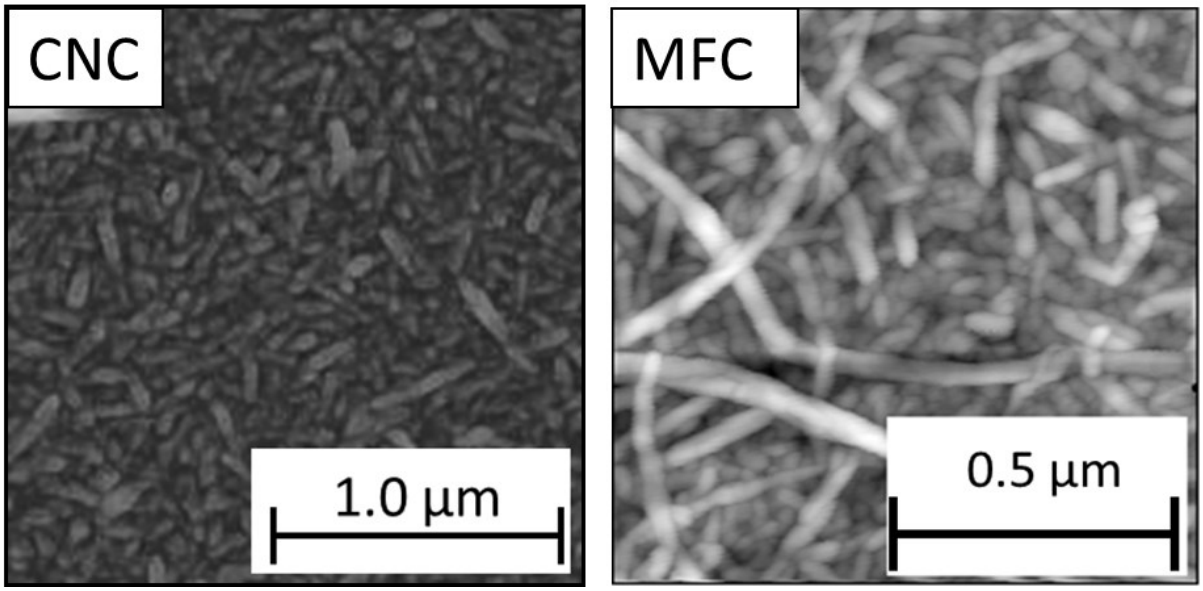

Figure 2-7. AFM height image of CNC (left) and MFC (right) on an AUT derived SAM.

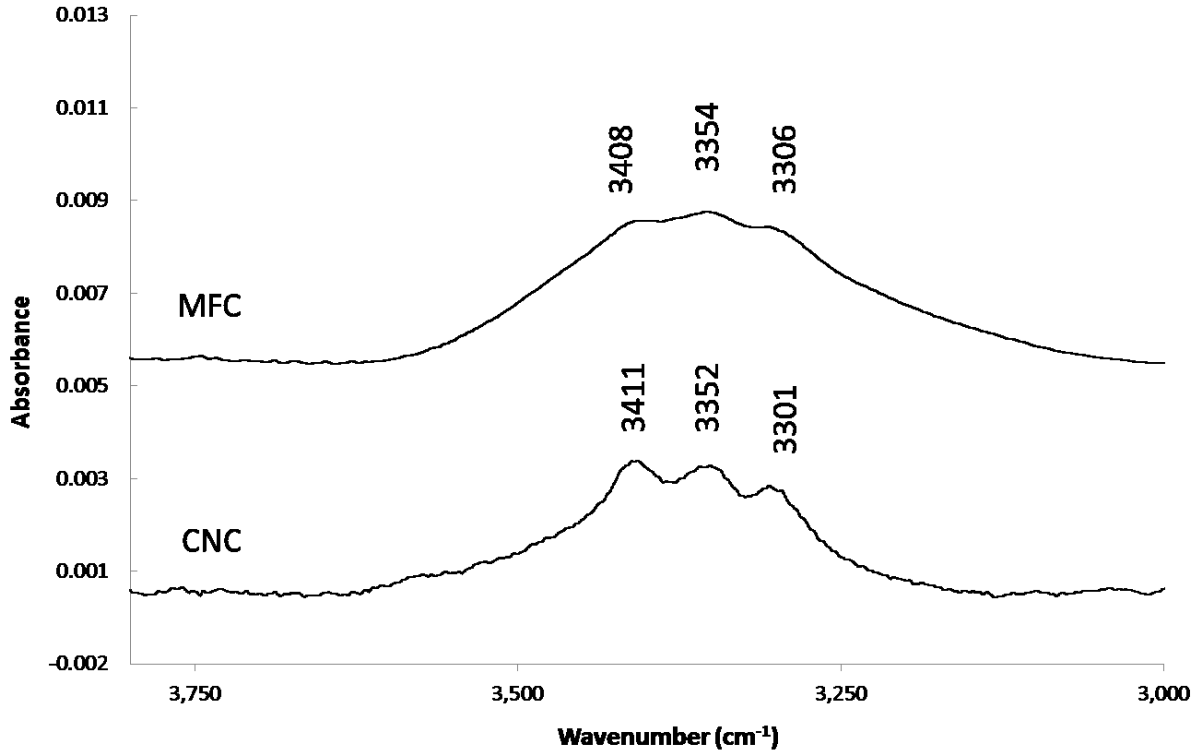

Figure 2-8. IRRAS of CNC and MFC in the OH region. The MFC spectrum was divided by 4 and then shifted upwards 0.005. The IRRAS spectrum was unchanged on these axes.

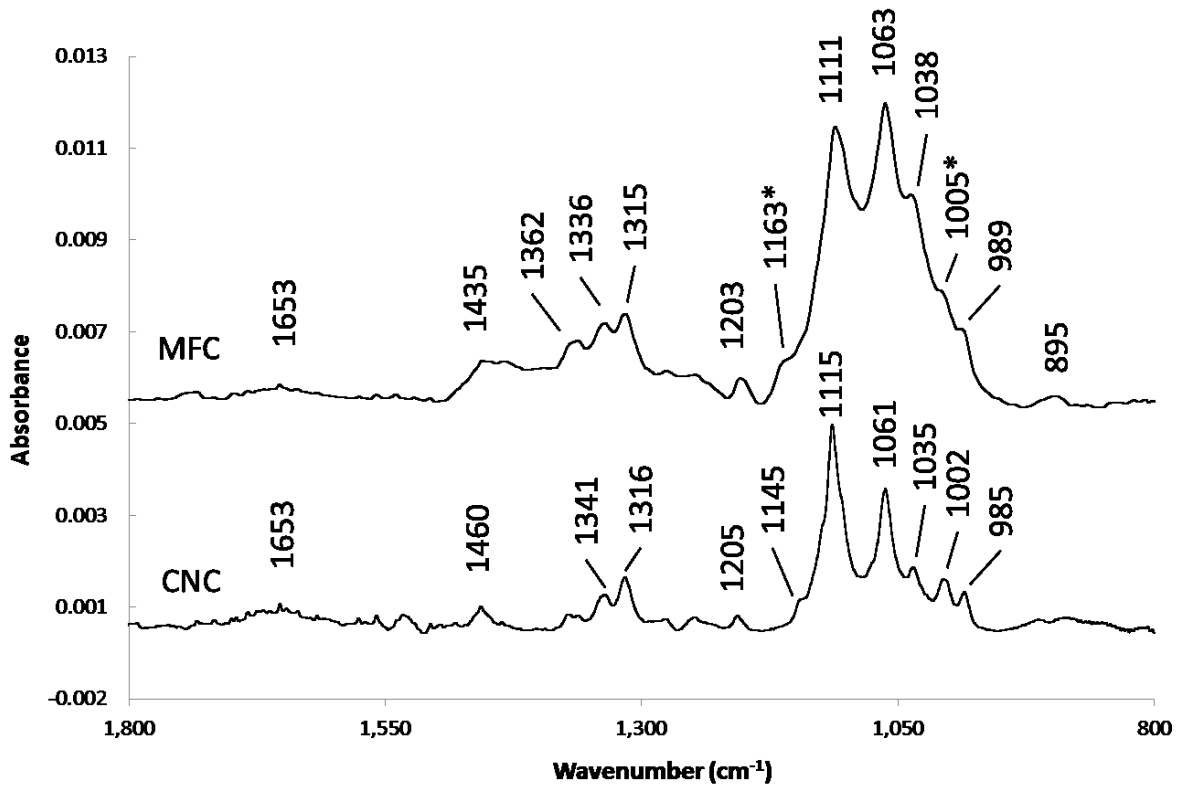

Figure 2-9. IRRAS of CNC and MFC in the CO region. * indicates peak positions determined by 2nd derivative analysis using Savitsky-Golay Quadratic/Cubic. The manipulation was done with Essential FTIR v3.00040 and used a software Smoothing Window value of 11. The transmission spectrum as divided by 4 and then shifted upwards 0.005. The IRRAS spectra was unchanged on these axes.

and particles not adsorbing parallel to the surface. This region is composed of many vibrational contributions, of which only several are assigned and magnitude differences between the two spectra could be due to a change in magnitude of any number of underlying bands.

2nd Derivative Spectrum

Second derivative data analysis has been applied to the IR spectra of cellulose[21,131,132] with the limitation arising from lack of detail in the original spectra. The detail present in the IRRAS spectrum in the CO region is better than can be obtained by transmission IR spectroscopy. Its 2nd derivative was calculated to gain the position of some bands that were not fully resolved. Small contributing bands that are overshadowed by larger ones are more likely to yield incorrect results using this data analysis.[133] The IRRAS spectrum of CNC is compared with its 2nd derivative in Figure 2-10 across the CO stretching region.

There are many possible peaks revealed that are not easily visualized when looking at the original spectrum. However, due to the sloping background in the lower wavenumbers and a parabolic background across the entire spectrum it is possible that these band positions are artifacts due to the operation. With that disclaimer, a list of possible band positions in this CO region of CNC follows with the resolved bands in the original spectrum in bold: 1456, 1436, 1317, **1207**, **1146**, 1134, 1125, **1115**, 1103, 1093, 1086, 1077, **1062**, 1045, **1035**, 1020, 1007, **1003**, **984**, 967 cm^{-1}. Although bands at some of these positions have never appeared in vibrational spectra of CNC and support their observation as an artifact of the calculation, some have been observed. For example, a Raman spectrum of the same CNC used in these experiments shows shifts

at 1127, 1098, 1077, 1064, 1045, 1038, 1000 and 964 cm^{-1} among others. Raman spectrum of tunicate show strong peaks at 1095 cm^{-1} and are assigned to the glycosidic bond.[38] Samples of CNC isolated from Whatman show strong Raman peaks at 1094 cm^{-1} and 1120 cm^{-1}.[71] An infrared band at 1075 cm^{-1} has been assigned to a ring C-O-C mode.[77]

Figure 2-8 shows the OH stretching region in the IRRAS spectrum of CNC and reveals more noise than the CO stretching region and many 2nd derivative band positions collected in the OH region are likely artifacts of the mathematical operation. When this approach was attempted on our cotton samples, which is dominantly I_β with a small amount of I_α, bands at 3270 cm^{-1} and 3242 cm^{-1} could be seen. These bands are assigned specifically to the I_β and I_α crystal phases respectively.[18,21,117] However, to manipulate the software's "smoothing window" figure to obtain these designations, a large number of other bands appeared that could not be interpreted. For this reason it is currently not suitable to assign bands in the OH stretching region of an IRRAS spectrum of CNC based on 2nd derivative analysis.

If bond to band specificity were fully assigned for CNC then simple deconvolution calculations could follow specific bonds through processes such as crystal phase changes or chemical reactions. However, it is unlikely that complete band assignments will be comprehensive in this complex fingerprint region. With the work that has been done here, we offer new insight into the structure of CNC and offer a method to observe cellulose materials.

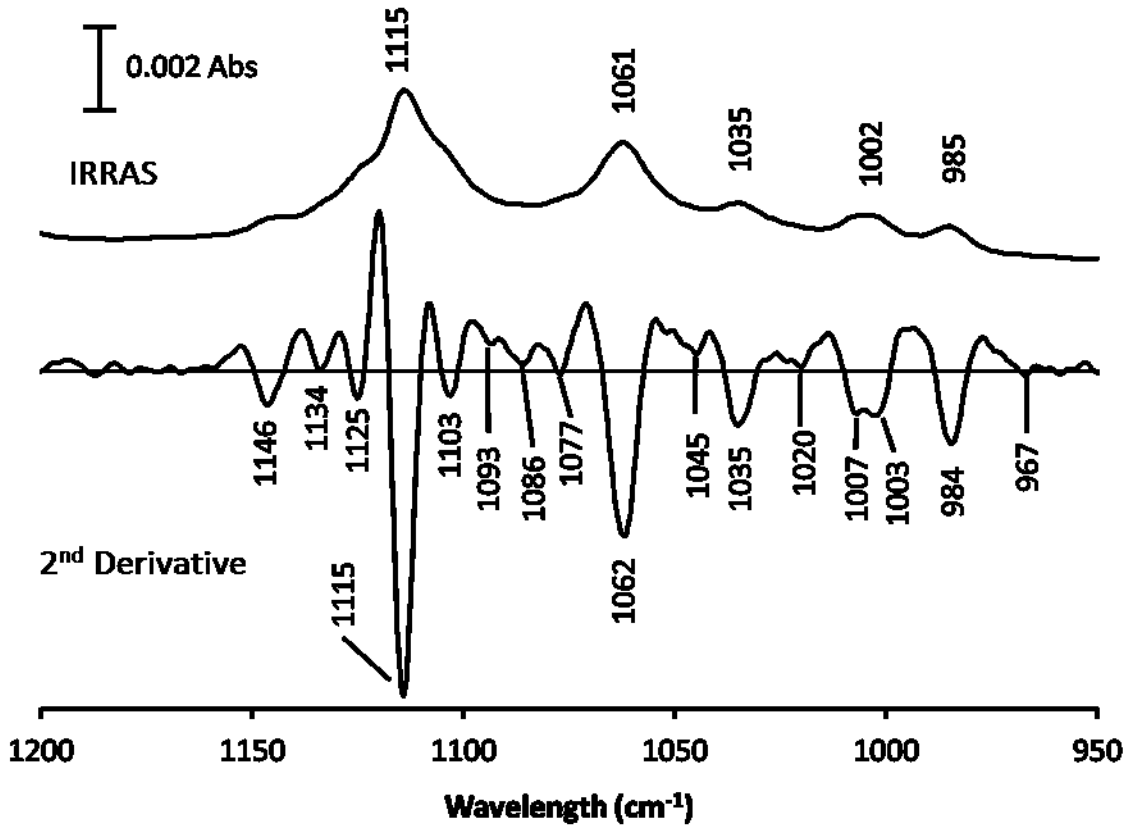

Figure 2-10. 2nd derivative of IRRAS CNC on the bottom with the original CNC above for comparison within the CO region. The operation was done with the Savitsky-Golay Quadratic/Cubic in Essential FTIR v3.00040 and used a software Smoothing Window value of 11.

Table 2-2. Wavenumber assignments for peaks observed in IRRAS of cotton CNC.

Wavenumber (cm^{-1})	Assignment	Type	References
3411	O6-H6	Stretch	77,117,128
3352	O3-H3	Stretch	77,117,128,134
3301	O6-H6	Stretch	77,117,128,134,135
2922	CH_2 Asymmetric C_{11} AUT	Stretch	27
2854	CH_2 Symmetric C_{11} AUT	Stretch	27
~1650	Broad Absorbed Water	Bending	127
1460	CH_2 of Cellulose and AUT	Bending scissor	27,119
1366	(minor peak) CH or OH	Bending	122
1336	OH	In plane bending	77,127
1315	OH	In plane bending	77,127
1205	C1-O5-C5	Pyranose Ring mode	77
1145	C1-O5-C5	Pyranose Ring mode	
1115	C2-O2	Stretch	77
1161 (not present)	C1-O1-C4	Glycosidic Asymmetric Stretch	77,119,127,135
1090-1095 (Raman)	C1-O1-C4	Stretch	39,136
1056	C3-O3	Stretch	77,119,127
1034	O6-C6	Stretch – Dominant conformation	77,119,127,132
1016 (not present)	C6-O6 Minor conformation?	Stretch – minor conformation	77,127
1005	O6-C6 Minor conformation	Stretch - Secondary conformation	127
985	O6-C6 Minor conformation/ CH_2?	Stretch/bend	127

Conclusion

The detailed IRRAS spectrum of CNC has been recorded and analyzed and a list of band assignments are presented in Table 2-2. IRRAS offers unique insight into the structure of this abundant polymer with many band assignments agreeing with literature. It does open some room for disagreeing with pervious assignments due to the complexity of bonding modes absorbing in the fingerprint region. We have confirmed assignments in the CO stretching region by relating band magnitudes with their known angles to the c-axis based on the selection rules inherent in IRRAS. We have assigned the bands at 1205 cm^{-1} to a ring mode and observed for the first time a band at 1145 cm^{-1} in the IR spectrum of CNC. We assign this to a ring mode. Some assignments have been left with a "?" indicating that this work offers no elucidation into the bands origin. In these experiments, a gold surface with an amine/ammonium terminated alkanethiol derived SAM was used to adsorb CNC to collect an IRRAS spectrum. This situation offers the possibility for a myriad of unique surface environments that interact with CNC. The nature of CNC to adsorb to different surfaces functionalities is of value and will be the topic of Chapter 3.

Chapter 3
Adsorption of CNC to Organically Tailored SAMs

Introduction

In Chapter 2 the acquisition and interpretation of IRRAS spectra of CNC was described. In this chapter, IRRAS will be used to explore the nature of CNC to adsorb on functionally controlled surfaces.

Cellulose nanocrystals (CNC) are a promising nano material with potential applications across many fields. Their strategic implementation with other materials has been used to influence properties such as rheology, mechanical strength, and optics.[7,50,95,96,105,137–144] This is accomplished by incorporating CNC in some form into a host material. One challenge faced when CNC is mixed with materials such as polymers is the hydrophilicity of the CNC surface. This ultimately governs the interfacial interactions of the material.

The interactions between CNC and various functional groups are of great interest in employing CNC as an additive to any chemical system. CNCs can be modified to meet certain compatibility criteria. Sulphuric acid isolated CNCs have negative surface sulphate groups which permit stable aqueous suspensions on account of electrostatic effects. This is useful for suspension in polar solvents and permits mixing with polar polymers but these CNC are not well suspended in non-polar solvents. If this is desired a surface modification is performed. IRRAS can offer a method to monitor the attraction

between CNC and a surface tailored with a functional group to model the expected interactions that would be present in a composite system.

Chemical force microscopy has previously been used to directly monitor the attractive forces between functional groups and cellulose materials.[145] In this work, gold AFM tips were modified with functionalized alkane thiols, much like in the procedure outlined in this chapter. The pull-off-force or adhesion force required to remove the tip after contact with a cellulose film was monitored with several functional groups over several pH's.

Tunable cellulose surfaces have been prepared via layer by layer (LbL) assembly.[146–148] The LbL technique involves alternating immersion between a CNC solution and another solution or repeated application of a CNC solution via spin coating. The difference between these methods to grow CNC layers and the current research is that in the former, polyelectrolyte multilayers were formed with CNC and poly(allylamine hydrochloride) or poly(di allylamine hydrochloride) with the intent of increasing the mechanical strength of the layers. This layering of alternating anionic and cationic species allows continual film growth up to 500 nm. The experiments presented here are not focused on mechanical strength or increasing layer thickness but rather the natural tendency for CNC to adsorb from aqueous solution to surfaces.

When forming a film at an air/liquid interface, the solvent will evaporate and the CNC concentration will increase. Past some critical value, a liquid nematic phase will form.[149] Varying the ionic strength of the aqueous CNC suspension will alter the pitch of the cholesteric planes resulting in some control over the colour of iridescence.[49,150] A

decrease in double layer thickness increases the chiral interactions between the crystallites resulting in a blue shift in iridescence. As well, CNC surface chemistry alters the gelling nature of concentrated CNC suspensions.[151]

In Chapter 2, an NH_2/NH_3^+ terminated alkane thiol was used to create a spontaneously adsorbed monolayer (SAM) on a gold slide for the purpose of collecting IRRAS spectra of CNC. This satisfied the IRRAS requirement of a reflective smooth surface as well as offers the means to control the terminal group of the SAM. The SAM allows an electrostatic means for the negatively surface charged CNC to spontaneously adsorb to the positive amine/ammonium. Thiols with a variety of terminal functional groups can also be utilized to monitor the adsorption to these surfaces from solutions of various compositions. Two parameters, the surface and the solution, were controlled and the resulting adsorbed CNC films were characterized.

Experimental

Reagents and Materials

CNC were obtained from Alberta Innovates Technology Futures (AITF) as dried powder samples from cotton and softwood sources. In both cases, the CNC was isolated using sulfuric acid hydrolysis.

Deuterated octadecanethiol [$HS(CD_2)_{17}CD_3$] (DODT) 98% was purchased from Aldrich (Milwaukee, WI). 11-amino-1-undecanethiol [$HS(CH_2)_{11}NH_2$] HCl (AUT), 11-hydroxyl-1-undecanethiol (HUT), 11-carboxyl-1-undecanethiol (CUT) and dodecanethiol (DDT) were purchased from ProChimea (Sopot, Poland). All thiols were used as received.

Millimolar thiol solutions were prepared in anhydrous ethanol (Commercial Alcohols, Brampton Ontario).

Substrate Preparation

The glass substrates were pre-cleaned in piranha solution (1:3 H_2O_2:H_2SO_4) at 90ºC for 15 minutes, rinsed thoroughly with deionized water and dried under Argon. Glass slides were immediately introduced into the vacuum chamber of a thermal evaporation system (Torr International Inc.). A 10 nm adhesive under-layer of chromium was evaporated followed by 300 nm of gold (4n purity).

Monolayer Formation

Self-assembled monolayers (SAMs) of DODT and C_{11} thiols were prepared on gold substrates. One mM ethanolic solutions of each thiol were prepared and the gold substrate was immersed for 48 hours to ensure stable SAM formation. Slides were then removed and rinsed thoroughly with ethanol to remove unbound thiols. Thiol-derived monolayers were immediately used for experiments to avoid contamination. DODT were stored in a nitrogen purged environment and cleaned with ethanol before each use as a background signal.

Infrared Spectra Measurements

IRRAS spectra were collected with both a Mattson Infinity FT-IR spectrometer (Madison, WI) and a Bruker Vertex 70 FT-IR spectrometer equipped with low-noise mercury-cadmium-tellurium (MCT) detectors cooled with liquid nitrogen. In both instruments, the incident radiation was reflected from the sample at 80º. One thousand scans were collected with a wavenumber resolution of 2cm^{-1}. The sample chamber was

purged with nitrogen for 8 minutes prior to each measurement to limit atmosphere signals. A spectrum of the atmosphere of the purged chamber was subtracted from all spectra to reduce remaining unwanted signal. A background signal was collected using the DODT substrate. OPUS v. 5.5, Winfirst and Essential FTIR v. 3.00.040 software was used to collect and handle the data. All spectra were manually baselined at like wavenumbers: 4000, 3633, 3134, 3013, 2779, 1818, 1406, 1178, 949 and 821 cm^{-1}. A consequence of this background method are the apparent troughs and peaks that are a result of the signal dropping due to detector insensitivity towards $800cm^{-1}$ that can be observed in a single beam background spectrum. All samples were subject to mild mechanical stirring via a magnetic Teflon stir bar at minimal RPM to promote consistent liquid-substrate interactions.

Zeta Potential and Dynamic Light Scattering

A Zetasizer Nano-ZS of the nanoseries from Malvern (United Kingdoms) was used to collect zeta potential and dynamic light scattering measurements. All data presented on the sizes of CNC in solutions and the zeta potential was within the measurable ranges of the instrument specifications. The 1.0 M NaCl solution was not able to yield a zeta potential result due to the high ionic strength, this was expected.[152]

Procedure

A method was developed to observe IRRAS spectra of CNC and is depicted in Figure 3-1. As a metal surface was required to employ IRRAS, gold was chosen as it offered the freedom to create any functional group as terminal ends of an alkane chain that would be desired within the scope of this project. On the left side of Figure 3-1 this surface

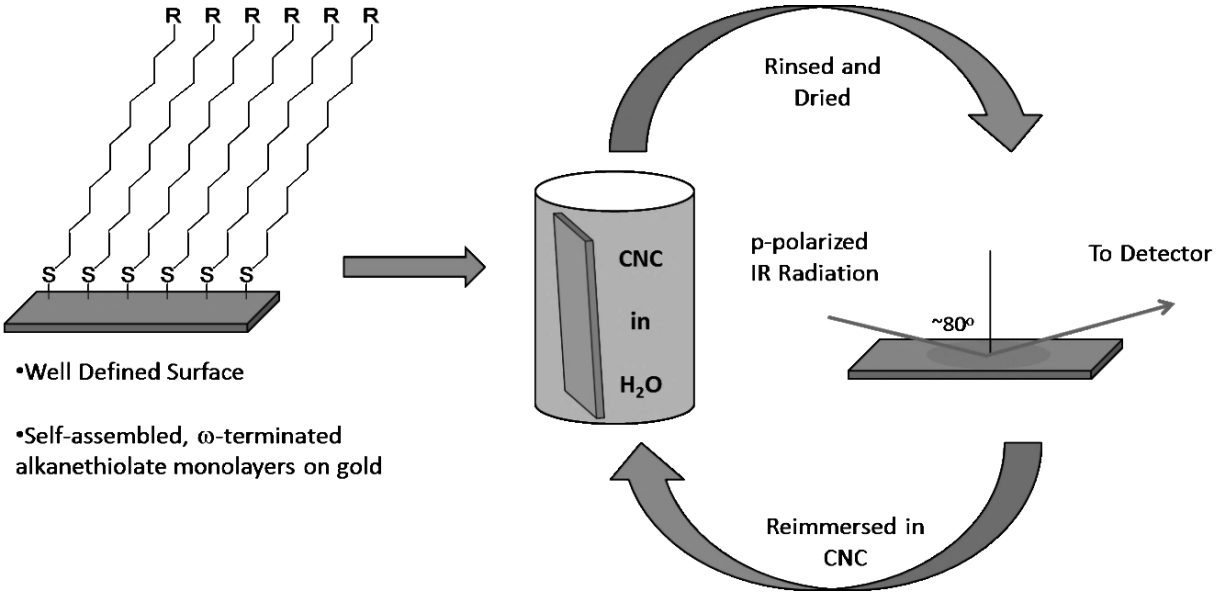

Figure 3-1. Diagram of method to obtain IRRAS of CNC over time by re-immersing slides.

modification is represented with a terminal group R. At time intervals the slide was removed, rinsed in 18 MΩ water, dried with argon and an IRRAS spectrum was collected. The sample was then re-immersed in the aqueous CNC solution until another sampling cycle was desired.

Mechanical stirring of the solution

Variable mass transport of CNC to the surface was thought to result in differences in signals for identical runs. A magnetic stir bar was added to the solutions to investigate this occurrence. Upon the addition of a stirrer, signals had lower standard deviation. All reported spectra and peak heights were obtained from a CNC solution with a stirrer present.

Peak height measurements and CNC surface coverage

Collected IRRAS spectra show a variety of bands in the IR region. To estimate a surface coverage from this data requires some assumptions. It is assumed that surface coverage is uniform across the slide area from which the incident beam reflects. This seems reasonable because the slides appear to be smooth to visible light and would be reflected even more regularly by longer wavelength IR radiation. It is assumed that surface coverage will scale linearly with signal. As a measure of surface coverage the absorbance of the most prominent band, which was the band at 1115 cm^{-1} was chosen. A baseline was made between nearby troughs at 1297 and 1015 cm^{-1}. The left point of the peak's baseline was close to zero absorbance. The right point was not near the baseline. Towards the lower wavenumbers the detector response starts to diminish and there is no response below 800 cm^{-1}. In different runs there are significant differences in the rate of signal drop off making the region below 950 cm^{-1} irreproducible and thus a poor choice for a baseline point when accurate band height is important to the method. For this reason, a trough between the two peaks at 1035 and 1001 cm^{-1} were chosen to mark the right boundary of the 1115 cm^{-1} band's baseline. As peaks become larger this trough will occur at a higher absorbance value and the surface coverage will be underestimated. This effect will not change the peak height significantly beyond what is required for this study. All surface coverage estimations were done using this metric.

Hornification

An unintended consequence of the cycling method is that the surface is continuously being dried and wetted. This has an effect on CNC as drying CNC will alter its properties. The term hornification is given to this phenomenon of the change in

properties of cellulose upon drying.[153] Hornification is described as the formation of irreversible or partially reversible hydrogen bonding in wood pulp upon drying. It is ascribed to the physically proximity between cellulose fibrils that is permitted when sufficient amounts of water are removed. Its importance in this project is that samples are continuously cycled through the CNC suspension and the instrument wherein each cycle involves drying and wetting. Changing the CNC-CNC interactions will invariable change the nature of CNC to adsorb from solution. Figure 3-2 illustrates this effect. Three identical samples with an AUT SAM were immersed at the same time (time zero) into an aqueous CNC solution and measured at various times.

Figure 3-2 shows the absorption at 1115 cm^{-1} vs. time for three samples that differ only in the measuring intervals. All were all immersed in identical CNC suspensions at time zero. All samples showed an increasing in surface coverage over time, which is expected with the initial assumption that more time would allow more CNC to adsorb. This plot indicates that a cycle of drying and wetting accelerates subsequent adsorption, presumably due to the surface adsorbed CNC stacking/settling upon drying that allow subsequent CNCs to adsorb. For this reason it is critically important to measure each sample identically if they are to be compared to one another.

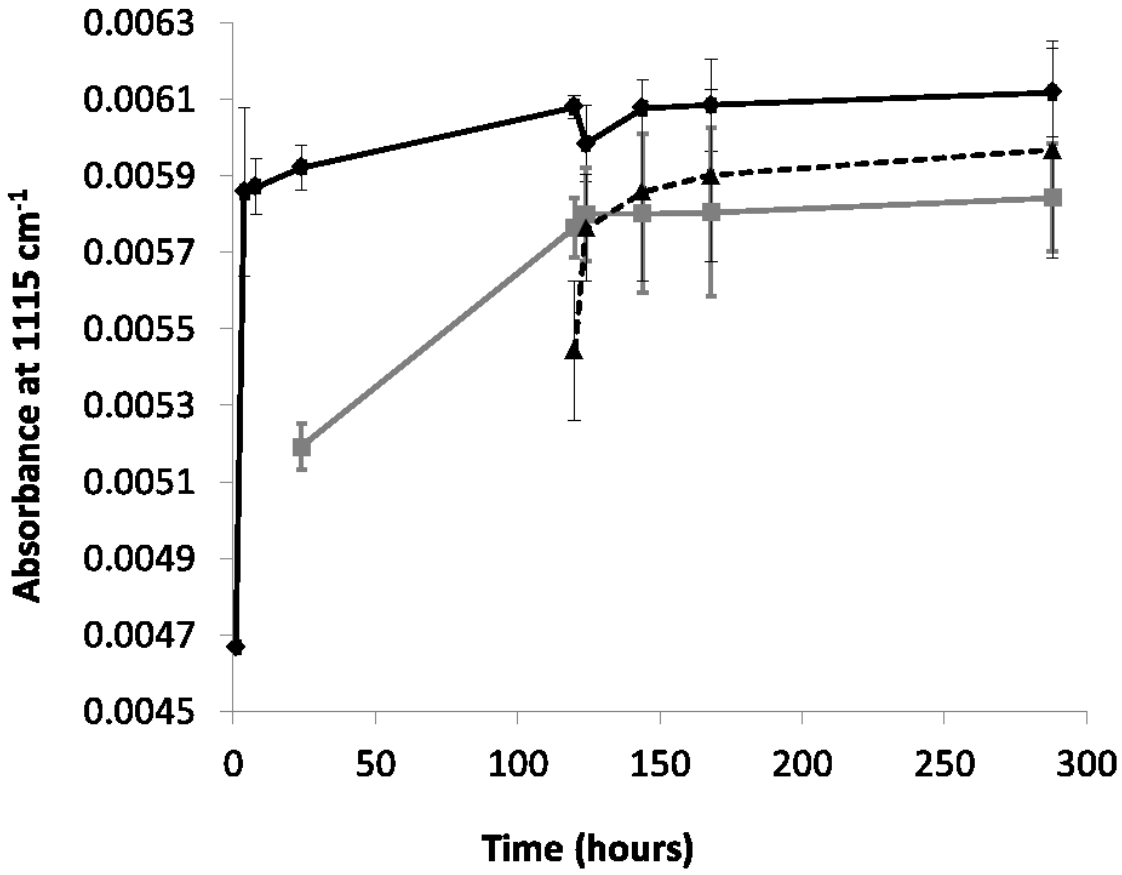

Figure 3-2. The effect of hornification. All samples were immersed at time zero and sampled at times shown. The diamond series was sampled at time intervals of 1, 4, 8, 24, 120, 124, 144, 168 and 288 hours. The square series was sampled at time intervals of 24, 120, 124, 144, 168 and 288 hours. The triangle series was sampled at 120, 124, 144, 168 and 288 hours.

Results and Discussion

This chapter explores the effect of surface chemistry on the adsorption of CNC from aqueous suspensions. The effects that CNC concentration has on films adsorbed to an 11-amino-1-undecanethiol [$HS(CH_2)_{11}NH_2$] HCl (AUT) SAM were investigated. The effect that the surface chemistry has on a 0.0015% (w/w) CNC suspension was also investigated. This was done by monitoring CNC films that adsorbed to four different functionally terminated SAMS. These four SAMS were prepared from four different thiols: AUT, 11-hydroxy-1-undecanethiol (HUT), 11-carboxy-1-undecanethiol (CUT), and DDT yielding surface functional groups of amine/ammonium, alcohol, carboxylic acid/carboxylate, and methyl, respectively. The effect that the ionic strength has on adsorbed CNC films was investigated by using a 0.0010% (w/w) CNC suspension and an AUT SAM while varying the ionic strength with NaCl.

Alkane thiols form SAMs on certain substrates.[80,81,83–85,88,89,92,93,154–156] This chemistry has been thoroughly researched and is well understood making it a powerful candidate for applications related to the work presented here. Early work includes the observation of layer formation of disulphides on gold by Allara and Nuzzo.[90] Several groups saw this stable surface as a candidate for uses such as protein adsorption and detection.[84,85,87–89,91–94] The combination of a controllable, organically terminated monolayer and a reflective metal surface lends itself directly to applications of IRRAS. It satisfies the mandatory condition of a reflective metal surface and allows flexibility of surface functionality. SAMs that form from sufficiently long alkane chains are stabilized via dispersive attractions as the chains stack adjacently. The quality of these layers can be estimated by the position of CH bands as observed in IRRAS. All the SAMs used in

this experiment were of thiols with eleven carbon alkane chains and remained as a stable monolayer through the experiments.

Effect of CNC Concentration

The range of CNC concentrations in water chosen were 1.5% (w/w) to 0.00015% (w/w) and at every order of magnitude in between. Vials of these 5 concentrations are shown in Figure 3-3. The concentration of 1.5% (w/w) was gel-like, as is known to occur in aqueous suspensions at high concentrations. For this reason, this sample was not used for experiments.

Adsorption of the 0.15 – 0.00015 % to an NH_2/NH_3^+ terminated SAM was monitored and the magnitude of the band at 1115 cm^{-1} is plotted in Figure 3-5. This surface was expected to have the strongest adsorption of all four functional groups that will be tested (NH_2/NH_3^+, OH, CH_3, $COOH/COO^-$) and will presumably give the greatest detail of any changes that occur. IRRAS spectra of these concentrations after one hour of immersion are shown in Figure 3-4. O-H stretching absorbs from 3200 to 3600 cm^-, C-H stretching absorbs around 2900 cm^{-1}, and the region from 1000 to 1200 cm^{-1} is predominantly C-O stretching with contributions from C-H bending occurring at around 1300 cm^{-1}. The negative bands around 2200 cm^{-1} are due to the reference (deuterated C_{18} SAM on a gold slide). The bands in the C-H region are due to the NH_2/NH_3^+ SAM that was used to adsorb and immobilize the CNC. The signal intensity of the C-H stretches increases with increasing concentrations of CNC. The band at 1115 cm^{-1} is clearl even at one hour of immersion in 0.00015% (w/w) CNC,

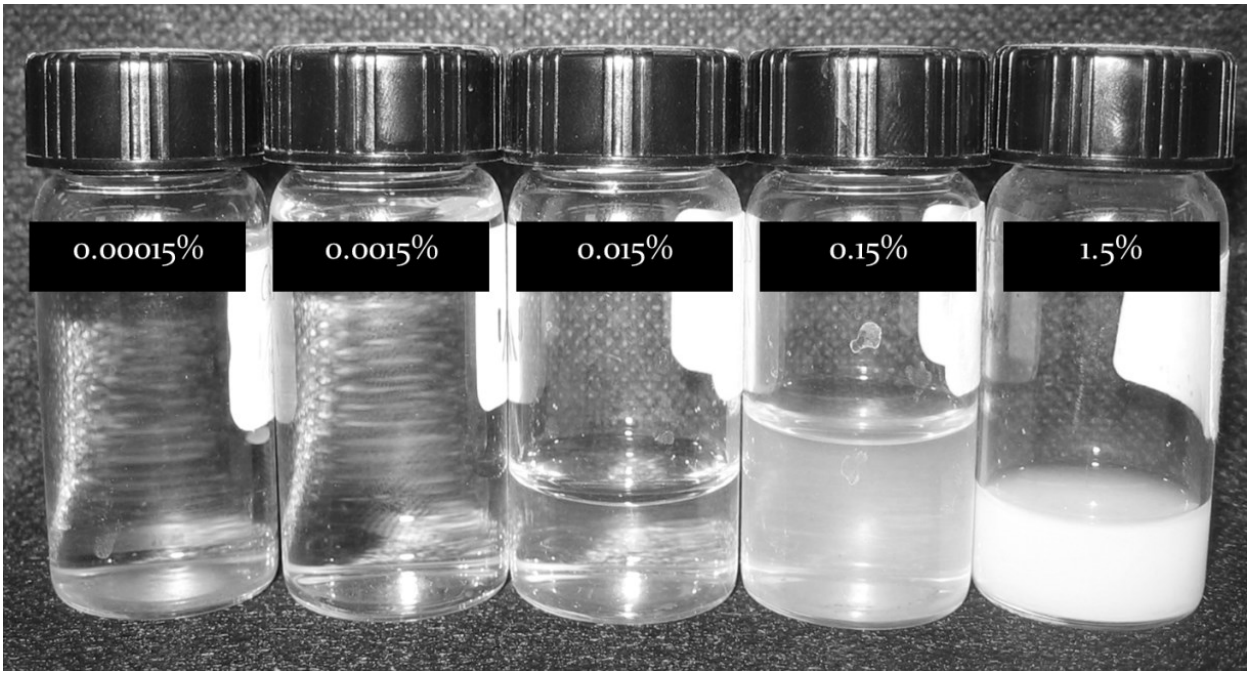

Figure 3-3. Photograph of different CNC concentrations (weight %) is water. The concentrations decrease from right to left. The concentrations in weight % are 1.5, 0.15, 0.015, 0.0015 and 0.00015.

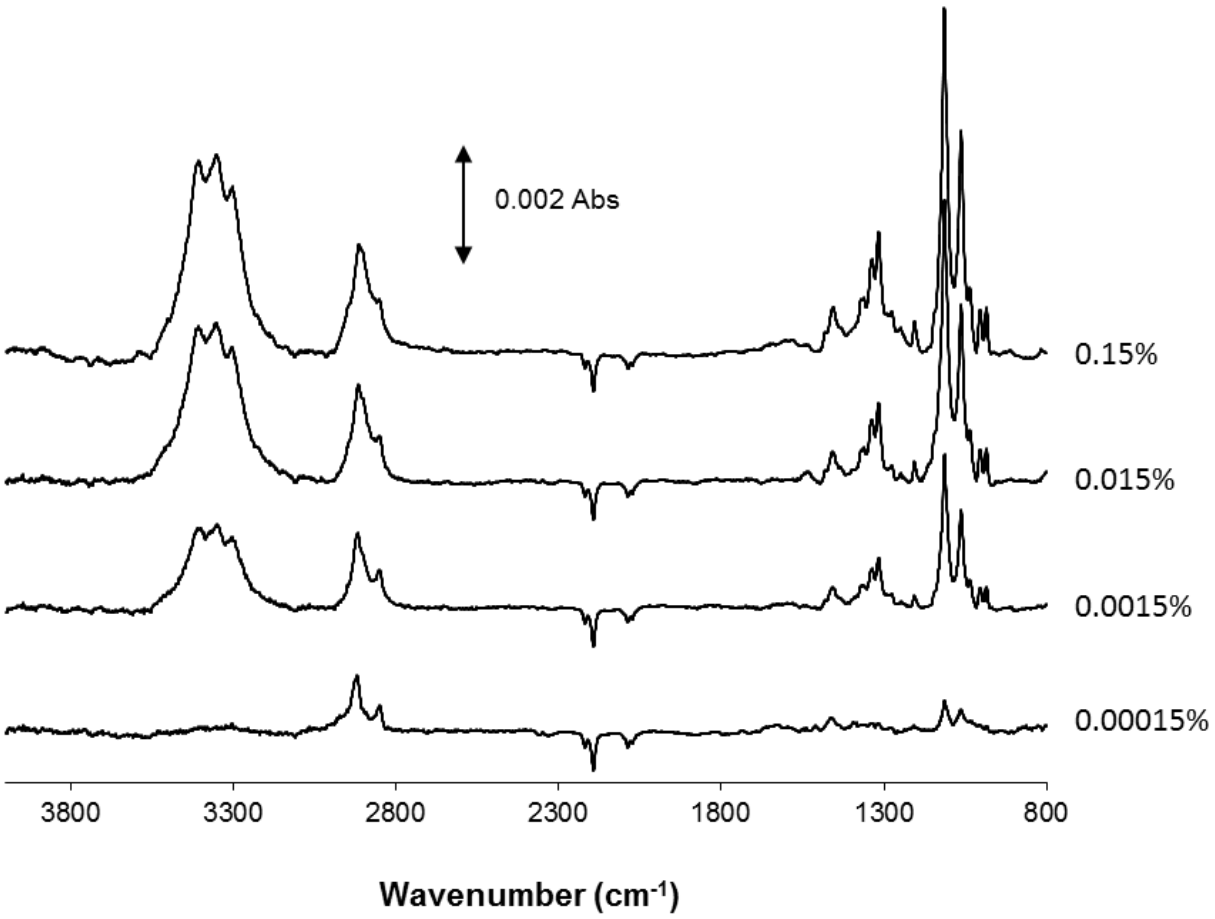

Figure 3-4. IRRAS spectra of CNC adsorbed to AUT on gold after one hour immersion.

providing an example of the surface sensitivity of the IRRAS technique to CNC adsorption. After this first IRRAS measurement at one hour, the slides were re-immersed in their respective CNC solution and further measurements were taken at later times. The absorbance of the 1115 cm^{-1} band is plotted vs time in Figure 3-5.

All concentrations plotted show a maximum surface coverage achieved after 24 hours of immersion. The three highest CNC concentrations (0.15%, 0.015% and 0.0015%) exhibit a somewhat regular increase in surface coverage maximums. Interestingly, after 24 hours the lowest concentration reached the same surface coverage as the concentration that is 10 times higher (second lowest overall). This local adsorption signal is reached, but more slowly. This signal is estimated to be that of the surface coverage that allows sufficient interactions between the CNC and the SAM, any further adsorption would be stifled by the repulsive interactions involving two CNC rods. This is a surface coverage barrier that can be overcome by increasing the CNC concentration. AFM images of slides in Figure 3-5 were collected to gain insight into the nature of the adsorbed layers and are shown in Figure 3-6.

In Figure 3-6 the image of CNC adsorbed from high concentration (B) shows a “mat” of CNC with greater than monolayer coverage with CNC occasionally resting on top one another. This agrees with the higher IRRAS signal of the highest CNC concentration after 1 hour of immersion. The lowest concentration (A) at an immersion time of one hour shows sub-monolayer CNC surface coverage. Even at this low surface coverage an IRRAS signal is still observable at 1115 cm^{-1}. The background topology in Figure 3-6 is characteristic of the gold film substrate used here.

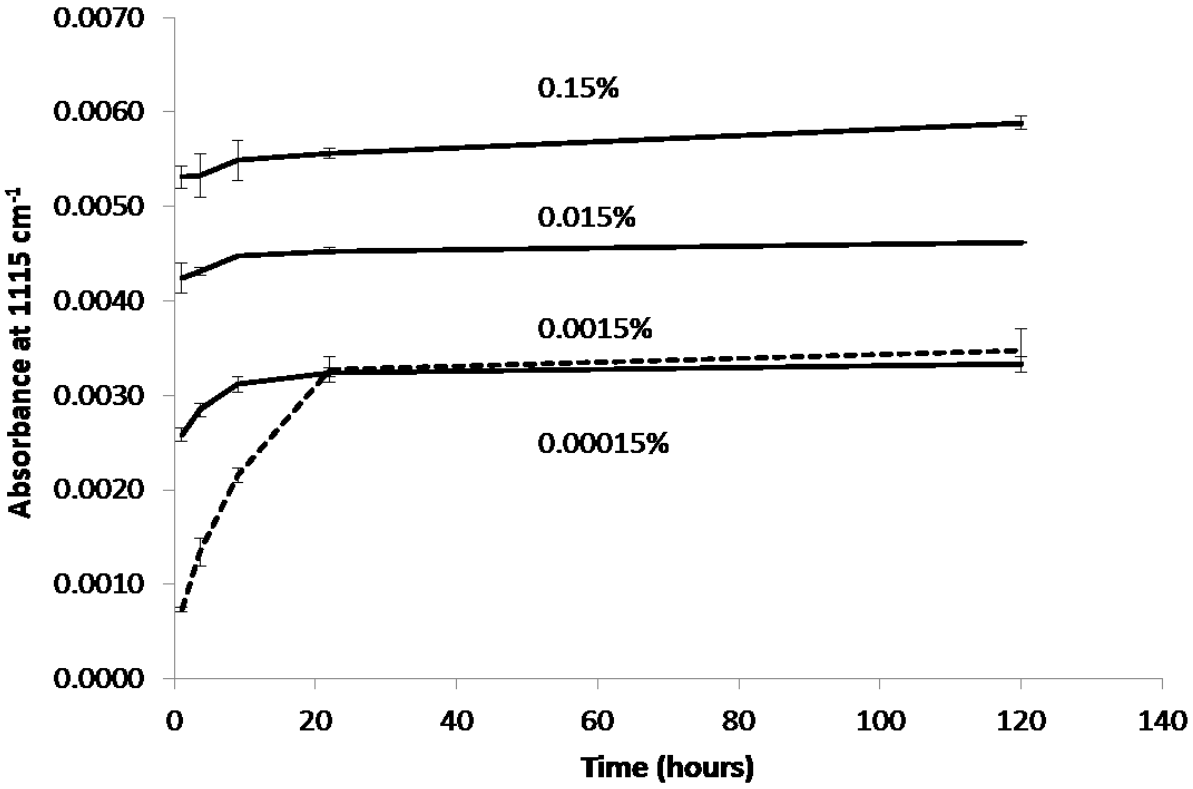

Figure 3-5. IRRAS adsorption of C-O stretch at 1115 cm^{-1} of 0.15%, 0.015%, 0.0015% and 0.00015% (w/w) [CNC] on a NH_2/NH_3^+ terminated C_{11} thiol SAM on gold. A spectrum of each concentration at 1 hour is plotted in Figure 3-4. Error bars represent one standard deviation.

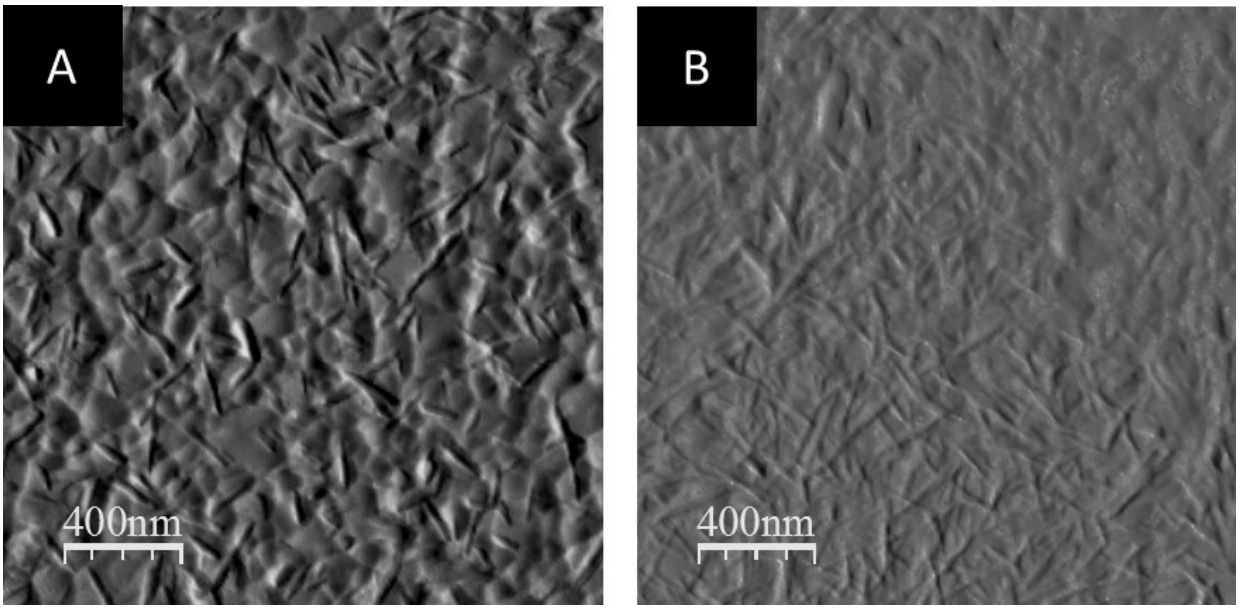

Figure 3-6. AFM of A) 0.00015%(w/w) CNC and B) 0.15%(w/w) CNC on the right adsorbed to an AUT SAM after one hour of immersion.

The surface thicknesses of the CNC films were measured using an AFM scratch test. This test involves using an AFM in contact mode over an area of 1 μm^2 multiple times to "scratch/plow" the surface adsorbed CNC to the edges of the imaging area. A voltage set point was chosen such that it did not scratch the gold substrate. This was confirmed during the scratch by observing the same surface features after sequential scratches. Next, the field of view was zoomed out to an area of 5 μm^2 centered about the scratched area and tapping mode was used to collect height images. A height profile is averaged across the scratched area and the height difference was calculated. An example of this procedure is shown in Figure 3-7.

This scratch test reveals that the thickness of films derived from the two lowest CNC concentrations (0.00015 and 0.0015 %) is 7 ± 1 nm. The thickness of individual CNCs from cotton sources is around 5-7 nm.[27,41,157] This implies that CNCs adsorb from aqueous solutions to an NH_2/NH_3^+ surface to form a monolayer regardless of the solution concentration. Once this monolayer of CNC has formed, further adsorption will have to endure less favorable CNC-CNC interaction rather than the attractive CNC-amine/ammonium interaction. Similar effects govern the thicknesses of individual layers in layer-by-layer films where each subsequent layer will adsorb to available surface areas until the surface is saturated.[147]

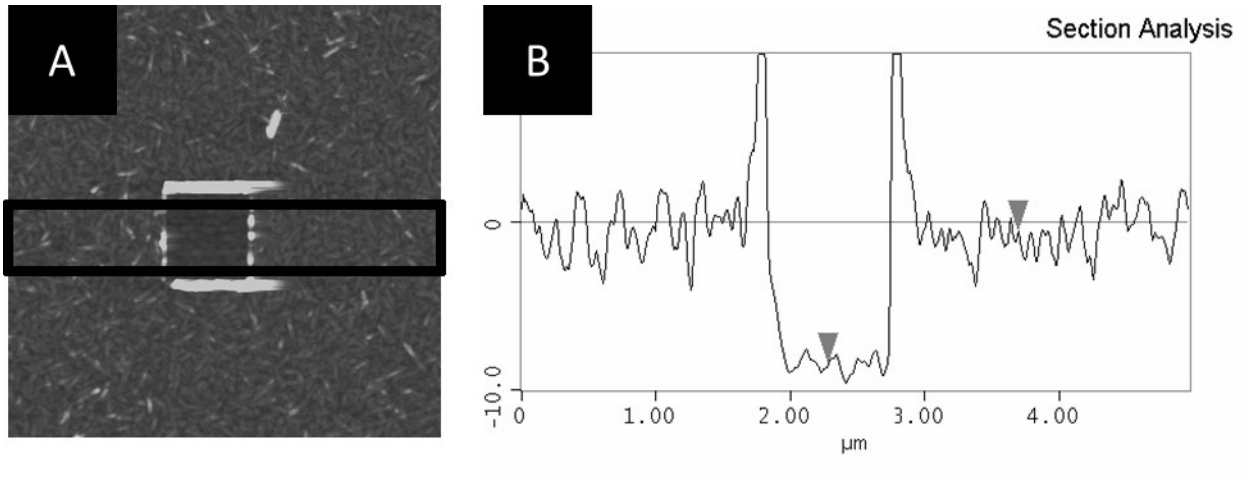

Figure 3-7. Example of scratch test. A: AFM image of the scratched region. The entire image is 5 x 5 µm and the scratched region in the center is 1 x 1 µm. B: Cross-section profile shows the average height of the black rectangle shown in A. The scratched CNC can be seen piled on the upper and lower regions of the scratched area in A. This example was performed on a NH_2/NH_3^+ SAM with CNC adsorbed from a 0.0015% w/w) aqueous suspension after 120 hours immersion and yields a CNC film height of 7 ± 1 nm. The SAM was incidentally removed in this process and has an independently measured thickness of 1.2 ± 0.9 nm which was subtracted from the total scratch height of 8.2 ± 0.6 nm.

Effect of Surface Functionality

The effect that the surface chemistry has on CNC adsorbed films was tested by using a 0.0015% (w/w) CNC suspension and varying the functionality of the SAM. This was done by creating SAMs with 4 different thiols; 11-amino-1-undecanethiol [$HS(CH_2)_{11}NH_2$] HCl (AUT), 11-hydroxyl-1-undecanethiol (HUT), 11-carboxyl-1-undecanethiol (CUT) and dodecanethiol (DDT). The results of the adsorption as a function of time are plotted in Figure 3-8.

The first measurements were performed 15 hours after immersion in the aqueous CNC suspension and each successive measurement showed higher surface coverages within error until the signal leveled off indicating a maximum coverage was reached. 15 hours was chosen rather than the time intervals present in Figure 3-5 because the relative trends were of interest more so than comparing the two data sets. In the experimental section, the effects of sampling have previously been shown to affect the amount of CNC that will adsorb. For this reason comparing the two data sets is not recommended although the signals in each (0.0015% CNC on an NH_2/NH_3^+ surface) do reach a similar maximum value.

We see a hierarchy of surface adsorption maxima. The SAM terminated with an amine/ammonium functional group adsorbed the greatest amount of CNC, followed by alcohol, methyl and finally carboxylic acid. The attraction between the CNC and amine/ammonium is likely electrostatic in nature, as there is a negative CNC surface charge due to the surface sulphate groups and a positive amine/ammonium surface at these pH's. The pKa of a NH_2/NH_3^+ SAM of this type is reported to be 7.4[158] which is above the pH values of these experiments. The attraction between CNC and alcohol

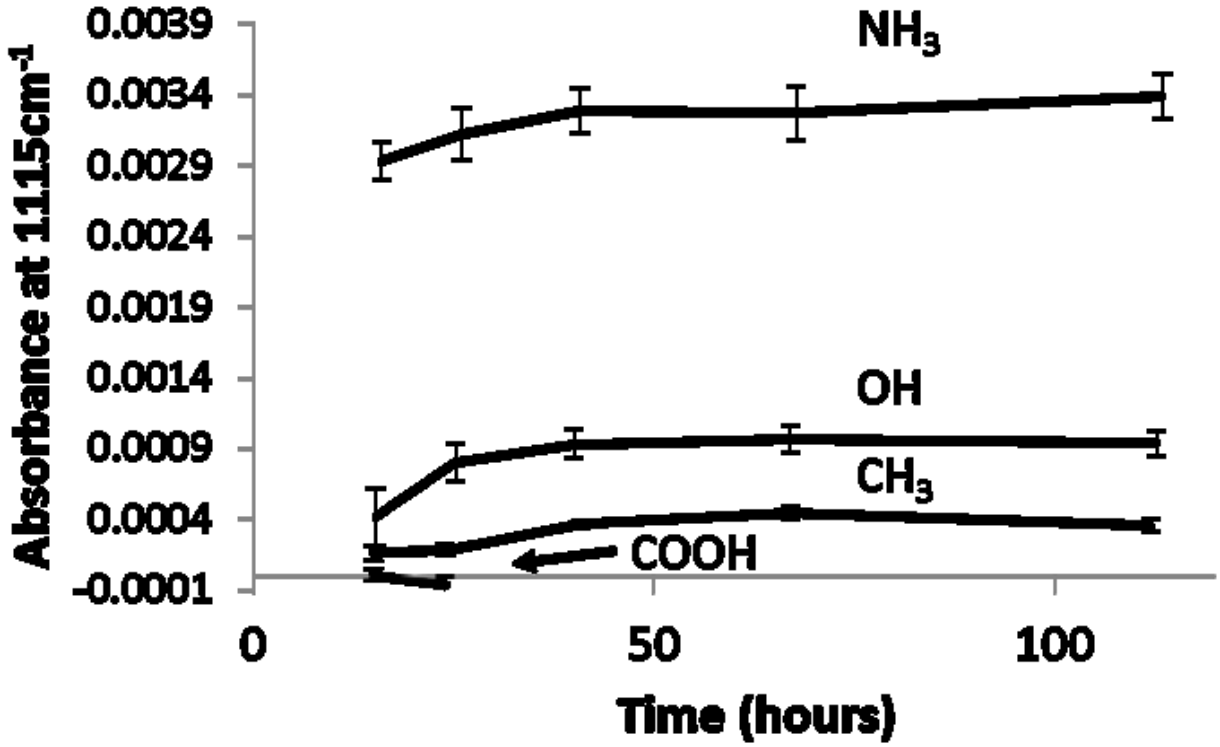

Figure 3-8. Effect of different surface functional groups on CNC adsorption. IRRAS adsorption of COC stretch at 1115 cm-1 of 0.0015 %(w/w) [CNC] on amine/ammonium, alcohol, carboxylic acid and methyl terminated C11 thiols on gold. The carboxylic acid showed no adsorption at any times and was not plotted after 24 hours. Each sample was run in triplicate and all three data points are plotted. Error bars represent one standard deviation.

would be of a hydrogen bonding nature as there is no charge on an alcohol group at these pH's. The attraction between the CNC and the methyl would be of a dispersive nature as the methyl group has neither charge nor a dipole. The repulsion between the CNC and the $COOH/COO^-$ would be of an electrostatic nature. The pKa of carboxylic acid terminated thiol derived SAMs is 5.5[159] and would be in its negative ionic form and would repel the negative surface charge of the CNC. IRRAS was not able to detect any adsorption of CNC to the $COOH/COO^-$ surface and is not plotted in Figure 3-8 for times greater than 24 hours. In Figure 3-4 IRRAS shows the sensitivity to yield a signal for sub-monolayer CNC coverage, which supports minimal adsorption to a carboxylic acid terminated SAM.

The results above agree with a related study on cellulose films.[145] In this study chemical force microscopy was performed with cellulose substrates and functionalized AFM tips. Briefly, a gold AFM tip was modified with a SAM formed from alcohol, methyl and carboxylic acid terminated thiols. The pull off force between the modified tip and a cellulose surface was monitored over a pH range. Below pH 4 the $COOH/COO^-$ functionalized tip showed a strong pull off force, which weakened as pH was increased above 4. The pKa of this SAM was between 4 and 6 which agree with previous work which estimates the pKa to be 5.5.[159] In the work presented here, the pH was monitored to be between 7.0 and 7.3, which is above the pKa of a SAM formed of $COOH/COO^-$ functionalized thiols, and the carboxylic acids are expected to be in its ionic form and repel suspended CNC. A hierarchy of intermolecular attractions between CNC and these four functional groups would be electrostatic > hydrogen bonding > dispersive. Of interest is the small amount of adsorption to the CH_3 terminated SAM.

This is empirical evidence of an attractive interaction between CNC and a non-polar non-charged surface. Figure 3-8 is evidence of the strength of different intermolecular interactions between CNC and these functional groups.

Effect of Ionic Strength

It is clear from the above that electrostatic interactions greatly influence the adsorption of CNC to modified surfaces. This is probed further by exploring the effect of ionic strength. Again, an amine/ammonium terminated SAM was used and the CNC concentration was constant at 0.0010%(w/w). NaCl was used to control the ionic strength in the range from 1.000 M to 0.001 M. The results are plotted in Figure 3-9.

Similar to controlling the CNC concentration, there is a difference in maximum surface coverage that depends on the ionic strength. The maximum surface coverage, as estimated by the absorbance at 1115 cm^{-1}, increases as ionic strength is increased from 0.000 M to 0.001 M to 0.010 M. As the salt concentration is increased further to 0.100 M and 1.000 M the maximum surface coverage decreases, with the 1.000 M having a lower coverage than the 0.000 M.

Increasing the ionic strength of nanoparticle suspensions is known to cause aggregation. To investigate the solutions and the films separately, a combination of AFM, DLS, and zeta potential were employed. The film thickness of the maximum surface coverage was obtained from AFM scratch tests as explained previously in this section. These results were compared to the IRRAS adsorption. The results are plotted in Figure 3-10 and are tabulated in Table 3-1.

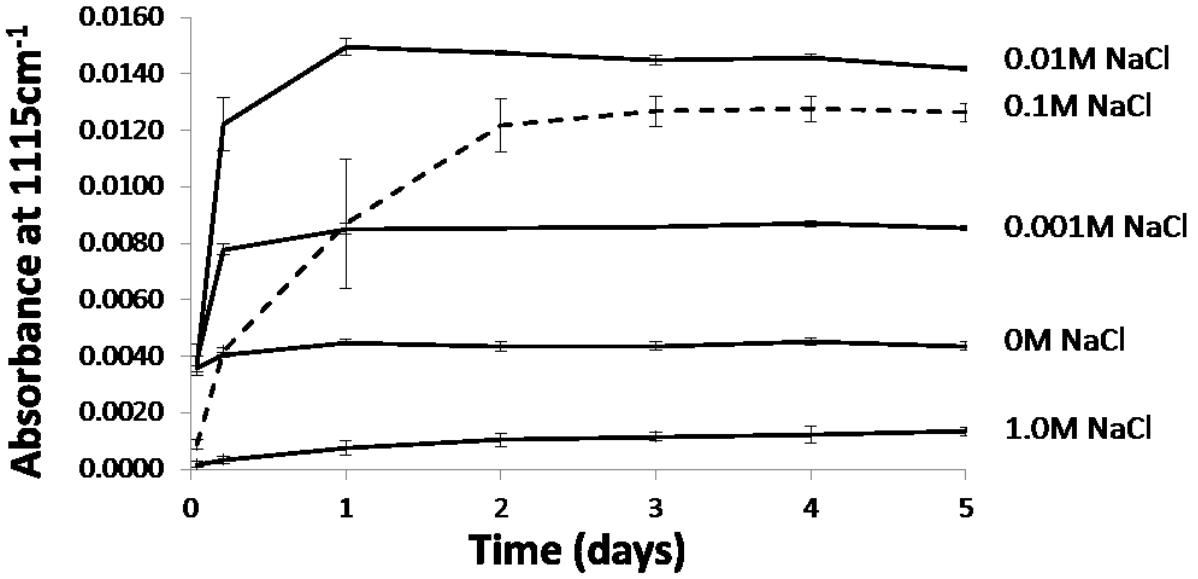

Figure 3-9. IRRAS of 0.001% (w/w) CNC suspension adsorbed to NH_2/NH_3^+ monolayers as ionic strength is varied. Error bars are standard deviations of three measurements.

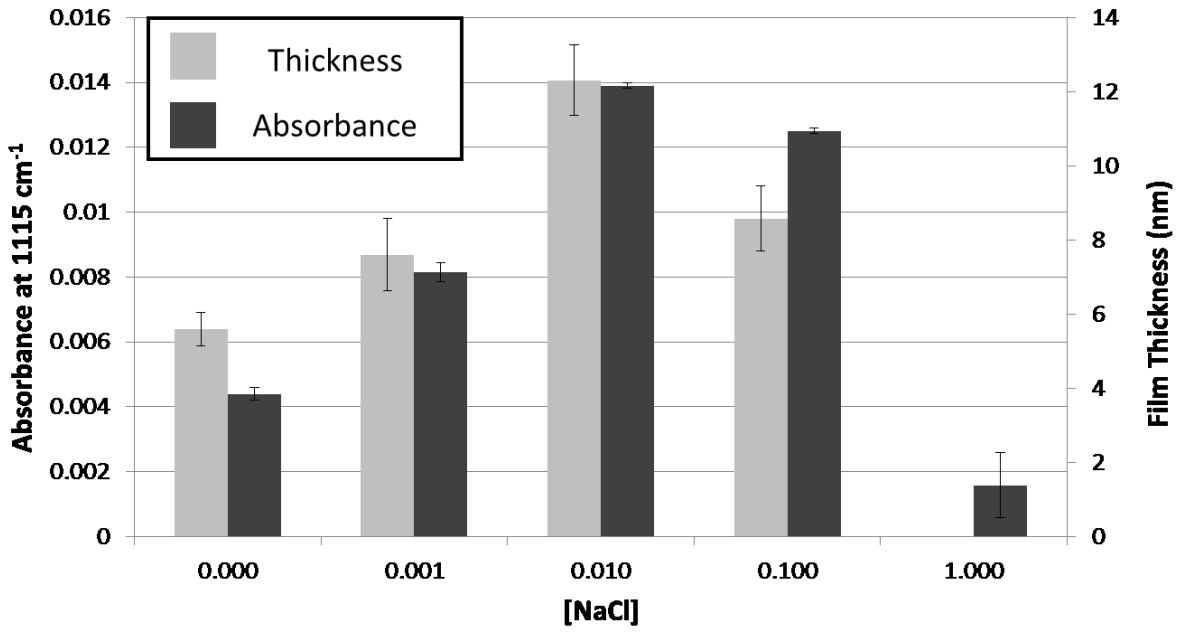

Figure 3-10. Comparison of CNC film thickness to IRRAS signal after 5 days of immersion. The CNC concentration was 0.0010% (w/w) and the SAM was NH_2/NH_3^+ terminated. Thicknesses could not be determined for 1.000 M solutions due to CNC aggregation; these aggregates would adsorb to the surface and yield an IRRAS signal. Error bars represent standard deviations of triplicate runs. Error bars are standard deviations of three measurements.

Table 3-1. Plotted values in Figure 3-10. Standard deviations of triplicates are shown.

[NaCl] (M)	0.000	0.001	0.010	0.100	1.000
Absorbance at 1115 cm^{-1}	0.0044 ± 0.0001	0.00815 ± 0.00008	0.01389 ± 0.00009	0.0125 ± 0.0003	0.0016 ± 0.0002
Thickness (nm)	5.6 ± 0.7	7.6 ± 0.9	12 ± 1	9 ± 1	N/A

From Figure 3-10 the trends in adsorption can be observed. Both the thickness and the IRRAS signal increase from zero to 0.010 M NaCl. After this point they decrease. The thickness at 1.000 M NaCl could not be determined as the surface was decorated with CNC aggregates. Aggregation is expected at these high salt concentrations. When a suspension that is stabilized by electrostatic repulsion experiences an increase in ionic strength, the electric double layer thickness will decrease and permit dispersive attractions to cause aggregation. Figure 3-11 shows AFM images of all five salt concentrations at their maximum surface coverages (immersion for 5 days).

All salt concentrations except the 1.000 M reveal a relatively homogeneous CNC film adsorbed to the SAM. Multiple scratch tests on different areas of individual slides show reproducible film heights, as expressed by standard deviations in Table 3-1. This adsorption trend is explainable considering CNC suspensions that are electrostatically stabilized. As salt concentration increases the electric double layers about suspended CNCs will decrease (their charges will be screened) but not so much as to permit aggregation (at least not at these three salt concentrations). This will result in a smaller

CNC-CNC distance of surface adsorbed CNCs and permit a more densely packed layer which not only has more CNC per area (higher IRRAS absorption) but also has thicker films (AFM scratch tests). Despite a homogeneous film, the 0.100M NaCl solution showed a decrease in surface coverage compared to the 0.010 M NaCl solution which is not in keeping with the explained trend of the three lowest salt concentrations. The 1.000 M NaCl sample revealed surface adsorbed aggregates of CNC which were not observable in the solution to the naked eye. Zeta potential and dynamic light scattering (DLS) were performed. The results are from the same solutions that gave rise to the AFM images in Figure 3-11. Zeta potential values are reported in Figure 3-12 and DLS of the two highest salt concentrations are shown in Figure 3-13.

Zeta potential is a calculation of the surface charge of a suspended colloid with the solvent's composition taken into account. As a generalization, suspensions become unstable and will aggregate/coagulate/flocculate when the absolute value of the zeta potential is below 25-30 mV.[152,160–162] The 0.000 M, 0.001 M, and 0.010 M NaCl solutions are outside of this range and no aggregation is observed either visibly in solution or on the SAM that is immersed in solution. The 0.100 M NaCl solution has a zeta potential of just under -25 mV which would raise suspicions about aggregates. However, the suspension still remains stable in solution and permits CNC layers to adsorb to the amine/ammonium slide. The decrease in surface coverage of the 0.100 M NaCl solution compared to the 0.010 M NaCl solution can be explained by the DLS data. The zeta potential of the 1.000 M solution could not be measured on account of the high degree of aggregation which is observed in the AFM of the adsorbed CNC.

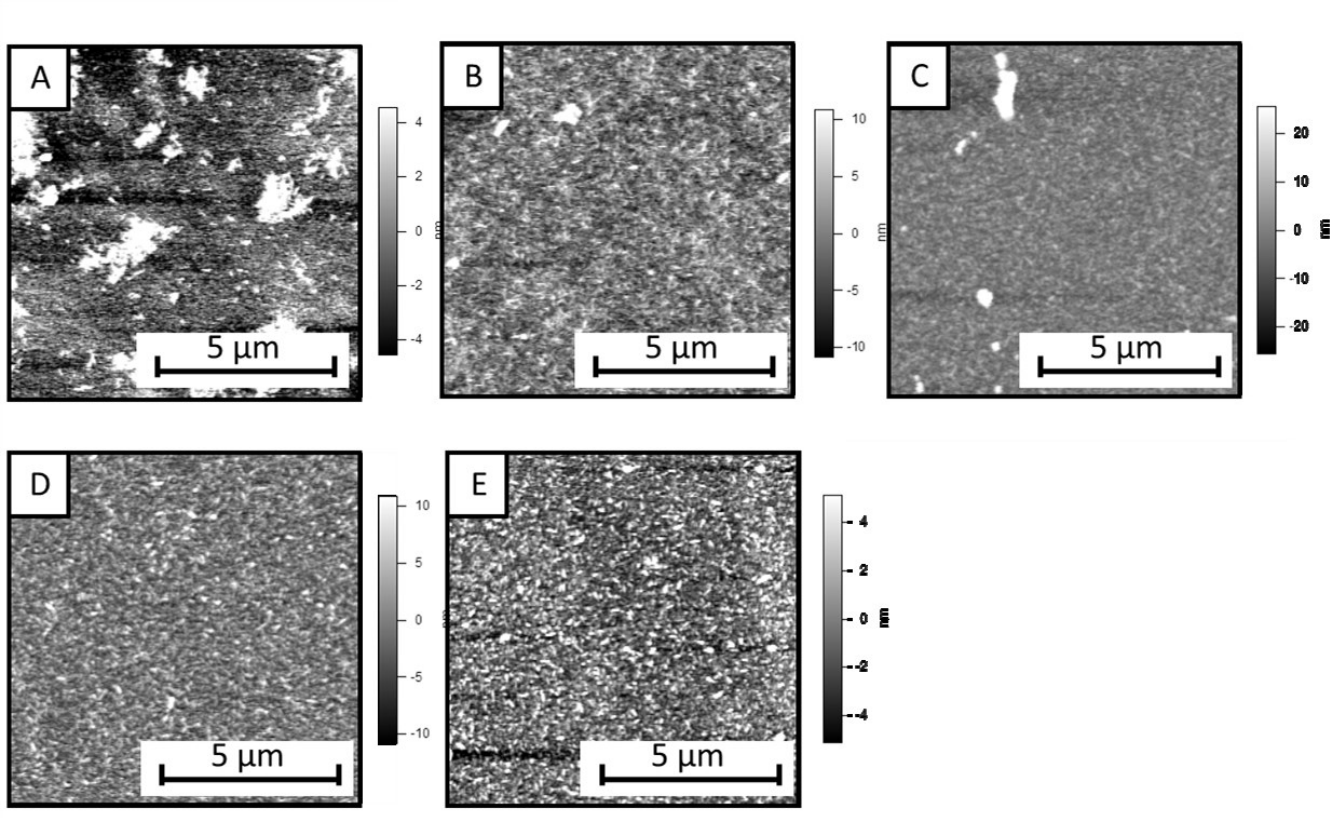

Figure 3-11. AFM height images of CNC films adsorbed from varying ionic strength solutions. A) 1.000 M B) 0.100 M C) 0.010 M D) 0.001M M E) 0.000 M. In all images the CNC suspension at 0.0010% (w/w) and NH_2/NH_3^+ SAMs were used. All CNC suspensions had no observable aggregation to the naked eye.

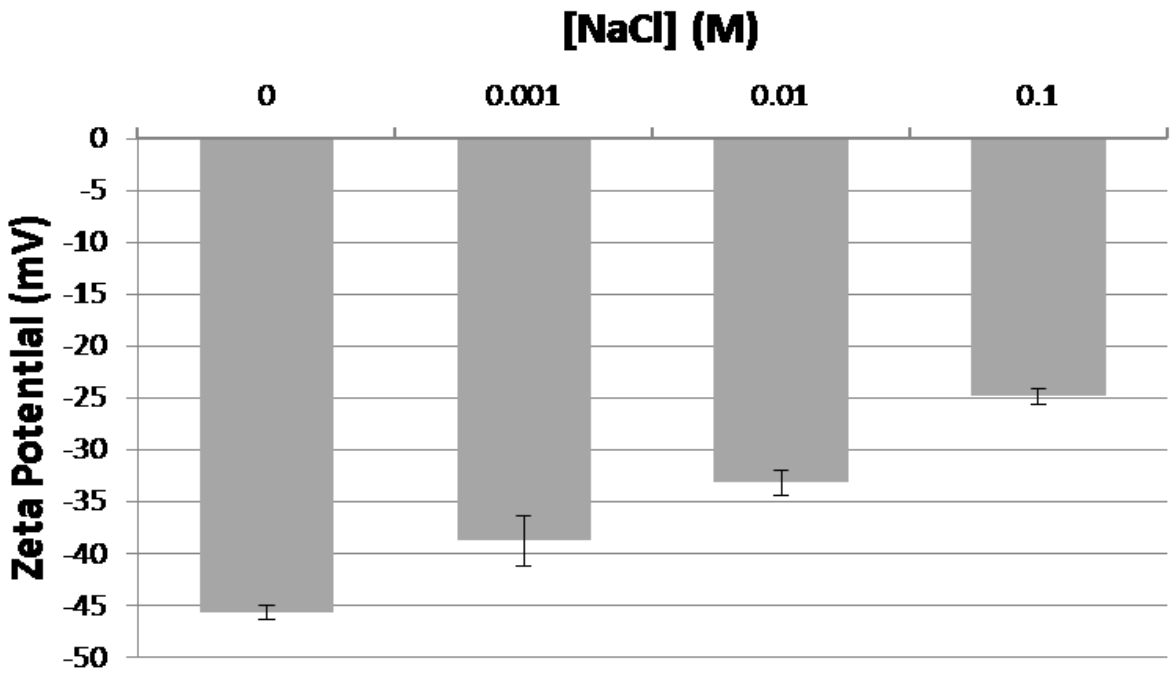

Figure 3-12. Zeta potential of aqueous CNC suspensions at different NaCl concentrations. In all solutions the CNC suspension at 0.0010% (w/w) and NH_2/NH_3^+ SAMs were used. All CNC suspensions had no observable aggregation to the naked eye.

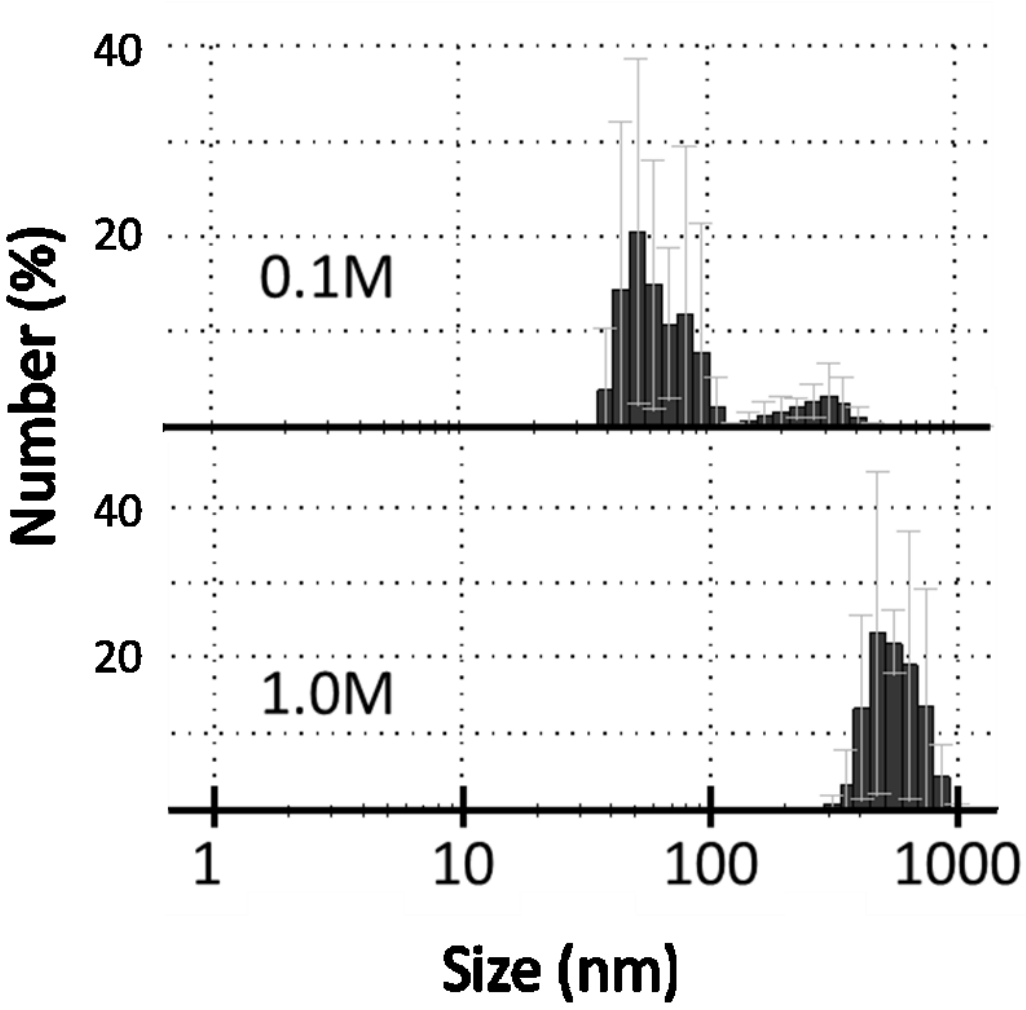

Figure 3-13. DLS of aqueous CNC suspensions at different NaCl concentrations. In both solutions the CNC suspension at 0.0010% (w/w). Neither CNC suspensions had observable aggregation to the naked eye.

The large aggregates observed in the AFM of the 1.000 M NaCl sample are occurring in solution as well. This is shown by the large particle size revealed in the DLS measurements and AFM images. CNC from cotton sources are typically 5-7 nm diameters and 100 nm lengths. The average particle size in the 1.000 M NaCl solution is 400 – 900 nm, indicating aggregation is occurring. The DLS results for the 0.100 M NaCl solution show a bimodal size distribution centred at 60 nm and 300 nm. These results support partial CNC aggregation where some CNC remains colloidally stable and others aggregate. This will result in an effective decrease in concentration of individually suspended CNC which could explain the decrease in surface coverage of this 0.100 M NaCl solution as we have previously seen a surface coverage dependence on concentration of CNC. However, this surface adsorbed decrease does not have an effect at very low concentrations as in Figure 3-5 the two lowest concentrations adsorbed to the same degree. Interestingly, this salt concentration which shows partial aggregation still has higher maximum surface coverage than both pure water (zero ionic strength) and 0.001 M NaCl. The CNC that remain suspended in the 0.100 M NaCl solution have a reduced double layer compared to the other solutions and can form more densely packed layers on the SAM. The decrease in adsorption of the 0.100 and 0.010 M NaCl is thus attributed to a balance in how close CNC particles can be with their attraction to the surface. Recall that CNC adsorbed very weakly to the methyl terminated SAM compared to the amine/ammonium terminated SAM. As the ionic strength increases the attraction of the surface to the CNC will be shielded and exhibit more of a dispersive attraction than the electrostatic. It is necessary to keep in mind that this explanation is comparing data of CNC adsorbing from 0 M NaCl to a methyl

terminated SAM with that of 0.100 and 0.010 M NaCl to an amine/ammonium terminated SAM.

Equilibrium Nature of Adsorbed CNC

Figure 3-14 is a continuation of the earlier experiment that is plotted in Figure 3-9. This figure shows the effect of immersing the slides in pure water after the measurement at day 5 and at all sequential days. In previous days (those days on the x-axis of Figure 3-9) the slides were immersed in salt solutions with 0.0010% CNC. This was done to investigate the reversibility of the adsorbed layers. Figure 3-14 shows that the CNC adsorbed layers are not in equilibrium between the solution and the surface. It is not uncommon of dried CNC layers to not re-disperse in aqueous media upon being re-immersed.

An interesting feature is the 1.000 M NaCl solution after being immersed in pure water after the IRRAS measurement on day 5. After this time the magnitude of the surface signal increases towards that of the 0.000 M NaCl solution. This is due to a reorganization of the previously adsorbed CNC aggregates as observed in AFM images before and after being immersed in pure water which are shown in Figure 3-15.

Scratch tests of image B in Figure 3-15 reveal a film height of 1.9 ± 0.9 nm. This is significantly less thick than the 0.000 M NaCl sample. Although these two slides differ in thickness, the have similar absorbance values, 0.0047 ± 0.0003 for the 0.000 M NaCl and 0.0038 ± 0.0004 for the 1.000 M NaCl at day 11. To have the same absorbance with different thicknesses, the CNC that make up the films of the 1.000 M NaCl sample on day 13 must be denser than the films of the 0.000 M NaCl sample. After dispersion

of the previously formed aggregates upon immersion into pure water, not all CNC re-disperse individually. Evidence for this is contained in Figure 3-15 B where CNC aggregates that appear to consist of several individual CNCs are observed.

Band Broadening in the IRRAS Signals of Cellulose

An observation of the IRRAS spectrum of CNC films adsorbed to an NH_2/NH_3^+ functionalized SAM was band broadening in the C-O stretching region. This was only observed in the 1.000 M NaCl solutions and only after the sample was immersed in pure water. Recall that CNC suspensions in 1.000 M NaCl contain aggregates in solution and resulted in aggregates adsorbed to an NH_2/NH_3^+ functionalized SAM. After immersion in pure water, AFM images reveal that these aggregates are no longer present on the SAM surface but instead a homogeneous surface coverage is observed. Lowering the ionic strength permits previous aggregates to re-disperse and then adsorb as a film on the SAM. This also results in an increase in the IRRAS adsorption as well as CO region band broadening.

The sharpness of IRRAS peaks of CNC samples is a result of their crystalline nature. Bonds are commonly in identical environments and they absorb the same frequency of infrared radiation. If the crystallinity were to be perturbed, this would be reflected in the broadness of the infrared adsorption bands. No broadening was observed in the CNC IRRAS signals as films adsorbed at any ionic strength suggesting that the internal crystallinity was unaffected by the presence of NaCl. The broadening that was observed was after CNC aggregates were re-dispersed. The profile of this broadening is illustrated in Figure 3-16 A, where the signal after re-immersion in pure water is subtracted from a signal of CNC collected from a suspension of 0.000 M NaCl.

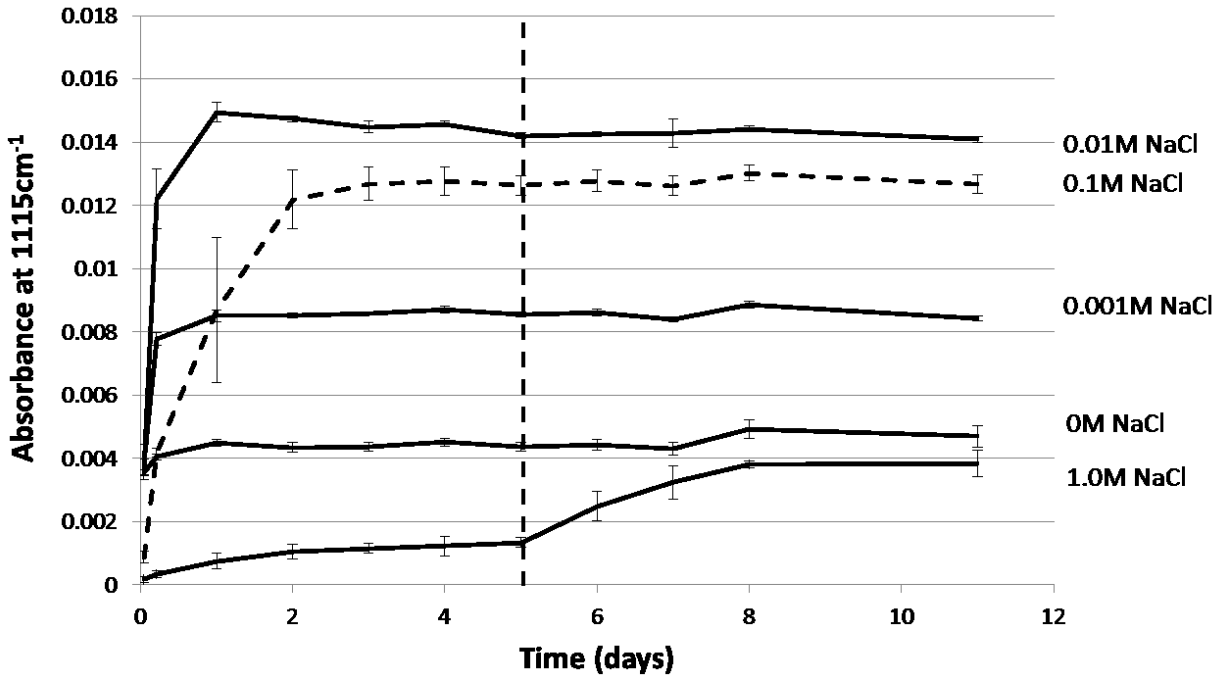

Figure 3-14. IRRAS of 0.001% (w/w) CNC suspension adsorbed to NH_2/NH_3^+ monolayers as ionic strength is varied. The vertical dotted line denotes that after this time, all samples were immersed in pure water (18.2 MΩ) rather than aqueous CNC. Error bars are standard deviations of three measurements.

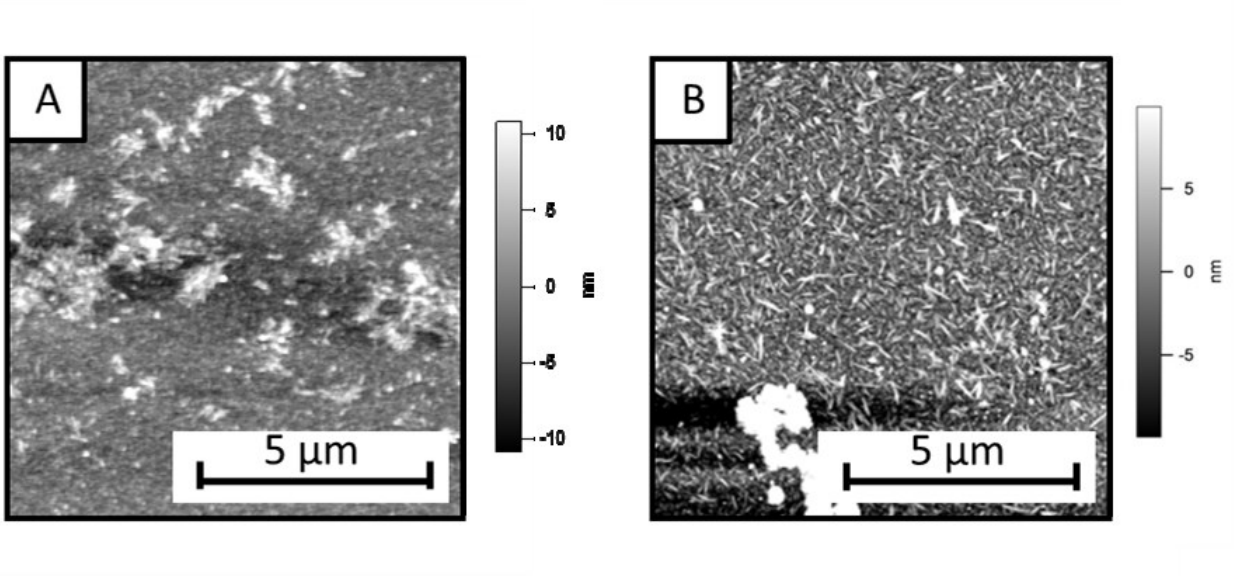

Figure 3-15. AFM height images of CNC films adsorbed from solution. A) After 5 days of immersion in 1.000 M NaCl B) The same slide as in A but after being immersed in pure water from day 5 to 13, the image was taken on day 13. Until day 5 the CNC suspension was constant at 0.0010% (w/w) and the ionic strength was constant at 1.000 M NaCl. Both the CNC suspension and the pure water had no observable aggregation to the naked eye.

In Figure 3-16-A, the difference spectrum is a profile of the broadening that is occurring after the CNC aggregates are introduced to pure water. To explore the possibility of a change in the crystallinity of the CNC, this broadening profile can be compared to a less crystalline sample of CNC. This sample is in a form of cellulose referred to as microcrystalline cellulose (MFC). This form of cellulose has similar diameters to CNC but longer lengths; this is achieved during the isolation step from the natural host material, cotton in this case. By controlling the acid hydrolysis and not removing the amorphous regions that connect crystalline regions, MFC can be collected. An IRRAS spectrum of MFC was collected in the same manner as CNC and is presented in Figure 3-16-B. The difference spectrum in part B is a profile of IRRAS peak broadening on account of having less crystalline cellulose. If the crystallinity is disrupted, each band would be expected to broaden to approximately the same extent.

The broadening of the MFC profile illustrates this form of broadening with the broadening occurring directly around each existing band. The IRRAS of MFC as compared to CNC differs in more ways than just band broadening. The absolute magnitudes of the largest bands change as well as the appearance of a band around 1160 cm^{-1}. This band is assigned to the glycosidic stretch and is absent from IRRAS of CNC on account of it being surface parallel, as explained in Chapter 2. The amorphous regions of MFC contain glycosidic linkages that are in non-surface parallel environments giving rise to this band being observed. As well, AFM images in Figure 3-15 of adsorbed films of MFC reveal that not all regions of the cellulose fibrils are surface parallel; this too would alter the bond angles relative to the surface and alter their magnitudes.

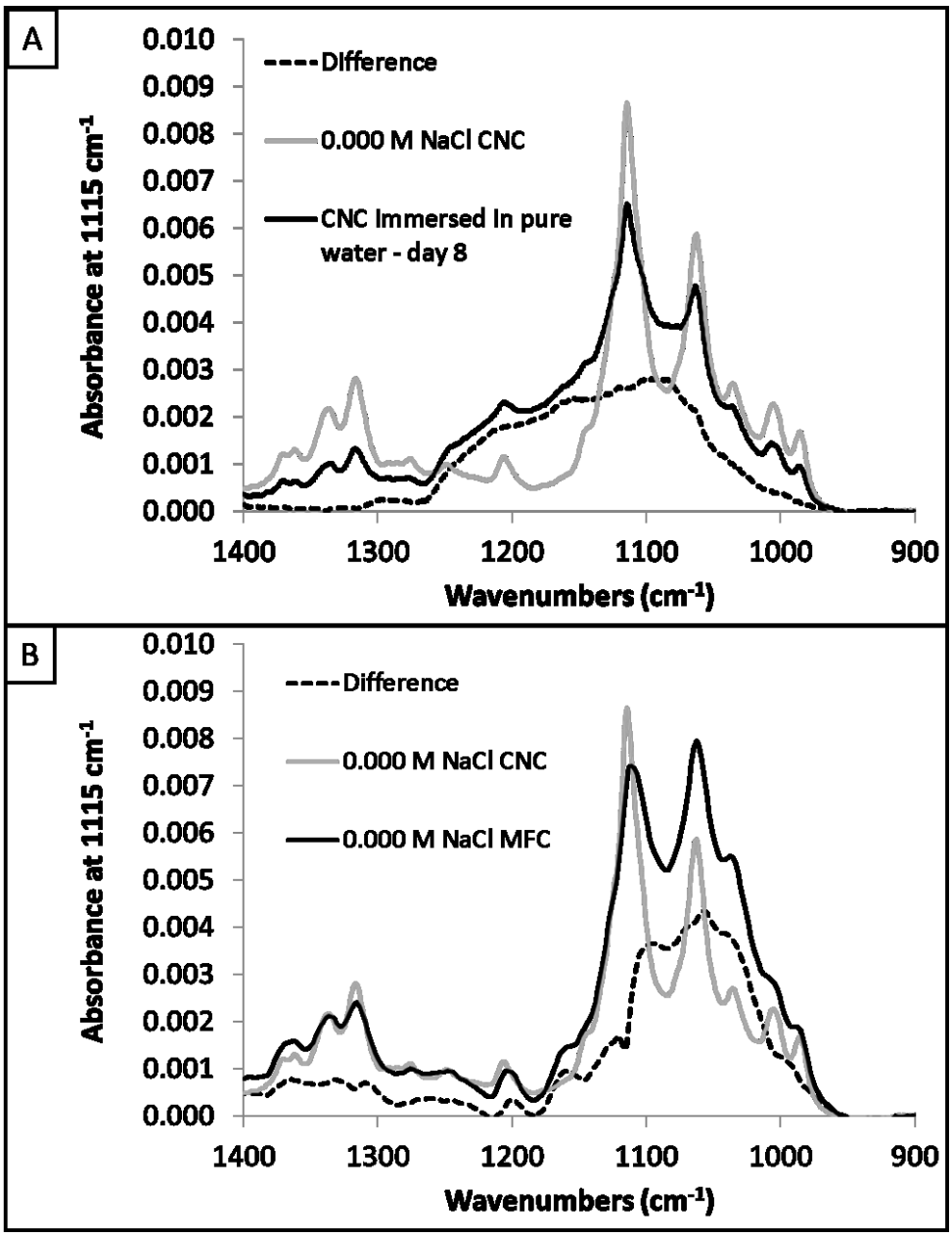

Figure 3-16. A) IRRAS spectra of a CNC film adsorbed from pure water and a film adsorbed for 5 days from a 1.000 M NaCl CNC suspension of 0.0010% (w/w) CNC and then 3 days in pure water. The days of immersion correspond to Figure 3-14. NH_2/NH_3^+ SAM were used to adsorb CNC from solution for all collected spectra. B) IRRAS spectra of a CNC and MFC film adsorbed from pure water to an NH_2/NH_3^+ SAM. The CNC and MFC concentration were 0.0010% (w/w).

By comparing the broadening in CNC spectra from ionic strength with that of MFC, their differences support that the aggregation and subsequent re-dispersion upon being exposed to pure water do not have an effect on the crystallinity. The source of the broadening is unknown at this time and we will be investigating in subsequent experiments that are not included in this thesis. Our current hypothesis is that dispersion after aggregation is not totally reversible. It is possible that aggregations of several CNC still remain which changes the environment of the surface available atoms enough to give rise to the observed broadening.

Conclusion

The work done in this chapter lends a method to empirically measure the affinity of CNC to a variety of model surfaces. With this method it is possible to rank CNC-surface attractions in aqueous media which could be useful in choosing functional groups in mixtures when attempting to use CNC as an additive. The observed trends are explainable when considering the molecular interactions of the suspended CNC and the surface. Electrostatic forces dominate the amine/ammonium – CNC interaction and show the greatest final surface coverage of all tested SAMs. Hydrogen bonding dominates the alcohol – CNC interaction and exhibits the next greatest final surface coverage. Weaker dispersive forces provide a small amount of CNC to adsorb to the methyl terminated SAM. This result is promising in that it gives evidence that CNC produced from sulpuric acid hydrolysis do have an attractive affinity for nonpolar surfaces via dispersive interactions. Finally, no adsorption was observed to the surface carboxylic acid terminated SAMs which were expected at these pH's of just over 7.0, the negatively charged surface electrostatically repelled the suspended CNC.

Varying the concentration of the CNC in suspension reveals some interesting results. In all CNC concentrations tested, a maximum stable surface coverage was reached. Subsequent studies reveal that this is not an equilibrium adsorption. Adsorbed species were resistant to desorb from the surface when placed in pure water. As such, a Langmuir isotherm is not appropriate to model these systems to calculate surface adsorption equilibrium constant to numerically rank them. The lowest CNC concentration adsorbed to the same maximum as a sample with ten times the CNC present but reached this maximum more slowly. This is consistent with an irreversibly absorbing species.

The combination of the IRRAS spectra and the surface layer thickness offers insight into the density of the adsorbed layer. The density will be a direct result of the CNC-CNC interactions as they are mutually repelled by their like surface charges. The ionic strength of the solutions was varied which decreased the double layer thickness of the CNCs and allowed them to pack more densely. The CNC surface coverage does not directly correlate with the ionic strength across all ionic strengths investigated. There was a maximum adsorption, as measured by IRRAS band intensity at 1115 cm^{-1} and AFM scratch thickness at 0.010 M NaCl. Increasing the ionic strength beyond this concentration allowed the CNC to interact closely enough to aggregate. Partial aggregation was observed from DLS in a 0.100 M NaCl solution and severe aggregation was observed at 1.000 M NaCl by both DLS and adsorbed aggregates on an amine/ammonium terminated SAM. Upon re-immersion in pure water, the surface adsorbed aggregates that formed at 1.000 M NaCl re-dispersed on the amine/ammonium SAM to form a homogeneous film. The IRRAS spectrum of this film

differed from the IRRAS of CNC that did not undergo this process of aggregation and re-dispersion. By comparing these spectra to MFC spectra, we conclude that this process of increasing ionic strength does not alter the crystallinity of the CNC.

In the interest of furthering the understanding of the interactions of suspensions of CNC with functional groups, modified applications of this method could involve controlling the pH of the CNC suspension, using a SAM that is a mix of desirable functional groups and changing the suspension medium.

Chapter 4
Cellulose Nanocrystals with Diazonium Salt Derived Aryl Groups

Introduction

Chapters 2 and 3 have sequentially introduced a method to obtain IRRAS spectra of CNC as well as an application of that method to gather information about the interactions of CNC and functional groups. In this chapter, this method will be further employed to estimate the compatibility of chemically modified CNC with various functional groups.

As the market for materials with unique and superior properties advances, the understanding of the nature of CNC is integral in employing them to meet these demands. Environmental awareness is driving the prospect of using naturally occurring fibers such as cellulose. Altering the surface chemistry of hydrophilic cellulose is at the heart of achieving dispersions in hydrophobic mixtures and methods to characterize these interactions are necessary to provide valuable feedback during these processes.

The polymer industry's most produced polymers are hydrophobic, the "big four" being polyethylene, polypropylene, polyvinylchloride, and polystyrene.[163] When used alone these polymers offer a host of useful properties, there is great interest in mixing polymers with both other polymers and additives to gain a unique property set which can be tailored for the desired product. This approach has interest in lowering production cost with inexpensive fillers as well as creating unique materials.

CNC have the pedigree to assist in achieving the goals of polymer manipulation. They are naturally sourced and biocompatible but their most sought after property is mechanical strength. If strain on a material could be concentrated on a CNC network within a polymer, the resulting properties could be invaluable. The main challenge is evenly distributing the CNC into a matrix. The controlling factor is the surface chemistry of the CNC and the interaction it has with the host matrix. Surface modification of CNC to control its surface chemistry is common.[7,50]

In this Chapter, a novel chemical surface modification of CNC will be characterized and the previously explained method to use IRRAS to monitor CNC-SAM affinity will be used. The modification will use a diazonium radical to form a covalent bond to the CNC surface. Diazonium salts are known for their radical activity and spontaneously form multilayers with covalent bonds on certain substrates.[80,81] This reactivity and the flexibility of functional groups that can be para to the N_2 make this reaction even more desirable as a means to modify CNC surfaces. Diazonium salts have been used to modify cellulose sheets for immunoassay membranes.[164]

Experimental

Reagents and Materials

CNC were obtained from Alberta Innovates Technology Futures (AITF) as dried powder samples from cotton and softwood sources.

Tetrafluoroboric acid (5% in water), 4-(trifluromethyl)aniline, 4-nitrobenzenediazonium tetrafluoroborate, sodium nitrate, diethyl ether, acetonitrile, l-ascorbic acid, were purchased from Aldrich and used as is. Amicon Ultra-15 centrifugal filters with Ultracel-

3 membranes with a molecular weight cut off of 3000 were purchased from EDM Millipore (Darmstadt, Germany) and used as is. Deuterated octadecanethiol [$HS(CD_2)_{17}CD_3$] (DODT) 98% was purchased from Aldrich (Milwaukee, WI). 11-amino-1-undecanethiol [$HS(CH_2)_{11}NH_2$] HCl (AUT) was purchased from ProChimea (Sopot, Poland). All thiols were used as received. Millimolar thiol solutions were prepared in anhydrous ethanol (Commercial Alcohols, Brampton Ontario).

Substrate Preparation

The glass substrates were pre-cleaned in piranha solution (1:3 H_2O_2:H_2SO_4) for 15 minutes, rinsed thoroughly with deionized water and dried under Argon. Glass slides were immediately introduced into the vacuum chamber of a thermal evaporation system (Torr International Inc.). A 10 nm adhesive under-layer of chromium was evaporated followed by 300 nm of gold (4n purity).

Monolayer Formation

Self-assembled monolayers (SAMs) of DODT and AUT were prepared on gold substrates. 1 mM ethanolic solutions of each thiol were prepared and the gold substrate was immersed for 48 hours to ensure stable SAM formation. Slides were then removed and rinsed thoroughly with ethanol to remove unbound thiols. AUT-derived monolayers were immediately used for experiments to avoid contamination. DODT were stored in a nitrogen purged environment and cleaned with ethanol before each use as a background signal.

Infrared Spectra Measurements

IRRAS spectra were collected with both a Mattson Infinity FT-IR spectrometer (Madison, WI) and a Bruker Vertex 70 FT-IR spectrometer equipped with low-noise mercury-cadmium-tellurium (MCT) detectors cooled with liquid nitrogen. In both instruments, the incident radiation was reflected from the sample at 80º. 1000 scans were collected with a wavenumber resolution of $2cm^{-1}$. The sample chamber was purged with nitrogen for 8 minutes prior to each measurement to limit atmosphere signals. A spectrum of the atmosphere of the purged chamber was subtracted from all spectra to reduce remaining unwanted signal. A background signal was collected using the DODT substrate. OPUS v. 5.5, Winfirst and Essential FTIR v. 3.00.040 software was used to collect and handle the data. All spectra were manually baselined at like wavenumbers: 4000, 3633, 3134, 3013, 2779, 1818, 1406, 1178, 949 and $821cm^{-1}$.

Transmission IR spectra were collected using a Thermo Nicolet 8700 with attached Continuum FTIR microscope. Data was collected with OMNIC v. 8.3 software and handled with Essential FTIR v. 3.00.040 software. All samples were subject to mild mechanical stirring via a magnetic Teflon stir bar at minimal RPM to promote consistent liquid-substrate interactions.

Diazonium Salt Preparation

The 4-nitrobenzenediazonium tetrafluoroborate was purchased from Aldrich and the 4-(trifluromethyl)benzene diazonium tetrafluoroborate was prepared in lab. Sixty mL of 5% HBF_4 was used to dissolve 16 g of 4-(trifluromethyl) aniline and was cooled with icy water. 10 g of $NaNO_2$ was mixed with 20 mL of water and cooled in an icy water bath. The cool $NaNO_2$ solution was slowly added drop wise to the aniline solution and all

solutions were cooled by icy water the entire time. This mixture was stirred for 2 hours, filtered in a Buchner funnel and rinsed with cold HBF_4 and cold diethyl ether. The filtrate was dissolved in acetonitrile and re-crystallized in cold diethyl ether. Residual diethyl ether in the resulting white powder was removed by low pressure to assist evaporation, after ether removal the power was stored in a fridge for later use.

CNC Modification with Diazonium Salt

Two g of dried CNC were suspended in 100 mL of water to form a 2% (w/w) CNC suspension. Five mmoles of either diazonium salt was added and the contents were sonicated for 10 minutes. 0.5 mmoles of l-ascorbic acid from a 100 mM solution was added to the contents. This mixture was sonicated a further 1 hour. The reacted CNC were separated from solution by centrifuge filtration. The contents were evenly divided between 10 x 15 mL 3000 MW cutoff centrifuge filtration tubes. These were centrifuged at 4500 RPM at 20^{O} for 3 hours. At each hour 18 MΩ water was added to the filtrate to maintain a supply of rinse water. This final product was freeze dried and kept in storage vials for later use.

Results and Discussion

Surface Modification of CNC

CNC particles were modified with diazonium derived films of nitrobenzene (NO_2) and trifluoromethy benzene (CF_3). NO_2 and CF_3 functional groups were chosen to creating CNC surfaces with vastly different polarity. Based on previous reports of diazonium derived films on carbon and gold surfaces, we assume that the radical reaction of the diazonium will yield a covalent bond with the CNC surface and will orient the functional

group in the para position available to influence the solution – CNC interface.[80,81,83–85,88,89,92,93,154–156] Transmission IR and X-ray photon spectroscopy (XPS) were performed on the final products to confirm successful modification.

Figure 4-1 has transmission IR spectra of unmodified and nitrobenzene modified CNC. The spectrum of the CNC modified with diazonium derived nitrobenzene shows unique bands as compared to unmodified CNC. Two N-O stretching modes are present at 1348 and 1522 cm^{-1}. Two ring modes are present as well, C-C stretching in the benzene ring at 1597 cm^{-1} and CH out of plane deformation present in para substituted benzene rings at 854 cm^{-1}. These additional bands provide support for the successful modification of the CNC with nitrobenzene groups.

An IR spectrum tracking the modification of CNC with aryl tri-fluoromethane groups is shown in Figure 4-2. A band consistent with C-F stretch is observed at 1327 cm^{-1}. Also, characteristic ring modes at 1616 and 843 cm^{-1} are observed. Again, observation of these bands is consistent with modification of CNC with aryl-CF_3 groups.

To further confirm successful surface modification with the two diazonium salts of interest, XPS N 1s, C 1s, and F 1s XPS spectra were collected. Figure 4-3 shows the N 1s spectrum of both the NO_2 modified and unmodified CNC. The higher binding energy peak observed at approximately 405 eV is consistent with the nitro group that is expected to be present on the nitro benzene of its diazonium salt. The lower binding energy peak at approximately 400 eV is likely due to unreacted precursor as it is consistent with a nitrogen-nitrogen double bond or amine.

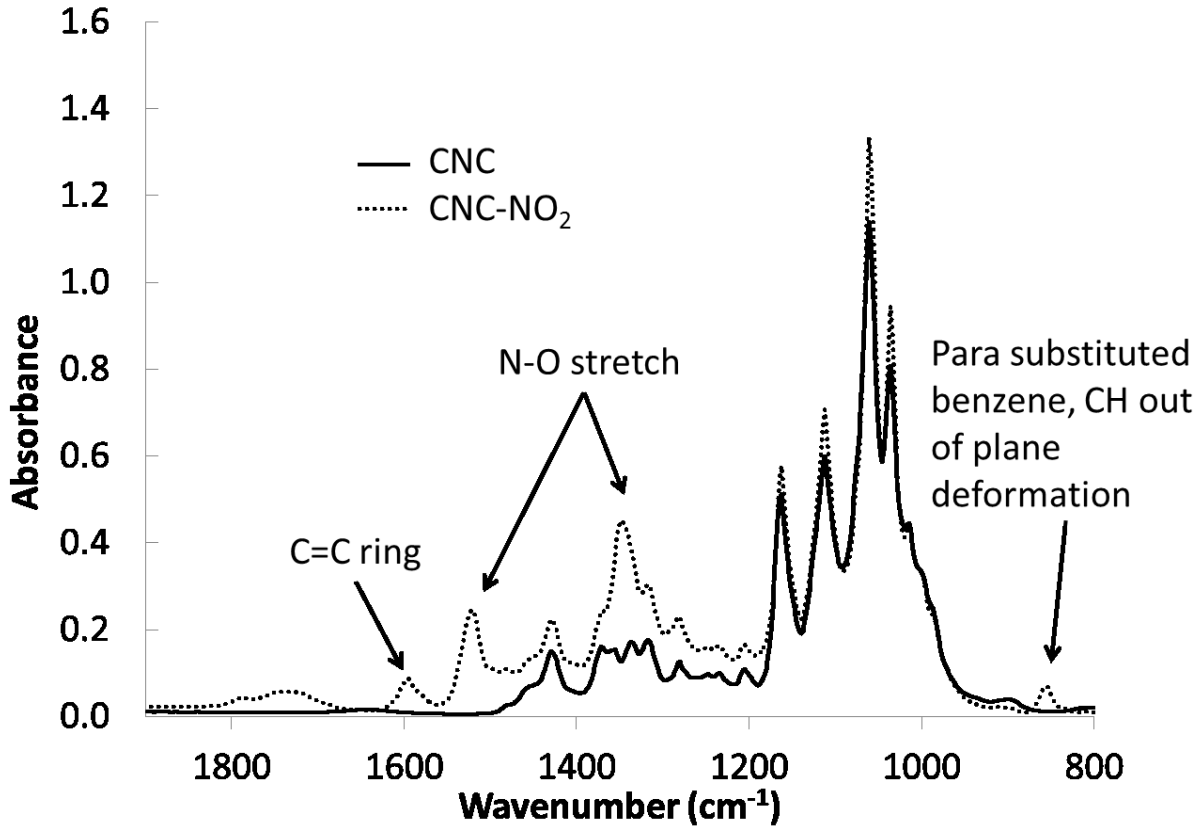

Figure 4-1. Transmission FTIR of CNC and diazonium derived nitrobenzene modified CNC with assignments to bands due to modification.

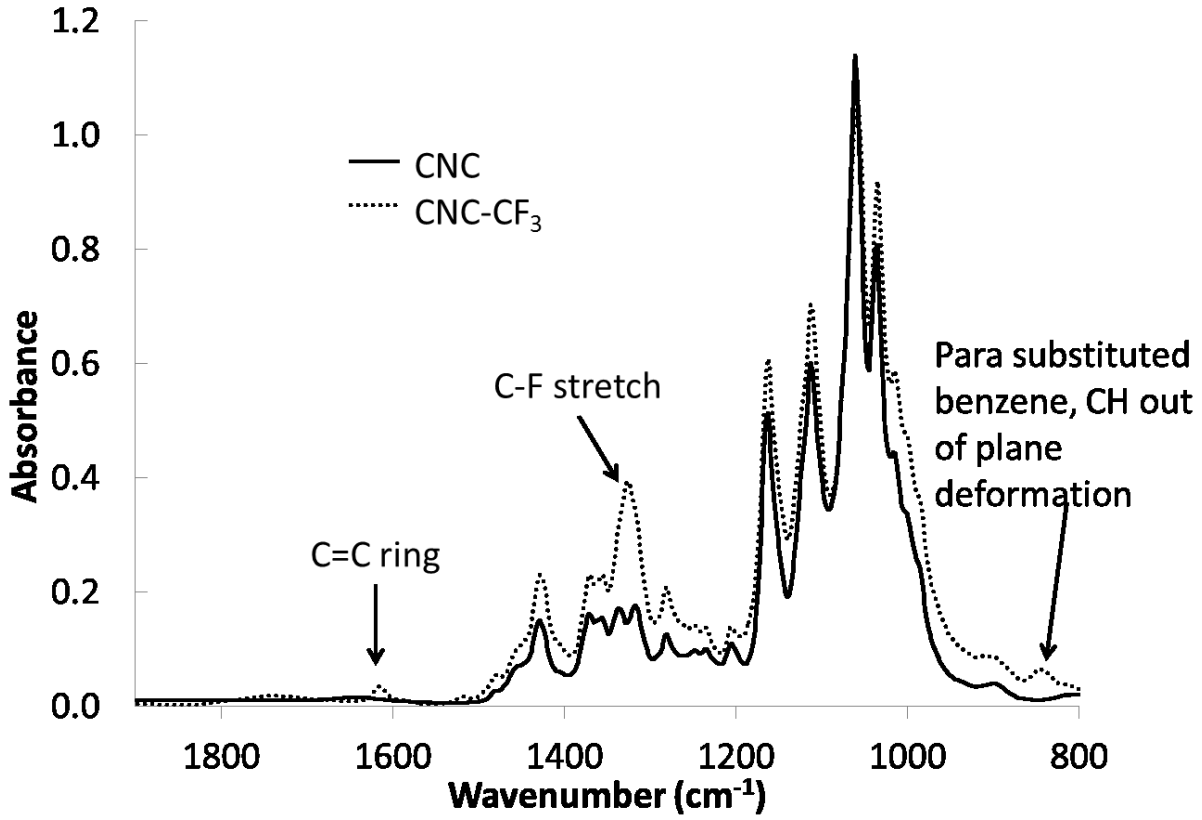

Figure 4-2. Transmission FTIR of CNC and diazonium derived from trifluoromethyl benzene modified CNC with assignments to bands due to modification.

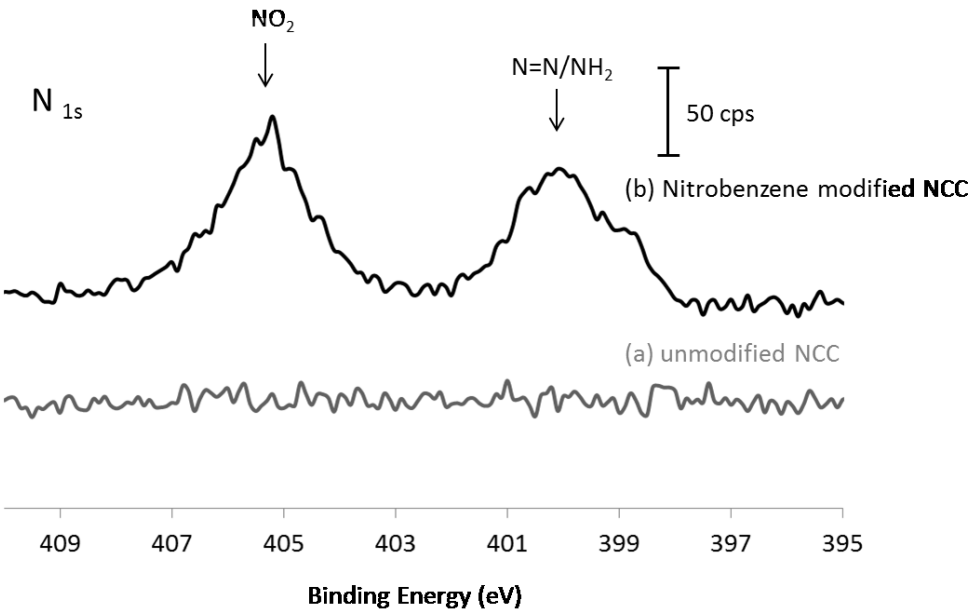

Figure 4-3. XPS of nitrobenzene modified CNC in the N_{1s} region. Sample Preparation and Spectra collected by Dr. Rongbing Du.

Figure 4-4 shows the carbon 1s region of CNC modified with trifluoro-methyl diazonium. The largest peak at 284.8 eV is due to the carbons present in the CNC. An expected peak at 286.9 eV arises from the numerous C-O and C-N present in CNC and modified CNC. The lowest binding energy peak present at 283.5 eV is less common but is likely due to the sp2 hybridized carbon in the benzene ring. A separate peak at 292 eV indicates the presence of fluorinated carbon introduced by successful CNC modification. This higher binding energy peak is consistent with other halogenated carbons in the literature.[165] The lower intensity of the C-F peak relative to the C-O peak suggests that only a fraction of the CNC surface is modified. To estimate the surface coverage some assumptions will need to be made. First, the diazonium may be added at any of the surface alcohol groups on a single cellobiose unit. Second, half of the C-O signal is due to non-alcohol functionality. Third, 55 % of all the C-O bonds are on the surface and available to be modified and the 10 to 25% that are modified with a sulphate group[76] are also available for modification. This assumption is based on a cotton sourced CNC particle being 6 x 6 cellulose chains[7] and of these 36 total chains, 20 run along the surface. Four, the $C1_s$ signals for the C-O and C-F have identical relative sensitivity factors. Five, the entire volume of a single CNC particle will be equally measured with the x-ray beam. Since CNCs are around 7 nm in diameter this assumption is valid. Six, multilayers of diazonium derived aryl groups are not present. This assumption is likely invalid as multilayers are known to form from a surface but this gives us a stage to estimate the surface coverage. With these considerations, a fully modified CNC particle would have a C-F signal that is 68 % the area of the C-O signal. Given that the area of the C-O peak is 20 times greater than the C-F peak, the degree of modification can

roughly be estimated to be no more than 7 % of surface available sites and is likely less when multilayers are considered.

Figure 4-5 shows the fluorine 1s region of CNC modified with a (triflurомethyl)benzene diazonium cation. This spectrum shows a single peak at approximately 685 eV that is consistent with other fluorine 1s spectra. In the un-modified CNC sample there is no signal in this binding energy range.

Adsorption of Modified CNC

The method introduced in Chapter 3 to monitor the adsorption of CNC from aqueous suspension to a controlled functional group was again employed with these modified CNCs. In contrast to the previous measurements which involved hydrophilic CNC adsorbing to various functional groups from aqueous solutions, these experiments involve a presumably less hydrophilic CNC. This will cause less CNC to be suspended in water with the possibility for agglomeration and results should not be directly compared to the previous chapters. Figure 4-6 shows IRRAS spectra of both the NO_2 and CF_3 modified CNC as they adsorbed from aqueous solution to an amine/ammonium and methyl terminated alkane thiolated SAM. CF_3 modified CNC showed no adsorption to the CH_3 SAM and is not plotted. This observation was unexpected as dispersive forces were expected to be strong enough to adsorb some of the trifluoromethyl modified CNC. Chapter 2 revealed that dispersive forces were enough to adsorb some unmodified CNC to a methyl terminated SAM. We conclude that altering a CNC surface to a trifluoromethyl group and suspending these CNC in water yields aggregates that are stabilized by the modified CNC-water interaction sufficiently so that they are reluctant to adsorb to a nonpolar, methyl terminated surface.

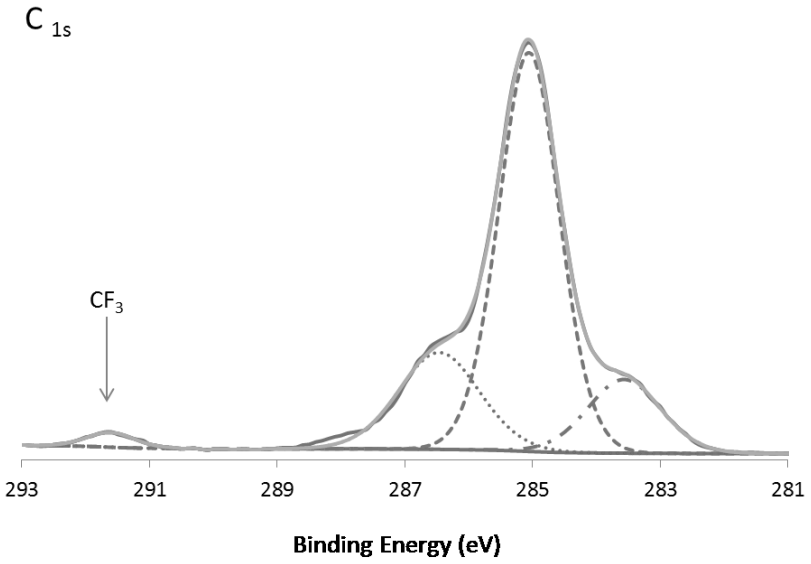

Figure 4-4. XPS of CF_3 modified CNC in the C1s region. Sample Preparation and Spectra collected by Dr. Rongbing Du.

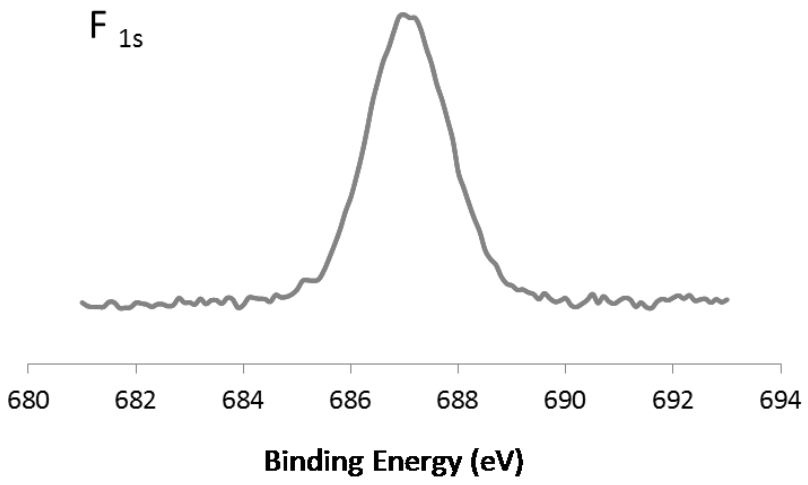

Figure 4-5. XPS of CF_3 modified CNC in the F1s region. Sample Preparation and Spectra collected by Dr. Rongbing Du.

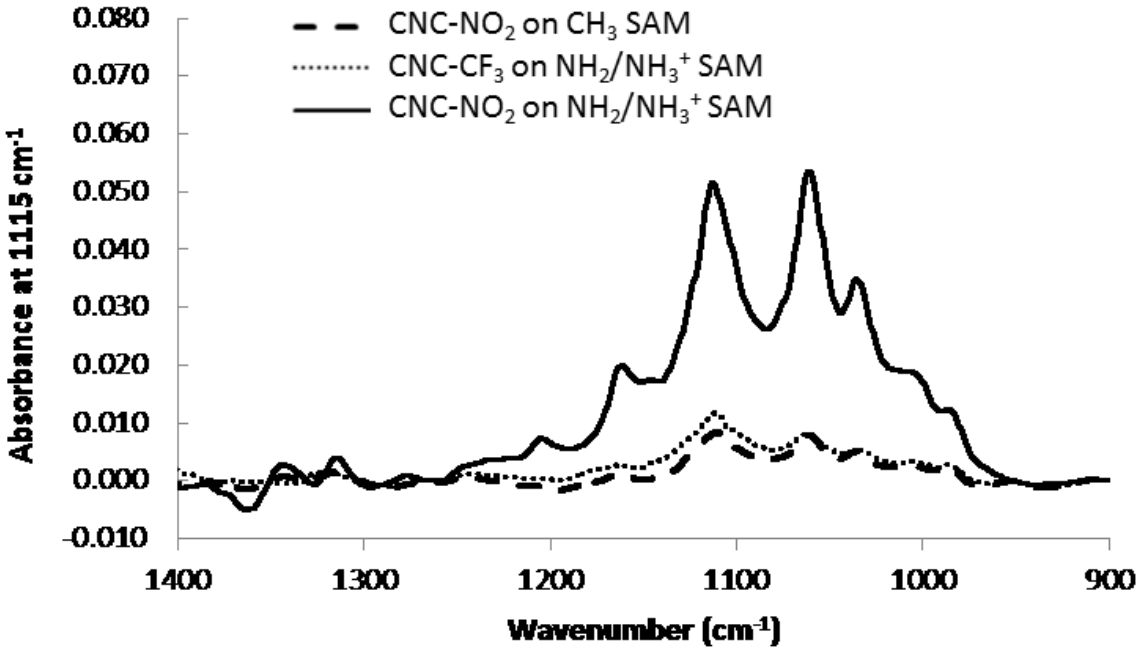

Figure 4-6. IRRAS of NO_2 and CF_3 modified CNC adsorbed to a CH_3 and a NH_2/NH_3^+ SAM from an aqueous suspension. The CF_3 modified CNC showed no adsorption to the CH_3 SAM and is not plotted. All aqueous sampels had 0.0150 % (w/w) modified CNC.

When the CF_3 and NO_2 modified CNC were introduced into water, they showed visible aggregation. As with all previously collected IRRAS spectra of adsorbed CNC to a SAM, magnetic stirring was used to promote sample homogeneity. This mixing assisted in the dispersion and adsorption of the modified CNC. As aggregates were stirred they would be forced into contact with the immersed slide. These interactions allowed some CNC to adsorb to the SAM.

The spectra of both modified CNCs show the presence of a band around 1160 cm^{-1}. This band is assigned to the glycosidic stretch and is absent from IRRAS spectra of CNC on account of the glycosidic bond angles relative to the surface, this effect is referred to as the surface selection rules and is described in Chapter 2. The appearance of this band supports that the adsorbed modified CNC are not completely parallel to the surface.

Figure 4-7 shows the change in surface coverage over time. As stated above, these modified CNC precipitate out of aqueous media. The different increase in signals over time of the two modified CNCs can be attributed to the relative affinities of each modified CNC to the SAM. The observed hierarchy of surface coverage supports successful modification to the extent that it is influencing the CNC surface chemistry of an aqueous particle and as an adsorbing species to an amine/ammonium terminated SAM.

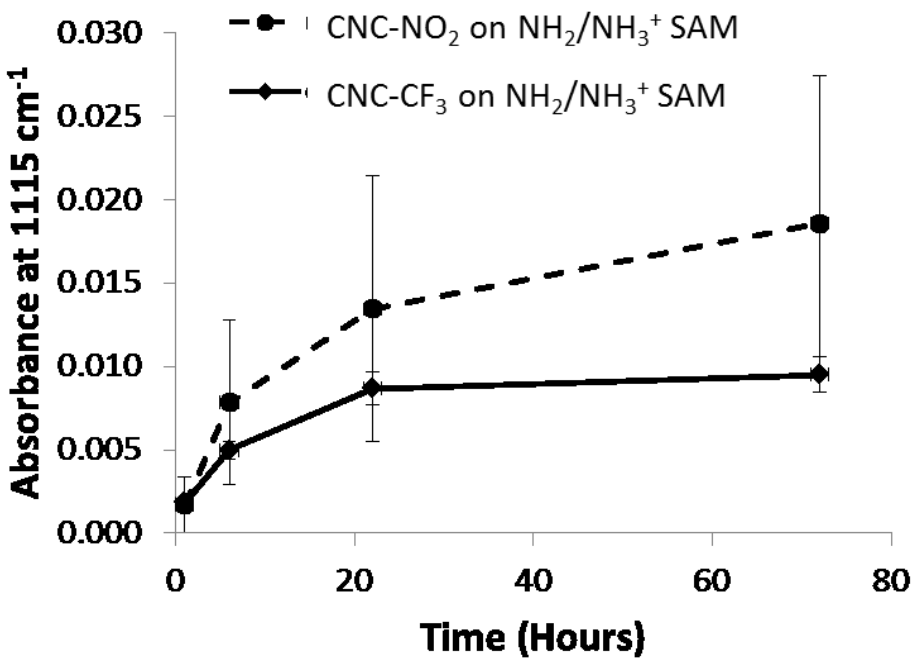

Figure 4-7. Surface coverage of NO_2 and CF_3 modified CNC adsorbed to a NH_2/NH_3^+ SAM from an aqueous suspension. All aqueous solutions had 0.0150 % (w/w) modified CNC. Error bars are standard deviations of three measurements.

Conclusion

This novel method of modifying CNC with the reactive radical from the reduction of the N_2 group on a functionalized diazonium is an effective method to attain desired surface chemistry on the CNC. The variability of functional groups that can be para to the N_2 makes this reaction even more desirable. On account of the relatively recent exploration into this method there is still fundamental background work that is being carried out to better understand the complexities of the reaction and to characterize the resulting modified CNC. Regardless, the application of the established IRRAS method to monitor surface adsorption onto tailored surfaces can give insight into the degree of attraction of the modified CNC and functional groups likely to be present in a different system.

Chapter 5
Mechanical Characterization of Polyethylene-Diazonium Modified CNC Nanocomposites

Introduction

CNC has many attractive properties as a polymer additive. Its high mechanical strength and appealing aspect ratios and surface area combined with a tailorable hydroxyl surface are part of the attraction. The fact that it is biologically produced from a renewable source permits human biocompatibility and biodegradability. With a wide range of unique properties, the focus of this work will be to harness the mechanical properties of CNC in polyethylene nanocomposites. CNC nanocomposites have been realized and review articles covering this topic are published.[50,95,105,137,138,142–144,166–170] In almost all CNC nanocomposites, a surface modification step is preformed to permit adequate miscibility of the notoriously hydrophilic CNC into a nonpolar polymer matrix. Polyethylene oxide, polyvinyl acetate, and polylactic acid has been incorporated with CNC to extruded a nanocomposite.[104,171–174] As well, all cellulose materials have been formed[175,176] and all cellulose nanocomposites extruded.[177]

Polyethylene (PE) is the most synthetically produced polymer, over $6x10^7$ tonnes per year.[178] There are three common types of PE; low density polyethylene (LDPE), linear low density polyethylene (LLDPE) and high density polyethylene (HDPE). These differ in density as a result of changes in the chain length and branching which in turn alters the polymer chain density. LDPE and LLDPE range between 0.915 and 0.940 g/mL

where HDPE ranges between 0.940 and 0.965 g/mL. LLDPE differs from LDPE in that it is polymerized in the presence of short chain alpha olefins giving the carbon backbone a highly branched structure. The common industrial uses of each are presented, according to The Essential Chemical Industry online, below in Figure 5-1.

With this wide range of uses the benefit of creating a mechanically superior material by forming a nanocomposite is apparent. One of the thermoplastic industries most common composite manufacturing processes is extruding. In this method a polymer in powder or pellet form is fed into a heated extruder along with additives and mixed. From this polymer melt a downstream product is formed which may be blow molded, injection molded or cast into a film.[163] Extruded PE composites primarily involve the addition of clay[179–181] and increasingly graphene.[182,183]

A PE-CNC nanocomposite would be the marriage of the most produced synthetic and natural polymers. Performing this composite manufacturing via melt extrusion would be easily adoptable by current industry. CNC has been combined with low density polyethylene and extruded without the use of any cellulose modification.[103] In this work, the composite was extruded from a melt mixer where water was added to the melt mix which was then sealed to prevent evaporation. This water injection-assisted high-shear extrusion improved CNC dispersion and resulted in an increase in the Young's modulus of the extruded films. Maleated PE via ball milling has been used to form extruded CNC nanocomposites with an increase in toughness and ductility.[184] Organic acid chlorides have been used to graft aliphatic chains to ramie fibers allowing successful extrusion with LDPE.[185]

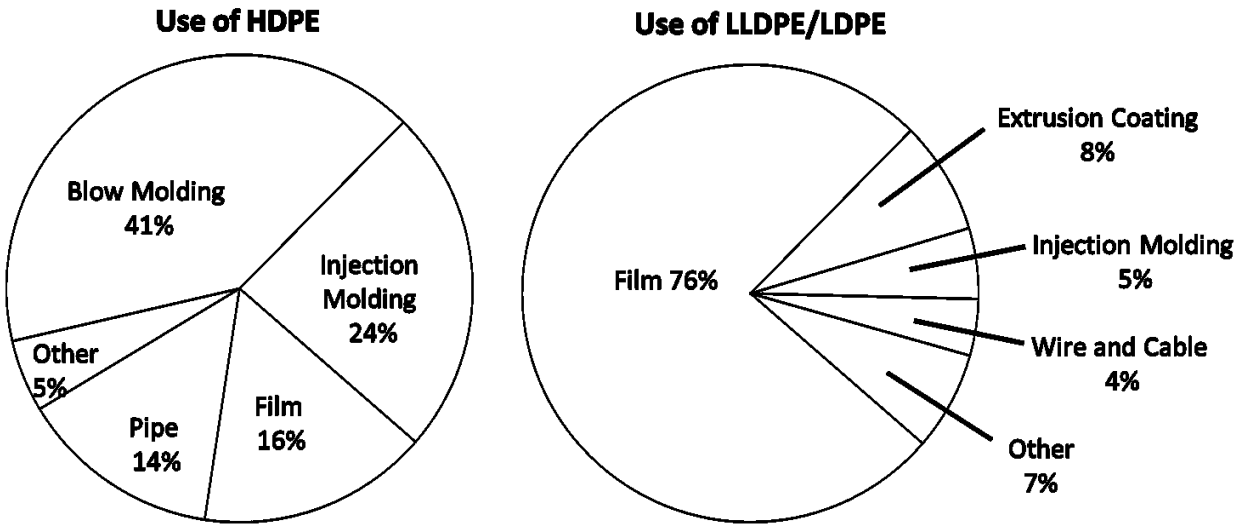

Figure 5-1. Uses of Polyethylene according to The Essential Chemical Industry online.

Using the modification scheme outlined in Chapter 4, trifluoromethyl benzene (TFMB) modified CNC was melt mixed with high density polyethylene and extruded into ribbons. This work describes the mechanical advantages of reinforcing HDPE with TFMB modified CNC.

Experimental

Reagents and Materials

CNC were obtained from Alberta Innovates Technology Futures (AITF) as dried powder samples from cotton and softwood sources.

Tetrafluoroboric acid (5% in water), 4-(triflurомethyl)aniline, sodium nitrate, diethyl ether, acetonitrile, l-ascorbic acid, were purchased from Aldrich and used as is. Amicon Ultra-15 centrifugal filters with Ultracel-3 membranes with a molecular weight cut off of 3000 were purchased from EDM Millipore (Darmstadt, Germany) and used as is.

High density polyethylene, DMDH 6400 – film blowing grade was used from Dr. Yaman Boluk's lab. This type of HDPE is multi-purpose and designed for blow molding.

Diazonium Preparation

The 4-(triflurомethyl)benzenediazonium tetrafluoroborate was prepared in lab. 60 mL of 5% HBF_4 was used to dissolve 16 g of 4-(triflurомethyl) aniline and was cooled with ice water. Ten grams of $NaNO_2$ was mixed with 20 mL of water and cooled in an ice water bath. The cool $NaNO_2$ dilution was slowly added drop wise to the aniline solution and all solutions were cooled by ice water the entire time. This mixture was stirred for 2 hours, filtered in a Buchner funnel and rinsed with cold HBF_4 and cold diethyl ether.

The filtrate was dissolved in acetonitrile and re-crystallized in cold diethyl ether. Residual diethyl ether in the resulting white powder was removed by low pressure to assist evaporation, after ether removal the power was stored in a fridge for later use.

CNC Modification with Diazonium Salts

2 g of dried CNC were suspended in 100 mL of water to form a 2% (w/w) CNC suspension. 5 mmoles of either diazonium salt was added and the contents were sonicated for 10 minutes. 0.5 mmoles of l-ascorbic acid from a 100mM solution was added to the contents. This mixture was sonicated a further 1 hour. The reacted CNC were separated from solution by centrifuge filtration. The contents were evenly divided between 10 x 15 mL 3000 MW cutoff centrifuge filtration tubes. These were centrifuged at 4500 RPM at 20^{O} for 3 hours. At each hour 18MΩ water was added to the filtrate to maintain a supply of rinse water. This final product was freeze dried and kept in storage vials for later use.

Melt Mixing

A Dynamico single screw benchtop melt mixer was used to extrude polymer ribbons. An operating temperature of 170 ^{o}C was maintained for both the hopper and the drive shaft. Dried polyethylene pellets and freeze dried CNC or modified CNC were added to the hopper and allowed to mix in the heated chamber before being extruded. A shaft-head distance of 1.3 mm was maintained to promote mixing time and control the ribbon thickness. A puller was used to extrude the ribbons at a constant rate. A picture the melt mixer with an expanded view into the hopper is shown in Figure 5-2.

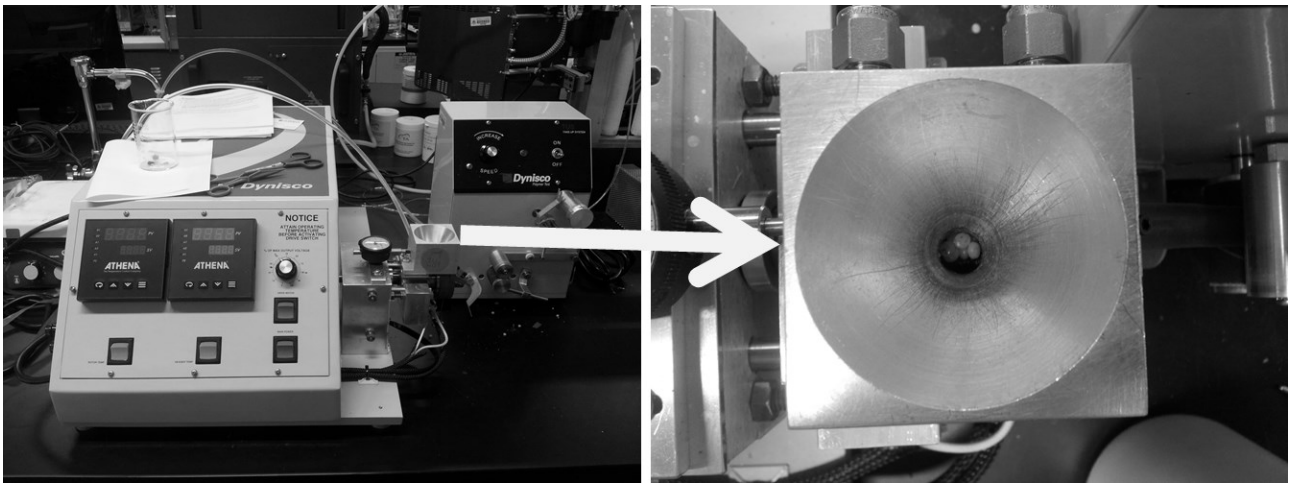

Figure 5-2. Benchtop melt mixer used to melt PE and mix CNC. The image on the right is looking down into the hopper.

Mechanical Testing

A BOSE Electroforce 3200 Series III Test Instrument with a 100 foot pound load cell was used to obtain stress strain curves of the extruded ribbons. WinTest 7 and Excel 2010 software were used to collect and handle the data. A displacement rate of 0.5 mm/min was used for all samples and gauge length varied between 4 and 8 cm. Triplicates of each ribbon were run for each sample.

Results and Discussion

The mixing of nanomaterials with polymers to produce nanocomposites with enhanced properties has been the subject of intense research and is the basis for many commercial products. A common method of composite formation is to melt mix the components and extrude them via a screw extruder. In the work presented in this Chapter, HDPE was melt mixed with diazonium derived trifluoromethyl benzene (TFMB) modified CNC (here after designated as CF_3-CNC) and unmodified CNC. The details on the modification of the CNC with diazonium cations are found in Chapter 4. The mechanical properties of the resulting materials were then tested.

Material testing is an integral component in the manufacturing of new products. Obviously, the interest of incorporating CNC into PE is to increase the mechanical stiffness and strength. There are many methods to measure and compare the strength of materials. A common approach to quantify this property is to construct a uniaxial tensile test that reveals a stress vs strain curve where a tension load is measured as the sample is continually stretched until it eventually fails.

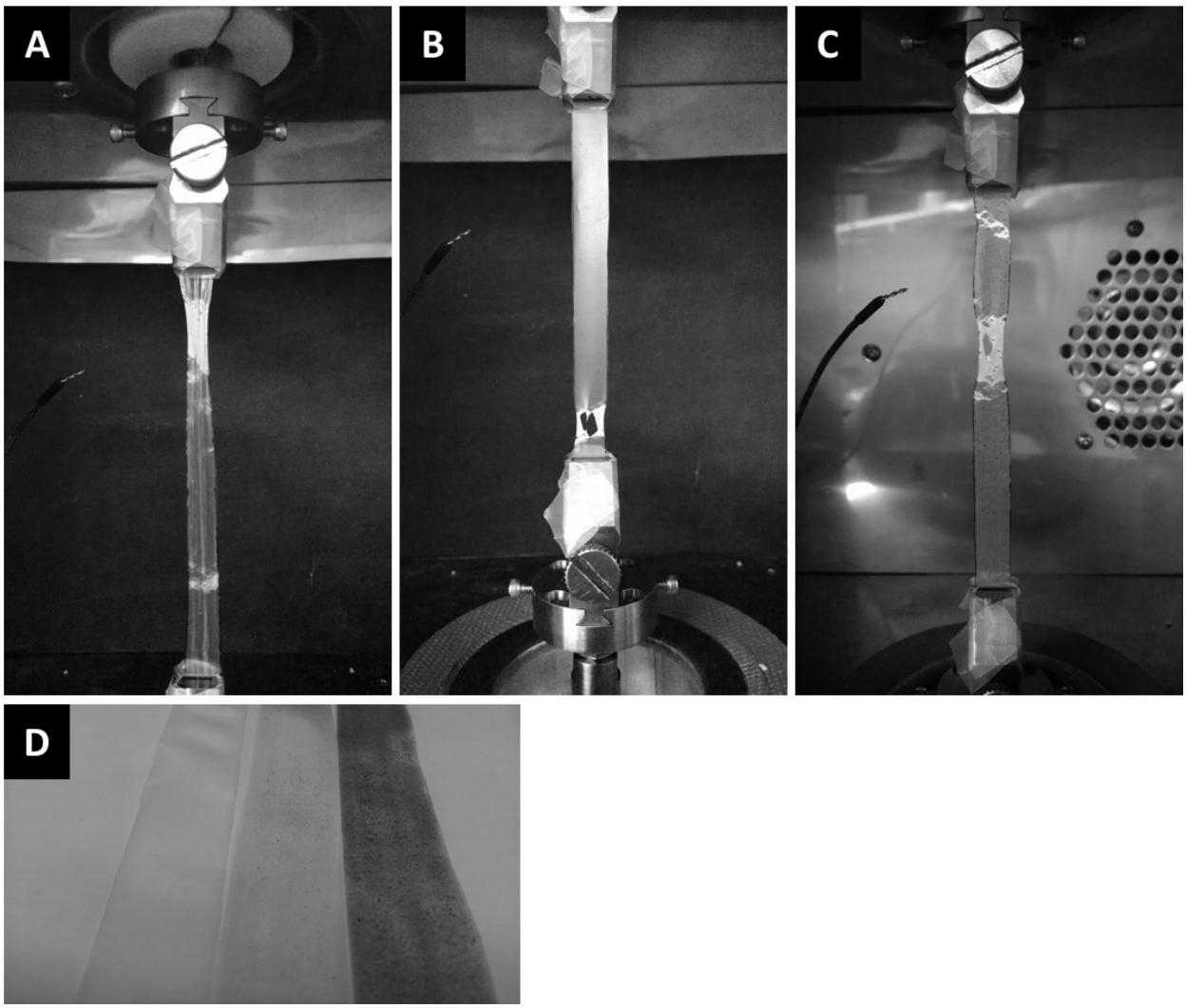

Figure 5-3. Photographs of the stress-strain measurement. A) Virgin PE B) 3% CNC in PE C) 6% CNC in PE before stretching D) Photos of the samples, from left to right; 0%, 3%, 6% CNC mixed with PE. All CNC are unmodified.

Stress-strain curves for the materials prepared here were acquired to investigate the mechanical properties of the nanocomposites. Photographs of the melt mixed ribbons in the testing apparatus near or at failure are shown in Figure 5-3. For all samples the region of the ribbon that failed was not at the clamp head. This confirms that the act of clamping the ribbon did not introduce a weak point (stress concentration) and cause premature failure. An example of a stress strain curve for CF_3-CNC-PE where the amount of CNC is 6% by weight is in Figure 5-4.

This is an expected stress strain curve for a thermoplastic material. The initial linear increase in stress as the sample is strained reveals the region where this material is behaving elastically. The Young's modulus of a material is the slope of this initial (elastic) portion of the curve. The ultimate tensile strength (UTS) is the maximum stress recorded over the entire curve, for this material it occurs just after the elastic region. As the material is continually strained beyond the UTS point visual signs of sample failure can be noticed following initiation of a necking region. Figure 5-3 C shows a photograph of the sample in Figure 5-4 in the stress-strain region after the UTS and before complete sample failure. As strain is continually applied the sample will, at some point, yield. This is referred to as the yield point.

Three aspects of the curve in Figure 5-5 will be analyzed. These are the elastic region, UTS point, and the yield point. The effect of incorporating surface modified CNC on these aspects will be discussed below. Each of the three effects can be visualized by its referring to the corresponding region in Figure 5-4.

Young's modulus

The elastic region of the curve in Figure 5-4 is expanded in Figure 5-5. The data are fit using least squares linear regression and the slope determined.

The observed downward facing curve in the data is typical and due to an imperfect elastic response. A similar range of strain values was used to estimate the Young's modulus of each sample. The magnitude of the Young's modulus for each sample prepared is shown in Figure 5-6. The Young's modulus for virgin HDPE is measured to be 0.36 ± 0.09 GPa. The HDPE used here is multipurpose with blow molding as the suggested use. A suitable literature values for the Young's modulus on www.matweb.com would be injection molded HDPE as it would be of a similar type and has values that range from 0.45 to 1.50 GPa.[186] The ribbons formed in this work have a lower Young's modulus than the mentioned literature value range and can be accounted for by the specifics of the extruder used and the exact type of HDPE. Ultimately, when investigating the effect of a polymer additive (CNC in this case) to increase mechanical strength, using the same process and the same polymer for both virgin and composite material will highlight the effectiveness of the additive. The Young's modulus of the nanocomposites containing CF_3-CNC is markedly higher than both the virgin PE and the PE composite formed with unmodified CNC. There is no statistical difference in the Young's modulus observed between the 3% and 6% materials for either the modified CNC or unmodified CNC. The lower modulus of the material containing unmodified CNC as compared to the modified is not surprising as there were aggregates visible to the naked eye within the unmodified CNC-PE ribbon (Figure 5-4 D). The interactions between the unmodified CNC and PE are expected to be weak and the aggregates would yield a similar result as having voids.

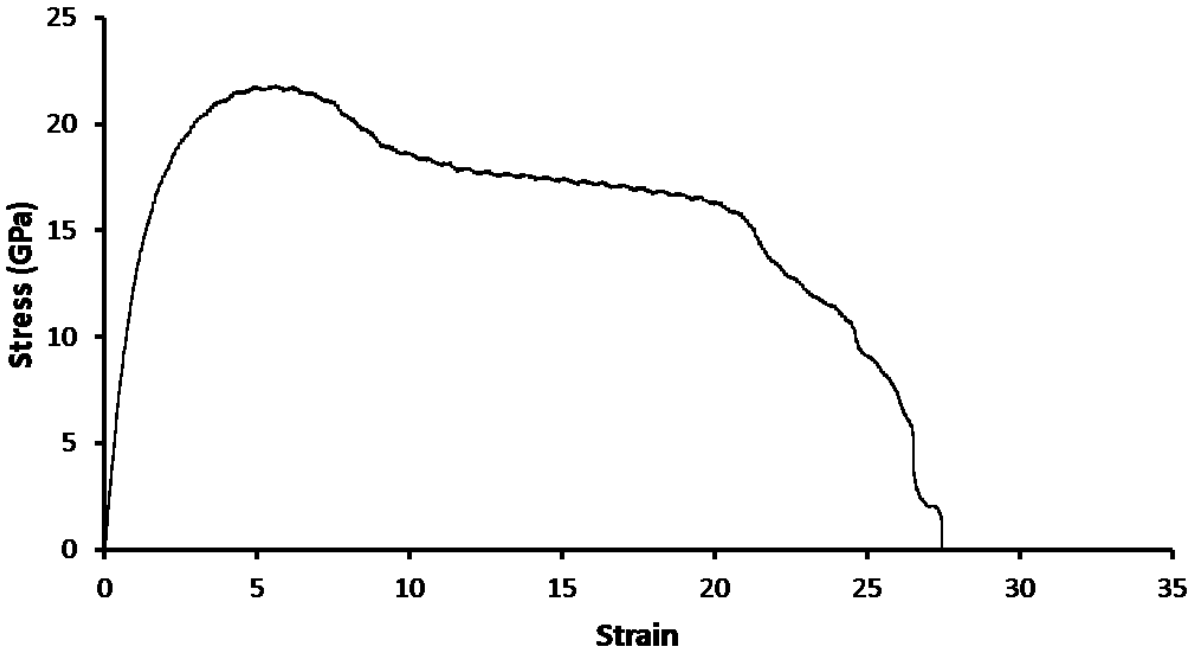

Figure 5-4. Stress vs. Strain Curve of 6% wt/wt CNC Melt Mixed with PE

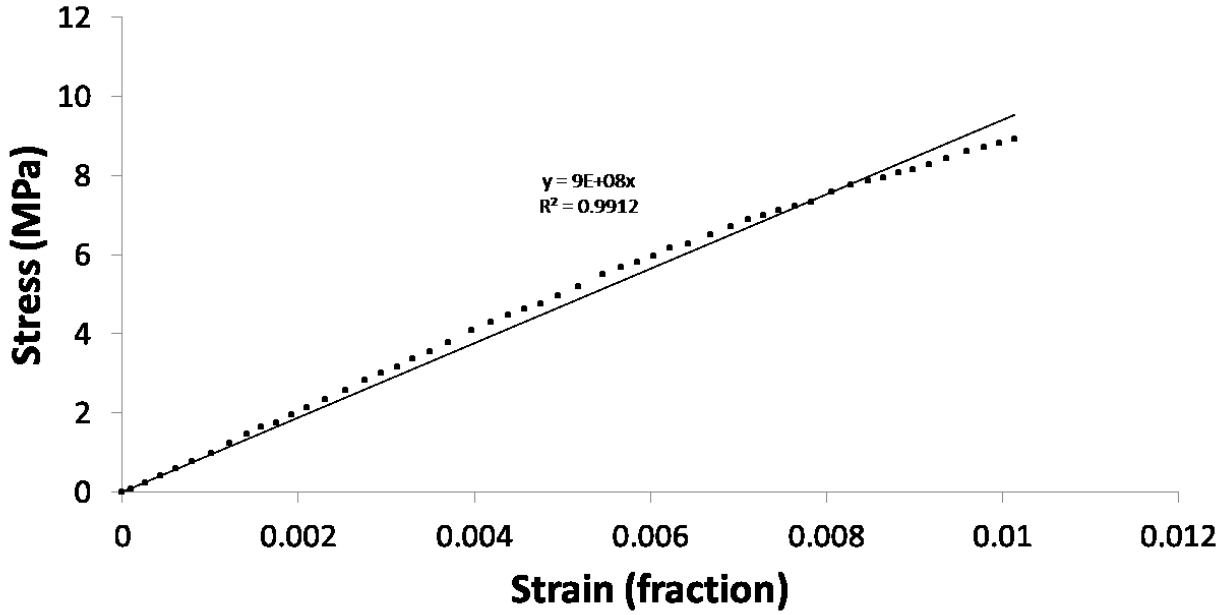

Figure 5-5. Stress vs. Strain in Elastic Region of 6% CNC Melt Mixed in PE. The dots are the original data points and the solid line through the data is the linear least-squares fit.

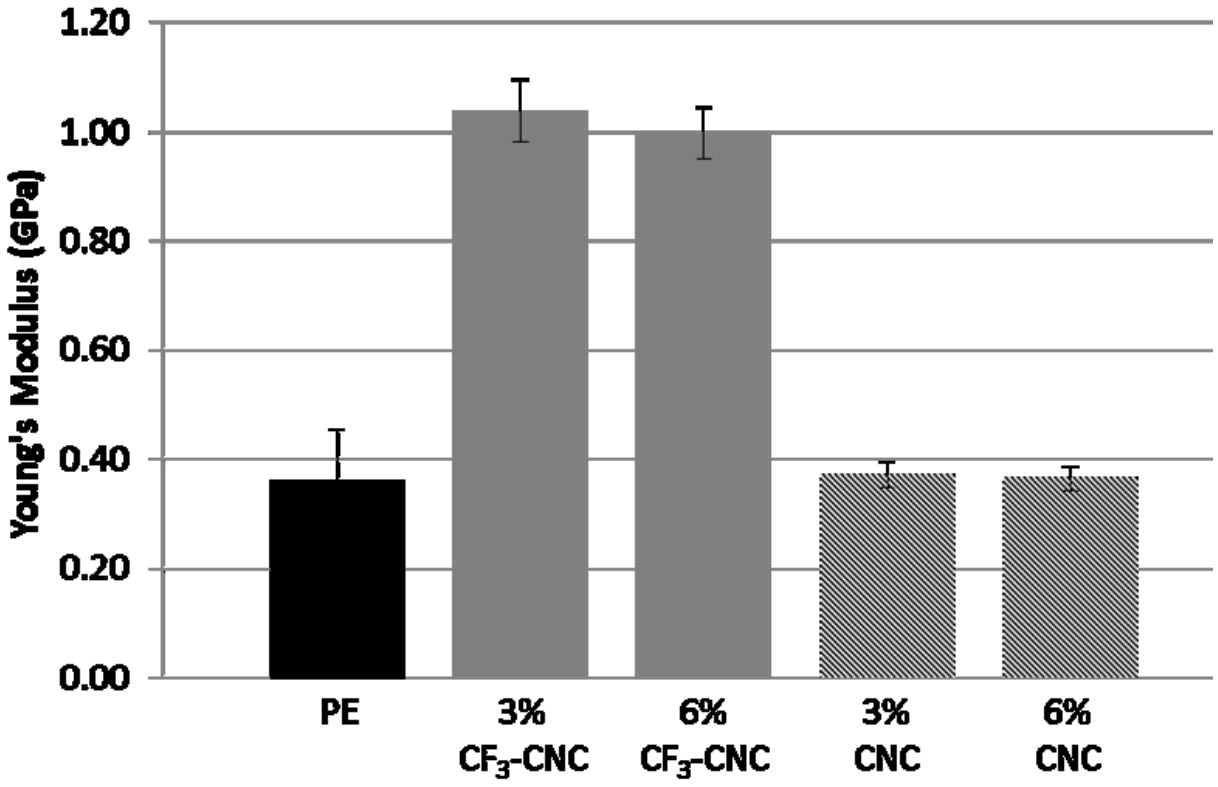

Figure 5-6. Young's Modulus of Polyethylene (PE), PE mixed with CNC, and PE mixed with CF_3 modified CNC.

Any stress applied to the ribbon, it would be focused through the PE network and not through the CNC. The higher Young's modulus of the modified CNC is consistent with well-dispersed nanoparticles and stronger interactions between the CF_3-CNC and the matrix. This allows an applied force to be partially transferred through the network of modified CNC.

Other CNC-PE composites have been created. High pressure steam extruded MCC-powdered LDPE composites with 5-10% cellulose content were prepared and yield a Young's modulus between 0.200 and 0.250 GPa, however a virgin material was not tested for comparison.[103] Poor adhesion between the unmodified cellulose and the matrix was observed and their reported mechanical enhancement results can be improved with an appropriate additive. Nanofibrillated cellulose and bacterial cellulose epoxy resin composites with around 50% volume cellulose additive increased the Young's modulus from 3.9 GPa for neat resin to 7.1 and 8.5 GPa for BC and NFC respectively.[187] HDPE and Kraft pulp (fiber sized from 0.1 to 1.0 mm) shows an increase in tensile modulus from less than 2 GPa to just under 5 GPa at 40% pulp.[188]

The nanocomposite ribbons created in this Chapter can be modeled by representing each mass fraction by its respective Young's modulus by the Rule of Mixtures. The Rule of Mixtures predicts the expected Young's modulus as a sum of each of the components represented by their mass fraction. From Figure 5-7 the Young's modulus of the native PE is 0.36 ± 0.09 GPa. The Young's modulus of CNC is between 120 – 170 GPa.[50] Using spectroscopic information Eichhorn and coworkers determined the modulus of cotton CNC to be 105 GPa[37] and will make a suitable reference for this system.

Applying these values to the Rule of Mixtures yields the following predictions:

3% CF_3-CNC: $(0.970 \text{ x } 0.36 \text{ GPa}) + (0.030 \text{ x } 105 \text{ GPa}) = 3.5 \text{ GPa}$ 5-1

6% CF_3-CNC: $(0.940 \text{ x } 0.36 \text{ GPa}) + (0.060 \text{ x } 105 \text{ GPa}) = 6.6 \text{ GPa}$ 5-2

The experimental values for the composites of 3% and 6% CF_3-CNC-PE are 1.0 ± 0.6 GPa and 1.0 ± 0.5 GPa, respectively. The lack of agreement between our experimental results and this relatively simple model is likely due to the random orientation of the rod-like CNC particles within in the polymer. The model assumes that all particles are aligned in the direction of tension.

An approach to account for random fiber orientation is the Nielson modified Halpin-Tsai equation.[189,190]

$$E_c = E_m \left[\frac{1 + A\eta V_f}{1 - \Psi\eta V_f}\right] \quad 5\text{-}3$$

Where

$$\Psi = 1 + \left(\frac{1 - \Phi_{max}}{\Phi_{max}^2}\right) V_f \quad 5\text{-}4$$

$$\eta = \left(\frac{\frac{E_f}{E_m} - 1}{\frac{E_f}{E_m} + A}\right) \quad 5\text{-}5$$

$$A = 2\frac{l}{d} \quad 5\text{-}6$$

In these equations, *l* and *d* are the length and diameter of the particles, E_c is the elastic modulus of the composite, E_f is the elastic modulus of the particles and E_m is the elastic modulus of the matrix. V_f is the volume fraction of the CNC to matrix. Φ_{max} is the maximum packing fraction of reinforcement. This value is taken as 0.82 for randomly oriented fibers.[191] These films were prepared using mass fractions but the densities of both materials are well known so estimating V_f is straightforward. The densities of polystyrene and CNC are 1.05[163] and 1.6 g/mL[7], respectively. A mass percentage of 3.0% CNC is equal to 2.0 % by volume and 6.0% CNC by mass is equal to 4.0% by volume.

The Nielson modified Halpin-Tsai equation yields a theoretical Young's modulus of 0.62 GPa for 3% CF_3-CNC in PE and 0.90 GPa for 6% CF_3-CNC in PE. The improved accuracy of this equation when compared to the Rule of Mixtures supports that the fibers are not completely aligned in the direction of tension which is what would be expected for a composite material extruded in this manner.

Ultimate tensile strength

Figure 5-7 shows representative stress strain curve for virgin PE, PE mixed with 3% unmodified CNC, and PE mixed with 3% TFMB modified CNC. Figure 5-6 clearly shows the differences in Young's modulus discussed above. These curves all exhibit a similar maximum stress indicating similar ultimate tensile strengths (UTS).

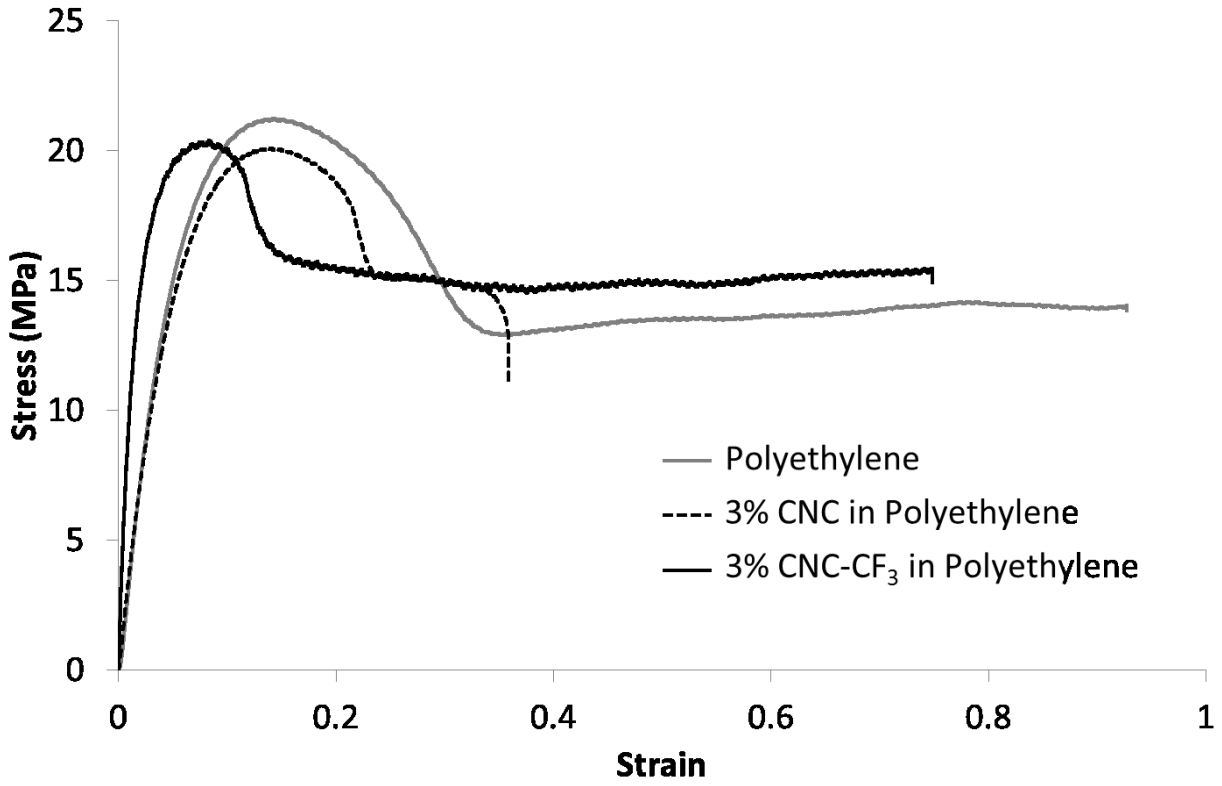

Figure 5-7. Stress strain curves for virgin PE, 3% CNC in PE, and 3% CF_3 modified CNC in PE.

Figure 5-8 plots the UTS for all the samples. The reported UTS for HDPE is around 21 MPa[186], which is similar to the virgin PE measured here, 18 ± 0.6 MPa. Across all samples there is no statistical difference in the UTS. Although the modified CNC provided a stiffer sample, as seen from the increase in Young's modulus, the maximum pressure it can withstand before yielding remained the same. Once stretched past the elastic region any high aspect ratio additives will begin to orient along the axis of elongation which requires slippage between the matrix and the additive and ultimately compromises the integrity of the matrix-additive interphase. As elongation increases the stress is transferred less so through the ridged CNC network more so through the PE. This provides evidence that the added CNC does not bear stress after the sample is elongated past the strain of the UTS but does bear load in within the elastic region.

Elongation and Tensile Strength at Break

Another figure of strength visible in Figure 5-7 is the elongation at break (the distance the ribbon can be stretched before it breaks) and the corresponding tensile strength at which this occurs. All three samples show similar tensile strength at break but different elongation at break. Incorporating unmodified CNC decreases the elongation at break considerably. This is consistent with having voids in the PE as poor CNC-PE adhesion is expected. The CF_3-CNC decreases elongation at break also but not to the same extent indicating better additive-matrix adhesion. The similar tensile strengths at break indicate that at this point the material bearing the load is PE and the added CNC offer little strength to this value. This is consistent with a sample where embedded rods are no longer adhered to the matrix and thus cannot bear load. As a comparison value,

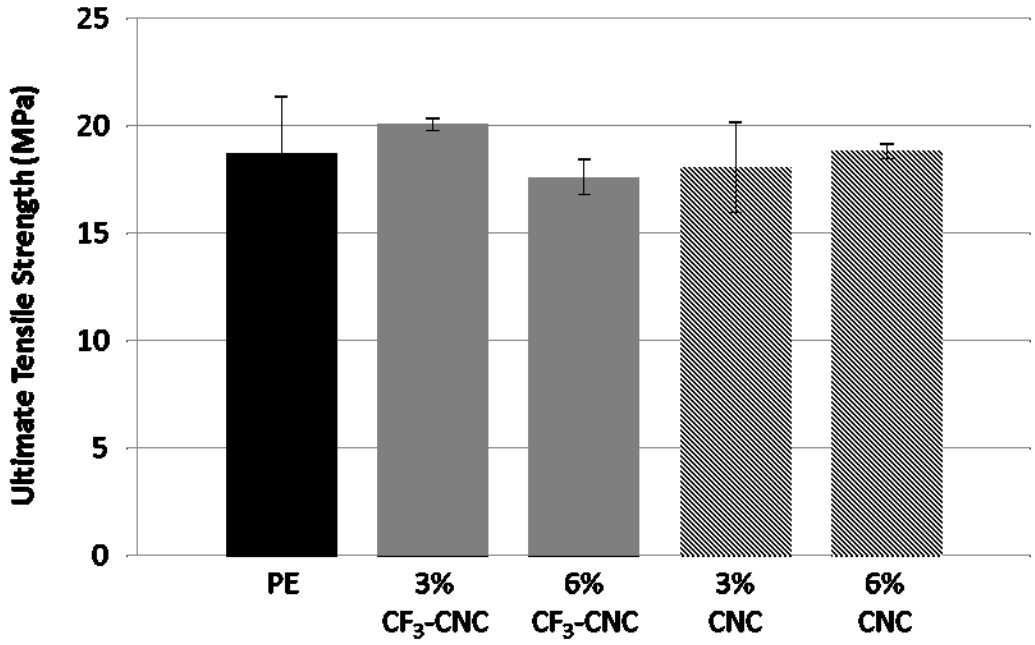

Figure 5-8. Ultimate Tensile Strength (UTS) of polyethylene (PE), PE mixed with CNC, and PE mixed with CNC modified CF_3.

MFC with fiber lengths of 240 μm were surface modified with silanes or benzoyl peroxide under various temperatures to create LLDPE composites that had yield strengths ranging between 10 and 20 MPa.[192] This is in the range of the current work as all composites and virgin material broke at stresses between 13 and 15 MPa.

Conclusion

The modification of CNC with diazonium cations is novel and effective. This work details modified CNC's increased miscibility with non-polar polymers, something that is difficult to achieve at an economic cost. Modifying CNC with a trifluoromethyl benzene group offers a mechanical advantage when forming composite materials via melt mixing with HPDE. The CF_3-CNC-PE nanocomposites that were extruded show an increase in Young's modulus of 2.7 times, from 3.6 ± 0.9 GPa to 1.0 ± 0.6 GPa. There was no change in the ultimate tensile strength and a decrease in elongation at failure with little change in tensile strength at failure. The Rule of Mixtures for the Young's modulus is within broad agreement while the Nielson modified Halpin-Tsai prediction is more accurate. This supports an increase in the strength of the interfacial interactions between the modified CNC-PE to that of unmodified CNC-PE. These interactions are still not as strong as those between PE chains making these composites less ductile. When observed with the naked eye, both the unmodified and modified CNC PE composites revealed aggregates. These were much larger in the unmodified ribbons. The task remains to further increase the mixing of the CNC within the PE to take full advantage of the superior mechanical properties that CNC can offer when employed as an additive to conventional thermoplastic polymers.

The temperatures used in this extrusion process are below that at which cellulose decomposes but these effects on the modified cellulose need to be investigated further. Other non-polar polymers such as polystyrene could be reinforced in a similar fashion with the introduction of this family of modified CNCs.

Chapter 6 Conclusion

The preceding collection of work outlines a small area of the total interest in taking advantage of the world's most abundant polymer. Each chapter contains its own conclusion that specifically summarizes the work done. This conclusion will serve as a field overview and will outline some of the bigger picture items that the above work served to advance. The scope of study of this nanoscale material is so broad and with so many applications that one could spend a lifetime reading peer-reviewed work without being inconvenienced to cover any material twice. Tangents of fundamental applications branch into industry to a level only limited by the imagination of the user. Focusing the dendroid nature of these innumerable avenues of application comes down to an economic balance between cost of manufacturing and the value that is added by this green incorporation. For this reason, the movement to advance material properties on account of CNC has not yet become common place. However, with the continued understanding, from harvesting to final product, of this ubiquitous polymer the uncertain potential can be realized and contribute to a future of materials to allow mankind to thrive in the next century and beyond. The challenges that encompass this field are solvable when approached with perseverance and ingenuity.

Government initiatives have been instrumental in moving towards connections between fundamental research and business. In Canada, ArboraNano has provided funding to this end with the Government of Canada's Business-led Centres of Excellence, FPInnovations and NanoQuebec.[193] In Finland, the Finnish Centre for Nanocellulose Technologies was established by the federal VTT Technical Research Center of

Finland, Aalto University UMP.[194] In the US, the National Nanotechnology Initiative (NNI) and within it the U.S. Department of Agriculture (USDA) serves to bridge the gap between science and industry.[195] In a more international role, the Technology Association of the Pulp and Paper Industry (TAPPI) has diverted much of its attention on this growing field of nano cellulose from its founding role of sharing industrial pulp and paper ideas. It brings together science and industry in an annual conference held around the world.[196] Continuing and expanding these collaborations and idea sharing will expedite the presentation of nano cellulose enhanced material to the world.

There are a wide variety of raw materials that can be exploited as a source for nano cellulose material. Some of these are waste byproducts of current industrial processes such as wood chips from lumber mills or pulp from pulp and paper manufacturers. From these different sources a variety of unique nano materials can result from the isolation process. Challenges for this genesis of cellulose nanomaterials research include improved consistency of isolated CNC with regards to internal damage of crystalline regions and size range of the final products. The implications of altering the surface of individual nano particles has been studied exhaustively and consistency will allow a more reproducible end product. Additional challenges include decreasing the cost of the extraction process while scaling to industrial volumes. Steps have been made towards these improvements with pilot plants opening and testing the potential of different methods including chemical treatment and chemical recycling.

Each area of study of cellulose nanomaterials has room for improvement. An improvement to one area might also allow new corridors for another with a cascade of improvement. For instance, if some of the challenges mentioned in the preceding

paragraph are address they could allow easier nanoparticle functionalization. This could be in the form of more complete surface reactions or at least more controllable ones that could be tailored to suit compatibility needs of certain systems. Using CNC as a composite carries all the uncertainty and property distributions of the individual particles. Since the end product's properties are a complicated collusion of many parameters, controlling them individually will invariably lead to more tunable materials. A further understanding of the interactions of cellulose nanomaterials with both themselves and with various matrix surfaces, that would be encountered when incorporated as an additive, would be of great value in advancing the field. These interactions on the nano particle scale are of obvious importance but so too are the macroscopic distributions of CNCs within a material. This is a rather difficult property to measure as it needs to be cross-sectioned or monitored in some way that penetrates the sample. AFM and EM are possible methods to probe distributions but suffer from lack of differentiation between the matrix and the cellulose. For the former, no imagine techniques that penetrate have sufficient resolution to imply information about the location of something as small as CNC. Ultimately, a well dispersed CNC will be characterized in whatever final material it is in, but understanding the step-by-step intricacies of its creation can help direct a method to a higher preforming product.

The field of characterizing individual cellulose nano particles and also materials made with its inclusion is possibly one of the areas that require the least advancement. This is largely in part owing to the fact that the techniques used have been developed externally and are well understood. This is especially true for characterizing macroscopic materials such as films or solid blocks, mechanical engineering has a

battery of tests to understand a materials bulk properties. Specifically to individual CNC or MFC, the exact structure is not readily interpretable. There are many crystal allomorphs that exist in non-identical sections and the nature of the crystal to connect these sections is speculative at best. That being said there is a growing understanding of the atomic configuration, something that the work presented in this thesis has advanced. By furthering this fundamental insight, projections towards other aspects can be better predicted. This includes all steps from raw source isolation to final product. This will be most valuable in modelling applications that require atomic positions to predict activities and properties of certain cellulose materials.

The work presented here provides new insight on the interactions between CNC and other materials through a method not previously applied to the structural analysis of cellulose, IRRAS. The results are complimentary to a wealth of previous infrared experiments with the introduction of bond orientation enhancement. This allowed the IR band assignments of previously inconclusive bands. Furthermore, this technique was expanded to permit a method of empirically monitoring the self-adsorption of CNC to controlled organic surfaces. This information was then used to compare the adsorption nature of several modified CNC and gain insight into mixing them with a hydrophobic polymer, namely polyethylene. Finally, the same modified CNC were melt-mixed with PE and the final product properties were explored.

This work provides advancement in the areas of structural characterization as well as monitoring both CNC-CNC interactions and CNC-functional group interactions. This fundamental work is necessary for the field to fully realize and implement the awesome potential of nanocrystalline cellulose.

Future Direction

Applications of the work described in this thesis lend themselves to the continued interest of finding a profitable industrial use that harnesses the unique property set of CNC. Proof of concept as an additive that offers a mechanical advantage is a proper first step in that direction. Projects involving the common hydrophilic polymer polystyrene and more specifically expanded polystyrene (EPS), trademark named as Styrofoam®, have been realized and funded. This work will attempt to use a surface modification to permit dispensability of CNC into a suspension polymerization of styrene monomer that will hopefully yield a more durable foam product. In exchange for the added price of production this process could offer longer lifetimes, increased vapor barrier properties and of course an increase in mechanical properties. Commercial applications of such foam would be useful when considering the lifetime expectancy of permanent concrete forms that are made of styrene which add insulation and water protection to a concrete foundation. Other areas include high impact foams for more mechanically demanding systems.

References

(1) Nickerson, R.; Habrle, J. Cellulose Intercrystalline Structure. *Industrial & Engineering Chemistry* **1947**, *39*, 1507–1512.

(2) Rånby, B. G.; Banderet, A.; Sillén, L. G. Aqueous Colloidal Solutions of Cellulose Micelles. **1949**.

(3) Rubinstein, C. V.; Gerrienne, P.; de la Puente, Gs.; Astini, R.; Steemans, P. Early Middle Ordovician Evidence for Land Plants in Argentina (eastern Gondwana). *New Phytologist* **2010**, *188*, 365–369.

(4) Taylor, T. N.; Osborn, J. M. The Importance of Fungi in Shaping the Paleoecosystem. *Review of Palaeobotany and Palynology* **1996**, *90*, 249–262.

(5) O'Sullivan, A. C. Cellulose: The Structure Slowly Unravels. *Cellulose* **1997**, *4*, 173–207.

(6) Ranby, B. G. Aqueous Colloidal Solutions of Cellulose Micelles. *Acta Chemica Scandinavica* **1949**, *3*, 649–650.

(7) Moon, R. J.; Martini, A.; Nairn, J.; Youngblood, J. Cellulose Nanomaterials Review: Structure, Properties and Nanocomposites. *Chemical Society Reviews* **2011**, *40*, 3941–3994.

(8) Klemm, D.; Heublein, B.; Fink, H.-P.; Bohn, A. Cellulose: Fascinating Biopolymer and Sustainable Raw Material. *Angewandte Chemie International Edition* **2005**, *44*, 3358–3393.

(9) Davis, W.; Barry, A.; Peterson, F.; King, A. X-Ray Studies of Reactions of Cellulose in Non-Aqueous Systems. II. Interaction of Cellulose and Primary Amines. *Journal of the American Chemical Society* **1943**, *65*, 1294–1299.

(10) Stipanovic, A. J.; Sarko, A. Packing Analysis of Carbohydrates and Polysaccharides. 6. Molecular and Crystal Structure of Regenerated Cellulose II. *Macromolecules* **1976**, *9*, 851–857.

(11) Wada, M.; Nishiyama, Y.; Chanzy, H.; Forsyth, T.; Langan, P. The Structure of Celluloses. *Powder Diffraction* **2008**, *23*, 92–95.

(12) Atalla, R. H.; Vanderhart, D. L. Native Cellulose: A Composite of Two Distinct Crystalline Forms. *Science* **1984**, *223*, 283.

(13) Sugiyama, J.; Vuong, R.; Chanzy, H. Electron Diffraction Study on the Two Crystalline Phases Occurring in Native Cellulose from an Algal Cell Wall. *Macromolecules* **1991**, *24*, 4168–4175.

(14) Horii, F.; Yamamoto, H.; Kitamaru, R.; Tanahashi, M.; Higuchi, T. Transformation of Native Cellulose Crystals Induced by Saturated Steam at High Temperatures. *Macromolecules* **1987**, *20*, 2946–2949.

(15) Sugiyama, J.; Persson, J.; Chanzy, H. Combined Infrared and Electron Diffraction Study of the Polymorphism of Native Celluloses. *Macromolecules* **1991**, *24*, 2461–2466.

(16) Horii, F.; Hirai, A.; Kitamaru, R. CP/MAS Carbon-13 NMR Spectra of the Crystalline Components of Native Celluloses. *Macromolecules* **1987**, *20*, 2117–2120.

(17) VanderHart, D. L.; Atalla, R. Studies of Microstructure in Native Celluloses Using Solid-State Carbon-13 NMR. *Macromolecules* **1984**, *17*, 1465–1472.

(18) Marrinan, H.; Mann, J. Infrared Spectra of the Crystalline Modifications of Cellulose. *Journal of polymer science* **1956**, *21*, 301–311.

(19) Nishiyama, Y.; Sugiyama, J.; Chanzy, H.; Langan, P. Crystal Structure and Hydrogen Bonding System in Cellulose 1(alpha), from Synchrotron X-Ray and Neutron Fiber Diffraction. *Journal of the American Chemical Society* **2003**, *125*, 14300–14306.

(20) Wada, M. Lateral Thermal Expansion of Cellulose I Beta and III1 Polymorphs. *Journal of Polymer Science Part B: Polymer Physics* **2002**, *40*, 1095–1102.

(21) Michell, A. J. Second-Derivative FT-IR Spectra of Native Celluloses. *Carbohydrate Research* **1990**, *197*, 53–60.

(22) Yamamoto, H.; Horii, F. CP/MAS I3C NMR Analysis of the Crystal Transformation Induced for Vdonia Cellulose by Annealing at High Temperatures. *Society* **1993**, 1313–1317.

(23) Elazzouzi-Hafraoui, S.; Nishiyama, Y.; Putaux, J.-L.; Heux, L.; Dubreuil, F.; Rochas, C. The Shape and Size Distribution of Crystalline Nanoparticles Prepared by Acid Hydrolysis of Native Cellulose. *Biomacromolecules* **2007**, *9*, 57–65.

(24) Saito, T.; Nishiyama, Y.; Putaux, J.-L.; Vignon, M.; Isogai, A. Homogeneous Suspensions of Individualized Microfibrils from TEMPO-Catalyzed Oxidation of Native Cellulose. *Biomacromolecules* **2006**, *7*, 1687–1691.

(25) Nishiyama, Y.; Langan, P.; Chanzy, H. Crystal Structure and Hydrogen-Bonding System in Cellulose I Beta from Synchrotron X-Ray and Neutron Fiber Diffraction. *Journal of the American Chemical Society* **2002**, *124*, 9074–9082.

(26) Dogsa, I.; Tomsic, M.; Orehek, J.; Benigar, E.; Jamnik, A.; Stopar, D. Amorphous Supramolecular Structure of Carboxymethyl Cellulose in Aqueous Solution at Different pH Values as Determined by Rheology, Small Angle X-Ray and Light Scattering. *Carbohydrate Polymers* **2014**.

(27) Beck-Candanedo, S.; Roman, M.; Gray, D. G. Effect of Reaction Conditions on the Properties and Behavior of Wood Cellulose Nanocrystal Suspensions. *Biomacromolecules* **2005**, *6*, 1048–1054.

(28) Dong, X. M.; Revol, J.; Gray, D. G. Effect of Microcrystallite Preparation Conditions on the Formation of Colloid Crystals of Cellulose. *Cellulose* **1998**, *5*, 19–32.

(29) Araki, J.; Wada, M.; Kuga, S.; Okano, T. Birefringent Glassy Phase of a Cellulose Microcrystal Suspension. *Langmuir* **2000**, *16*, 2413–2415.

(30) Postek, M. T.; Moon, R. J.; Rudie, A. W.; Bilodeau, M. A. *Production and Applications of Cellulose Nanomaterials*; 2013.

(31) Saito, T.; Kimura, S.; Nishiyama, Y. Cellulose Nanofibers Prepared by TEMPO-Mediated Oxidation of Native Cellulose. *Biomacromolecules* **2007**, *8*, 2485–2491.

(32) Habibi, Y.; Chanzy, H.; Vignon, M. R. TEMPO-Mediated Surface Oxidation of Cellulose Whiskers. *Cellulose* **2006**, *13*, 679–687.

(33) Diddens, I.; Murphy, B.; Krisch, M.; Müller, M. Anisotropic Elastic Properties of Cellulose Measured Using Inelastic X-Ray Scattering. *Macromolecules* **2008**, *41*, 9755–9759.

(34) Matsuo, M.; Sawatari, C.; Iwai, Y.; Ozaki, F. Effect of Orientation Distribution and Crystallinity on the Measurement by X-Ray Diffraction of the Crystal Lattice Moduli of Cellulose I and II. *Macromolecules* **1990**, *23*, 3266–3275.

(35) Sakurada, I.; Nukushina, Y.; Ito, T. Experimental Determination of the Elastic Modulus of Crystalline Regions in Oriented Polymers. *Journal of Polymer Science* **1962**, *57*, 651–660.

(36) Hsieh, Y.-C.; Yano, H.; Nogi, M.; Eichhorn, S. An Estimation of the Young's Modulus of Bacterial Cellulose Filaments. *Cellulose* **2008**, *15*, 507–513.

(37) Rusli, R.; Eichhorn, S. J. Determination of the Stiffness of Cellulose Nanowhiskers and the Fiber-Matrix Interface in a Nanocomposite Using Raman Spectroscopy. *Applied Physics Letters* **2008**, *93*, 033111.

(38) Sturcová, A.; Davies, G. R.; Eichhorn, S. J. Elastic Modulus and Stress-Transfer Properties of Tunicate Cellulose Whiskers. *Biomacromolecules* **2005**, *6*, 1055–1061.

(39) Eichhorn, S.; Young, R. The Young's Modulus of a Microcrystalline Cellulose. *Cellulose* **2001**, *8*, 197–207.

(40) Iwamoto, S.; Kai, W.; Isogai, A.; Iwata, T. Elastic Modulus of Single Cellulose Microfibrils from Tunicate Measured by Atomic Force Microscopy. *Biomacromolecules* **2009**, *10*, 2571–2576.

(41) Lahiji, R. R.; Xu, X.; Reifenberger, R.; Raman, A.; Rudie, A.; Moon, R. J. Atomic Force Microscopy Characterization of Cellulose Nanocrystals. *Langmuir* **2010**, *26*, 4480–4488.

(42) Postek, M. T.; Vladár, A.; Dagata, J.; Farkas, N.; Ming, B.; Wagner, R.; Raman, A.; Moon, R. J.; Sabo, R.; Wegner, T. H.; *et al.* Development of the Metrology and Imaging of Cellulose Nanocrystals. *Measurement Science and Technology* **2011**, *22*, 024005.

(43) George, J.; Sreekala, M.; Thomas, S. A Review on Interface Modification and Characterization. *Polymer engineering and science* **2001**, *41*.

(44) Kvien, I.; Tanem, B. Characterization of Cellulose Whiskers and Their Nanocomposites by Atomic Force and Electron Microscopy. *Biomacromolecules* **2005**, 3160–3165.

(45) Boluk, Y.; Danumah, C. Analysis of Cellulose Nanocrystal Rod Lengths by Dynamic Light Scattering and Electron Microscopy. *Journal of nanoparticle research* **2014**, *16*, 1–7.

(46) Elazzouzi-Hafraoui, S.; Nishiyama, Y.; Putaux, J. L.; Heux, L.; Dubreuil, F.; Rochas, C. The Shape and Size Distribution of Crystalline Nanoparticles Prepared by Acid Hydrolysis of Native Cellulose. *Biomacromolecules* **2007**, *9*, 57–65.

(47) Marchessault, R.; Morehead, F.; Walter, N. Liquid Crystal Systems from Fibrillar Polysaccharides. **1959**.

(48) Shopsowitz, K. E.; Qi, H.; Hamad, W. Y.; MacLachlan, M. J. Free-Standing Mesoporous Silica Films with Tunable Chiral Nematic Structures. *Nature* **2010**, *468*, 422–425.

(49) Dong, X. M.; Kimura, T.; Revol, J.-F.; Gray, D. G. Effects of Ionic Strength on the Isotropic-Chiral Nematic Phase Transition of Suspensions of Cellulose Crystallites. *Langmuir* **1996**, *12*, 2076–2082.

(50) Lin, N.; Huang, J.; Dufresne, A. Preparation, Properties and Applications of Polysaccharide Nanocrystals in Advanced Functional Nanomaterials: A Review. *Nanoscale* **2012**, *4*, 3274–3294.

(51) De Souza Lima, M. M.; Borsali, R. Rodlike Cellulose Microcrystals: Structure, Properties, and Applications. *Macromolecular Rapid Communications* **2004**, *25*, 771–787.

(52) Herschel, W. Experiments on the Refrangibility of the Invisible Rays of the Sun. By William Herschel, LL. DFRS. *Philosophical Transactions of the Royal Society of London* **1800**, 284–292.

(53) Francis, S.; Ellison, A. Infrared Spectra of Monolayers on Metal Mirrors. *JOSA* **1959**, *49*, 131–137.

(54) Pearce, H.; Sheppard, N. The Interpretation of the Infrared Spectra of Molecules Adsorbed on Particulate Metals; Infrared Spectra from Ethylene Chemisorbed on Silica-Supported Metal Catalysts. *Surface Science* **1976**, *59*, 205–217.

(55) Greenler, R. G. Infrared Study of Adsorbed Molecules on Metal Surfaces by Reflection Techniques. *The Journal of Chemical Physics* **1966**, *44*, 310.

(56) Porter, M.; Bright, T.; Allara, D.; Kuwana, T. Quantitative Aspects of Infrared External Reflection Spectroscopy: Polymer/glassy Carbon Interface. *Analytical Chemistry* **1986**, *58*, 2461–2465.

(57) Greenler, R. G. Reflection Method for Obtaining the Infrared Spectrum of a Thin Layer on a Metal Surface. *The Journal of Chemical Physics* **1969**, *50*, 1963.

(58) Pradier, C.; Salmain, M.; Zheng, L.; Jaouen, G. Specific Binding of Avidin to Biotin Immobilised on Modified Gold Surfaces: Fourier Transform Infrared Reflection Absorption Spectroscopy Analysis. *Surface science* **2002**, *503*, 193–202.

(59) Gilli, E.; Horvath, A. E.; Horvath, A. T.; Hirn, U.; Schennach, R. Analysis of CMC Attachment onto Cellulosic Fibers by Infrared Spectroscopy. *Cellulose* **2009**, *16*, 825–832.

(60) Mielczarski, J. A.; Mielczarski, E. Infrared External Reflection Spectroscopy of Adsorbed Monolayers in a Region of Strong Absorption of Substrate. *Journal of Physical Chemistry B* **1999**, *103*, 5852–5859.

(61) Kasai, W.; Tsutsumi, K.; Morita, M.; Kondo, T. Orientation of the Alkyl Side Chains and Glucopyranose Rings in Langmuir-Blodgett Films of a Regioselectively Substituted Cellulose Ether. *Colloid and Polymer Science* **2008**, *286*, 707–712.

(62) Foston, M. Advances in Solid-State NMR of Cellulose. *Current opinion in biotechnology* **2014**, *27*, 176–184.

(63) Atalla, R. H.; VanderHart, D. L. The Role of Solid State C-13 NMR Spectroscopy in Studies of the Nature of Native Celluloses. *Solid State Nuclear Magnetic Resonance* **1999**, *15*, 1–19.

(64) Wada, M.; Okano, T.; Sugiyama, J. Synchrotron-Radiated X-Ray and Neutron Diffraction Study of Native Cellulose. *Cellulose* **1997**, *4*, 221–232.

(65) Nishiyama, Y.; Langan, P.; Chanzy, H. Crystal Structure and Hydrogen-Bonding System in Cellulose 1 Beta from Synchrotron X-Ray and Neutron Fiber Diffraction. *Journal of the American Chemical Society* **2002**, *124*, 9074–9082.

(66) Xu, F.; Shi, Y.-C.; Wang, D. X-Ray Scattering Studies of Lignocellulosic Biomass: A Review. *Carbohydrate polymers* **2013**, *94*, 904–917.

(67) Kavcuráková, M.; Wilson, R. Developments in Mid-Infrared FT-IR Spectroscopy of Selected Carbohydrates. *Carbohydrate Polymers* **2001**, *44*, 291–303.

(68) Gu, J.; Catchmark, J. M.; Kaiser, E. Q.; Archibald, D. D. Quantification of Cellulose Nanowhiskers Sulfate Esterification Levels. *Carbohydrate polymers* **2013**, *92*, 1809–1816.

(69) Schulz, H.; Baranska, M. Identification and Quantification of Valuable Plant Substances by IR and Raman Spectroscopy. *Vibrational Spectroscopy* **2007**, *43*, 13–25.

(70) Gierlinger, N.; Schwanninger, M. The Potential of Raman Microscopy and Raman Imaging in Plant Research. *Spectroscopy* **2007**, *21*, 69–89.

(71) Agarwal, U. P.; Reiner, R. S.; Ralph, S. A. Cellulose I Crystallinity Determination Using FT–Raman Spectroscopy: Univariate and Multivariate Methods. *Cellulose* **2010**, *17*, 721–733.

(72) Agarwal, U. P.; Reiner, R. S. Near-IR Surface-Enhanced Raman Spectrum of Lignin. *Journal of Raman Spectroscopy* **2009**, *40*, 1527–1534.

(73) Wiley, J.; Atalla, R. Band Assignments in the Raman Spectra of Celluloses. *Carbohydrate Research* **1987**, *160*, 113–129.

(74) O'Connor, R. T.; DuPré, E. F.; McCall, E. R. Infrared Spectrophotometric Procedure for Analysis of Cellulose and Modified Cellulose. *Analytical Chemistry* **1957**, *29*, 998–1005.

(75) Nelson, M. L.; O'Connor, R. T. Relation of Certain Infrared Bands to Cellulose Crystallinity and Crystal Lattice Type. Part II. A New Infrared Ratio for Estimation of Crystallinity in Celluloses I and II. *Journal of Applied Polymer Science* **1964**, *8*, 1325–1341.

(76) Lin, N.; Dufresne, A. Surface Chemistry, Morphological Analysis and Properties of Cellulose Nanocrystals with Gradiented Sulfation Degrees. *Nanoscale* **2014**, *6*, 5384–5393.

(77) Marechal, Y.; Chanzy, H. The Hydrogen Bond Network in I-Beta Cellulose as Observed by Infrared Spectrometry. *Journal of Molecular Structure* **2000**, *523*, 183–196.

(78) Agarwal, U. P.; Ralph, S. a. FT-Raman Spectroscopy of Wood: Identifying Contributions of Lignin and Carbohydrate Polymers in the Spectrum of Black Spruce (Picea Mariana). *Applied Spectroscopy* **1997**, *51*, 1648–1655.

(79) Woods, D. A.; Petkov, J.; Bain, C. D. Surfactant Adsorption by Total Internal Reflection Raman Spectroscopy. Part III: Adsorption onto Cellulose. *Colloids and Surfaces A: Physicochemical and Engineering Aspects* **2011**, *391*, 10–18.

(80) Kariuki, J. K.; McDermott, M. T. Formation of Multilayers on Glassy Carbon Electrodes via the Reduction of Diazonium Salts. *Langmuir* **2001**, *17*, 5947–5951.

(81) Anariba, F.; DuVall, S. H.; McCreery, R. L. Mono-and Multilayer Formation by Diazonium Reduction on Carbon Surfaces Monitored with Atomic Force Microscopy "scratching."*Analytical chemistry* **2003**, *75*, 3837–3844.

(82) Delamar, M.; Hitmi, R.; Pinson, J.; Saveant, J. M. Covalent Modification of Carbon Surfaces by Grafting of Functionalized Aryl Radicals Produced from Electrochemical Reduction of Diazonium Salts. *Journal of the American Chemical Society* **1992**, *114*, 5883–5884.

(83) Pinson, J.; Podvorica, F. Attachment of Organic Layers to Conductive or Semiconductive Surfaces by Reduction of Diazonium Salts. *Chemical Society Reviews* **2005**, *34*, 429–439.

(84) Bain, C. D.; Whitesides, G. M. Formation of Two-Component Surfaces by the Spontaneous Assembly of Monolayers on Gold from Solutions Containing Mixtures of Organic Thiols. *Journal of the american chemical society* **1988**, *110*, 6560–6561.

(85) Bain, C. D.; Troughton, E. B.; Tao, Y. T.; Evall, J.; Whitesides, G. M.; Nuzzo, R. G. Formation of Monolayer Films by the Spontaneous Assembly of Organic Thiols from Solution onto Gold. *Journal of the American Chemical Society* **1989**, *111*, 321–335.

(86) Lebec, V.; Landoulsi, J.; Boujday, S.; Poleunis, C.; Pradier, C.-M.; Delcorte, A. Probing the Orientation of Beta-Lactoglobulin on Gold Surfaces Modified by Alkyl Thiol Self-Assembled Monolayers. *The Journal of Physical Chemistry C* **2013**, *117*, 11569–11577.

(87) Porter, M.; Bright, T. Spontaneously Organized Molecular Assemblies. 4. Structural Characterization of N-Alkyl Thiol Monolayers on Gold by Optical Ellipsometry, Infrared Spectroscopy, and Electrochemistry. *Journal of the American \ldots* **1987**, *109*, 3559–3573.

(88) Folkers, J.; Laibinis, P.; Whitesides, G. Self-Assembled Monolayers of Alkanethiols on Gold: Comparisons of Monolayers Containing Mixtures of Short-and Long-Chain

Constituents with Methyl and Hydroxyl Terminal Groups. *Langmuir* **1992**, *8*, 1330–1341.

(89) Laibinis, P.; Nuzzo, R. G.; Whitesides, G. M. Structure of Monolayers Formed by Coadsorption of Two N-Alkanethiols of Different Chain Lengths on Gold and Its Relation to Wetting. *The Journal of Physical Chemistry* **1992**, *96*, 5097–5105.

(90) Nuzzo, R.; Allara, D. Adsorption of Bifunctional Organic Disulfides on Gold Surfaces. *Journal of the American Chemical Society* **1983**, *105*, 4481–4483.

(91) Widrig, C. A.; Alves, C. A.; Porter, M. D. Scanning Tunneling Microscopy of Ethanethiolate and N-Octadecanethiolate Monolayers Spontaneously Absorbed at Gold Surfaces. *Journal of the American Chemical Society* **1991**, *113*, 2805–2810.

(92) Bain, C. D.; Evall, J.; Whitesides, G. M. Formation of Monolayers by the Coadsorption of Thiols on Gold: Variation in the Head Group, Tail Group, and Solvent. *Journal of the American Chemical Society* **1989**, *111*, 7155–7164.

(93) Laibinis, P.; Whitesides, G. Comparison of the Structures and Wetting Properties of Self-Assembled Monolayers of N-Alkanethiols on the Coinage Metal Surfaces, Copper, Silver, and Gold. *Journal of the American Chemical Society* **1991**, *113*, 7152–7167.

(94) Ulman, A. Formation and Structure of Self-Assembled Monolayers. *Chemical reviews* **1996**, *96*, 1533–1554.

(95) Habibi, Y.; Lucia, L. a; Rojas, O. J. Cellulose Nanocrystals: Chemistry, Self-Assembly, and Applications. *Chemical reviews* **2010**, *110*, 3479–3500.

(96) Roy, D.; Semsarilar, M.; Guthrie, J. T.; Perrier, S. Cellulose Modification by Polymer Grafting: A Review. *Chemical Society Reviews* **2009**, *38*, 2046–2064.

(97) Padalkar, S.; Capadona, J.; Rowan, S. J.; Weder, C.; Won, Y.-H.; Stanciu, L. A.; Moon, R. J. Natural Biopolymers: Novel Templates for the Synthesis of Nanostructures. *Langmuir* **2010**, *26*, 8497–8502.

(98) Ljungberg, N.; Bonini, C.; Bortolussi, F.; Boisson, C.; Heux, L.; Cavaillé, J.-Y. New Nanocomposite Materials Reinforced with Cellulose Whiskers in Atactic Polypropylene: Effect of Surface and Dispersion Characteristics. *Biomacromolecules* **2005**, *6*, 2732–2739.

(99) Aulin, C.; Varga, I.; Claesson, P. M.; Wågberg, L.; Lindström, T. Buildup of Polyelectrolyte Multilayers of Polyethyleneimine and Microfibrillated Cellulose Studied by in Situ Dual-Polarization Interferometry and Quartz Crystal Microbalance with Dissipation. *Langmuir* **2008**, *24*, 2509–2518.

(100) Cranston, E. D.; Gray, D. G.; Rutland, M. W. Direct Surface Force Measurements of Polyelectrolyte Multilayer Films Containing Nanocrystalline Cellulose. *Langmuir* **2010**, *26*, 17190–17197.

(101) Lin, Z.; Renneckar, S.; Hindman, D. P. Nanocomposite-Based Lignocellulosic Fibers 1. Thermal Stability of Modified Fibers with Clay-Polyelectrolyte Multilayers. *Cellulose* **2008**, *15*, 333–346.

(102) Kondo, T.; Dumitriu, S. *Hydrogen Bonds in Cellulose and Cellulose Derivatives*; Dekker: New York, 1998.

(103) Soulestin, J.; Quiévy, N.; Sclavons, M.; Devaux, J. Polyolefins-Biofibre Composites: A New Way for an Industrial Production. *Polymer Engineering & Science* **2007**, *47*, 467–476.

(104) Ben Azouz, K.; Ramires, E. C.; Van den Fonteyne, W.; El Kissi, N.; Dufresne, A. Simple Method for the Melt Extrusion of a Cellulose Nanocrystal Reinforced Hydrophobic Polymer. *ACS Macro Letters* **2011**, *1*, 236–240.

(105) Hubbe, M. A.; Rojas, O. J.; Lucia, L. A.; Sain, M. Cellulosic Nanocomposites: A Review. *BioResources* **2008**, *3*, 929–980.

(106) Azizi Samir, M. A. S.; Alloin, F.; Sanchez, J.-Y.; El Kissi, N.; Dufresne, A. Preparation of Cellulose Whiskers Reinforced Nanocomposites from an Organic Medium Suspension. *Macromolecules* **2004**, *37*, 1386–1393.

(107) Schroers, M.; Kokil, A.; Weder, C. Solid Polymer Electrolytes Based on Nanocomposites of Ethylene Oxide-Epichlorohydrin Copolymers and Cellulose Whiskers. *Journal of applied polymer science* **2004**, *93*, 2883–2888.

(108) Smith, P.; Lemstra, P.; Pijpers, J.; Kiel, A. Ultra-Drawing of High Molecular Weight Polyethylene Cast from Solution. *Colloid and Polymer Science* **1981**, *259*, 1070–1080.

(109) Bastiaansen, C. Influence of Initial Polymer Concentration in Solution and Weight-Average Molecular Weight on the Drawing Behavior of Polyethylenes. *Journal of Polymer Science Part B: Polymer Physics* **1990**, *28*, 1475–1482.

(110) Zoppe, J. O.; Peresin, M. S.; Habibi, Y.; Venditti, R. A.; Rojas, O. J. Reinforcing Poly Poly(ε-Caprolactone) Nanofibers with Cellulose Nanocrystals. *ACS applied materials \& interfaces* **2009**, *1*, 1996–2004.

(111) Peresin, M. S.; Habibi, Y.; Zoppe, J. O.; Pawlak, J. J.; Rojas, O. J. Nanofiber Composites of Polyvinyl Alcohol and Cellulose Nanocrystals: Manufacture and Characterization. *Biomacromolecules* **2010**, *11*, 674–681.

(112) Rojas, O. J.; Montero, G. A.; Habibi, Y. Electrospun Nanocomposites from Polystyrene Loaded with Cellulose Nanowhiskers. *Journal of applied polymer science* **2009**, *113*, 927–935.

(113) Biermann, C. J.; Chung, J. B.; Narayan, R. Grafting of Polystyrene onto Cellulose Acetate by Nucleophilic Displacement of Mesylate Groups Using the Polystyrylcarboxylate Anion. *Macromolecules* **1987**, *20*, 954–957.

(114) Månsson, P.; Westfelt, L. Grafting of Monodisperse Low-Molecular-Weight Polystyrene onto Cellulose Acetate. *Journal of Polymer Science: Polymer Chemistry Edition* **1981**, *19*, 1509–1515.

(115) Forziati, F. H.; Rowen, J. W. Effect of Changes in Crystalline Structure on the Infrared Absorption Spectrum of Cellulose. *J. Res. Nat. Bur. Stand* **1951**, *46*, 38–42.

(116) Ellis, J. W.; Bath, J. Hydrogen Bridging in Cellulose as Shown by Infrared Absorption Spectra. *Journal of the American Chemical Society* **1940**, *62*, 2859–2861.

(117) Kondo, T. The Assignment of IR Absorption Bands due to Free Hydroxyl Groups in Cellulose. *Cellulose* **1997**, *4*, 281–292.

(118) Horikawa, Y.; Sugiyama, J. Localization of Crystalline Allomorphs in Cellulose Microfibril. *Biomacromolecules* **2009**, *10*, 2235–2239.

(119) Sekkal, M.; Dincq, V.; Legrand, P.; Huvenne, J. Investigation of the Glycosidic Linkages in Several Oligosaccharides Using FT-IR and FT Raman Spectroscopies. *Journal of molecular structure* **1995**, *349*, 349–352.

(120) Oh, S. Y.; Yoo, D. I.; Shin, Y.; Seo, G. FTIR Analysis of Cellulose Treated with Sodium Hydroxide and Carbon Dioxide. *Carbohydrate research* **2005**, *340*, 417–428.

(121) Oh, S. Y.; Yoo, D. I.; Shin, Y.; Kim, H. C.; Kim, H. Y.; Chung, Y. S.; Park, W. H.; Youk, J. H. Crystalline Structure Analysis of Cellulose Treated with Sodium Hydroxide and Carbon Dioxide by Means of X-Ray Diffraction and FTIR Spectroscopy. *Carbohydrate Research* **2005**, *340*, 2376–2391.

(122) Vasko, P. D.; Blackwell, J.; Koenig, J. Infrared and Raman Spectroscopy of Carbohydrates: Part I: Identification of O-H and C-H-Related Vibrational Modes for D-Glucose, Maltose, Cellobiose, and Dextran by Deuterium-Substitution Methods. *Carbohydrate Research* **1971**, *19*, 297–310.

(123) Sirok`y, J.; Blackburn, R. S.; Bechtold, T.; Taylor, J.; White, P. Attenuated Total Reflectance Fourier-Transform Infrared Spectroscopy Analysis of Crystallinity Changes in Lyocell Following Continuous Treatment with Sodium Hydroxide. *Cellulose* **2010**, *17*, 103–115.

(124) Baldinger, T.; Moosbauer, J.; Sixta, H. Supermolecular Structure of Cellulosic Materials by Fourier Transform Infrared Spectroscopy (FTIR) Calibrated by WAXS and 13 C NMR. *Lenzing Berichte* **2000**, *79*, 15–17.

(125) Nishiyama, Y. Structure and Properties of the Cellulose Microfibril. *Journal of Wood Science* **2009**, *55*, 241–249.

(126) Marchessault, R. H.; Liang, C. Y. Infrared Spectra of Crystalline Polysaccharides .3. Mercerized Cellulose. *Journal of Polymer Science* **1960**, *43*, 71–84.

(127) Liang, C. Y.; Marchessault, R. H. Infrared Spectra of Crystalline Polysaccharides. II. Native Celluloses in the Region from 640 to 1700 Cm-1. *Journal of Polymer Science* **1959**, *39*, 269–278.

(128) Liang, C.; Marchessault, R. Infrared Spectra of Crystalline Polysaccharides. I. Hydrogen Bonds in Native Celluloses. *Journal of polymer science* **1959**, *37*, 385–395.

(129) NIST database http://sdbs.db.aist.go.jp/sdbs/cgi-bin/cre_index.cgi (accessed Sep 2, 2014).

(130) Haxaire, K.; Marechal, Y.; Milas, M.; Rinaudo, A. Hydration of Polysaccharide Hyaluronan Observed by IR Spectrometry. I. Preliminary Experiments and Band Assignments. *Biopolymers* **2003**, *72*, 10–20.

(131) Michell, A. J. Second-Derivative FTIR Spectra of Native Celluloses from Valonia and Tunicin. *Carbohydrate research* **1993**, *241*, 47–54.

(132) Langkilde, F.; Svantesson, A. Identification of Celluloses with Fourier-Transform (FT) Mid-Infrared, FT-Raman and near-Infrared Spectrometry. *Journal of pharmaceutical and biomedical analysis* **1995**, *13*, 409–414.

(133) Mark, H.; Workman Jr, J. Chemometrics: Derivatives in Spectroscopy, Part I-The Behavior of the Derivative-The Authors Begin a New Series of Columns about Derivatives of Spectra. *Spectroscopy-Eugene* **2003**, *18*, 32–37.

(134) Kokot, S.; Czarnik-Matusewicz, B.; Ozaki, Y. Two-Dimensional Correlation Spectroscopy and Principal Component Analysis Studies of Temperature-Dependent IR Spectra of Cotton–cellulose. *Biopolymers* **2002**, *67*, 456–469.

(135) Liang, C.; Marchessault, R. Infrared Spectra of Crystalline Polysaccharides. II. Native Celluloses in the Region from 640 to 1700 Cm.- 1. *Journal of Polymer Science* **1959**, *39*, 269–278.

(136) Eichhorn, S.; Hughes, M.; Snell, R.; Mott, L. Strain Induced Shifts in the Raman Spectra of Natural Cellulose Fibers. *Journal of materials science letters* **2000**, *19*, 721–723.

(137) Samir, M. A. S. A.; Alloin, F.; Dufresne, A. Review of Recent Research into Cellulosic Whiskers, Their Properties and Their Application in Nanocomposite Field. *Biomacromolecules* **2005**, *6*, 612–626.

(138) Siró, I.; Plackett, D. Microfibrillated Cellulose and New Nanocomposite Materials: A Review. *Cellulose* **2010**, *17*, 459–494.

(139) Klemm, D.; Kramer, F.; Moritz, S.; Lindström, T.; Ankerfors, M.; Gray, D.; Dorris, A. Nanocelluloses: A New Family of Nature-Based Materials. *Angewandte Chemie International Edition* **2011**, *50*, 5438–5466.

(140) Peng, B.; Dhar, N.; Liu, H.; Tam, K. Chemistry and Applications of Nanocrystalline Cellulose and Its Derivatives: A Nanotechnology Perspective. *The Canadian Journal of Chemical Engineering* **2011**, *89*, 1191–1206.

(141) Aspler, J. O. E.; Bouchard, J.; Hamad, W.; Berry, R.; Beck, S.; Drolet, F.; Zou, X. Review of Nanocellulosic Products and Their Applications. 461–508.

(142) Dufresne, A. Polysaccharide Nano Crystal Reinforced Nanocomposites. *Canadian Journal of Chemistry* **2008**, *86*, 484–494.

(143) Lee, K.-Y.; Aitomäki, Y.; Berglund, L. A.; Oksman, K.; Bismarck, A. On the Use of Nanocellulose as Reinforcement in Polymer Matrix Composites. *Composites Science and Technology* **2014**, *105*, 15–27.

(144) Dufresne, A.; Belgacem, M. N. Cellulose-Reinforced Composites: From Micro-to Nanoscale. *Polimeros* **2013**, *23*, 277–286.

(145) Bastidas, J. C.; Venditti, R.; Pawlak, J.; Gilbert, R.; Zauscher, S.; Kadla, J. F. Chemical Force Microscopy of Cellulosic Fibers. *Carbohydrate polymers* **2005**, *62*, 369–378.

(146) Cranston, E. D.; Gray, D. G. Formation of Cellulose-Based Electrostatic Layer-by-Layer Films in a Magnetic Field. *Science and Technology of Advanced Materials* **2006**, *7*, 319–321.

(147) Cranston, E. D.; Gray, D. G. Morphological and Optical Characterization of Polyelectrolyte Multilayers Incorporating Nanocrystalline Cellulose. *Biomacromolecules* **2006**, *7*, 2522–2530.

(148) Podsiadlo, P.; Choi, S.-Y.; Shim, B.; Lee, J.; Cuddihy, M.; Kotov, N. A. Molecularly Engineered Nanocomposites: Layer-by-Layer Assembly of Cellulose Nanocrystals. *Biomacromolecules* **2005**, *6*, 2914–2918.

(149) Revol, J.-F.; Bradford, H.; Giasson, J.; Marchessault, R.; Gray, D. Helicoidal Self-Ordering of Cellulose Microfibrils in Aqueous Suspension. *International journal of*

biological macromolecules **1992**, *14*, 170–172.

(150) Beck, S.; Bouchard, J.; Berry, R. Controlling the Reflection Wavelength of Iridescent Solid Films of Nanocrystalline Cellulose. *Biomacromolecules* **2010**, *12*, 167–172.

(151) Dorris, A.; Gray, D. G. Gelation of Cellulose Nanocrystal Suspensions in Glycerol. *Cellulose* **2012**, *19*, 687–694.

(152) Manual, Z. N. S. U. Malvern Instruments Ltd. *Manual Version IM* **2003**, *100*, 1–23.

(153) Fernandes Diniz, J.; Gil, M.; Castro, J. Hornification — Its Origin and Interpretation in Wood Pulps. *Wood Science and Technology* **2004**, *37*, 489–494.

(154) Combellas, C.; Kanoufi, F.; Pinson, J.; Podvorica, F. I. Sterically Hindered Diazonium Salts for the Grafting of a Monolayer on Metals. *Journal of the American Chemical Society* **2008**, *130*, 8576–8577.

(155) Podvorica, F. I.; Kanoufi, F.; Pinson, J.; Combellas, C. Spontaneous Grafting of Diazoates on Metals. *Electrochimica Acta* **2009**, *54*, 2164–2170.

(156) Laforgue, A.; Addou, T.; Bélanger, D. Characterization of the Deposition of Organic Molecules at the Surface of Gold by the Electrochemical Reduction of Aryldiazonium Cations. *Langmuir* **2005**, *21*, 6855–6865.

(157) Dufresne, A. Preparation of Cellulose Nanocomposite. *Interface Engineering of Natural Fiber Composites for Maximum Performance, ed. NE Zaferiropoulos, Woodhead Publishing in Materials, Philadelphia, USA* **2011**, 82–116.

(158) Zhang, H.; He, H.-X.; Wang, J.; Mu, T.; Liu, Z.-F. Force Titration of Amino Group-Terminated Self-Assembled Monolayers Using Chemical Force Microscopy. *Applied Physics A* **1998**, *66*, S269–S271.

(159) Vezenov, D. V.; Noy, A.; Rozsnyai, L. F.; Lieber, C. M. Force Titrations and Ionization State Sensitive Imaging of Functional Groups in Aqueous Solutions by Chemical Force Microscopy. *Journal of the American Chemical Society* **1997**, *119*, 2006–2015.

(160) Mirhosseini, H.; Tan, C. P.; Hamid, N. S.; Yusof, S. Effect of Arabic Gum, Xanthan Gum and Orange Oil Contents on ζ-Potential, Conductivity, Stability, Size Index and pH of Orange Beverage Emulsion. *Colloids and Surfaces A: Physicochemical and Engineering Aspects* **2008**, *315*, 47–56.

(161) Lahiji, R. R.; Boluk, Y.; McDermott, M. Adhesive Surface Interactions of Cellulose Nanocrystals from Different Sources. *Journal of Materials Science* **2012**, *47*, 3961–3970.

(162) Boluk, Y.; Lahiji, R.; Zhao, L.; McDermott, M. T. Suspension Viscosities and Shape Parameter of Cellulose Nanocrystals (CNC). *Colloids and Surfaces A: Physicochemical and Engineering Aspects* **2011**, *377*, 297–303.

(163) *Handbook of Plastic Materials and Technology*; Irvin I. Rubin, Ed.; Wiley & Sons, Inc., 1990.

(164) Credou, J.; Volland, H.; Dano, J.; Berthelot, T. A One-Step and Biocompatible Cellulose Functionalization for Covalent Antibody Immobilization on Immunoassay Membranes. *Journal of Materials Chemistry B* **2013**, *1*, 3277–3286.

(165) NIST X-ray Photoelectron Spectroscopy Database http://srdata.nist.gov/xps/ (accessed May 31, 2015).

(166) Kalia, S.; Kaith, B.; Kaur, I. *Cellulose Fibers: Bio-and Nano-Polymer Composites*; Springer, 2011.

(167) Dufresne, A. Polymer Nanocomposites from Biological Sources. *Encyclopedia of nanoscience and nanotechnology* **2010**, *21*, 219–250.

(168) Azizi Samir, M. A. S.; Alloin, F.; Dufresne, A. Review of Recent Research into Cellulosic Whiskers, Their Properties and Their Application in Nanocomposite Field. *Biomacromolecules* **2005**, *6*, 612–626.

(169) Bledzki, A.; Gassan, J. Composites Reinforced with Cellulose Based Fibres. *Progress in polymer science* **1999**, *24*, 221–274.

(170) Gauthier, R.; Joly, C.; Coupas, A.; Gauthier, H.; Escoubes, M. Interfaces in Polyolefin/cellulosic Fiber Composites: Chemical Coupling, Morphology, Correlation with Adhesion and Aging in Moisture. *Polymer Composites* **1998**, *19*, 287–300.

(171) Oksman, K.; Mathew, A.; Bondeson, D.; Kvien, I. Manufacturing Process of Cellulose Whiskers/polylactic Acid Nanocomposites. *Composites Science and Technology* **2006**, *66*, 2776–2784.

(172) Oksman, K.; Skrifvars, M.; Selin, J.-F. Natural Fibres as Reinforcement in Polylactic Acid (PLA) Composites. *Composites science and technology* **2003**, *63*, 1317–1324.

(173) Gong, G.; Oksman, K.; Mathew, A. P. Efficient Toughening and Reinforcing of Polyvinyl Acetate.

(174) Bondeson, D.; Oksman, K. Polylactic Acid/cellulose Whisker Nanocomposites Modified by Polyvinyl Alcohol. *Composites Part A: Applied Science and Manufacturing* **2007**, *38*, 2486–2492.

(175) Nishino, T.; Matsuda, I.; Hirao, K. All-Cellulose Composite. *Macromolecules* **2004**, *37*, 7683–7687.

(176) Han, D.; Yan, L. Preparation of All-Cellulose Composite by Selective Dissolving of Cellulose Surface in PEG/NaOH Aqueous Solution. *Carbohydrate Polymers* **2010**, *79*, 614–619.

(177) Bondeson, D.; Syre, P.; Niska, K. O. All Cellulose Nanocomposites Produced by Extrusion. *Journal of Biobased Materials and Bioenergy* **2007**, *1*, 367–371.

(178) http://www.essentialchemicalindustry.org/polymers/polyethene.html (accessed Nov 14, 2014).

(179) Gopakumar, T.; Lee, J.; Kontopoulou, M.; Parent, J. Influence of Clay Exfoliation on the Physical Properties of Montmorillonite/polyethylene Composites. *Polymer* **2002**, *43*, 5483–5491.

(180) Zhang, J.; Wilkie, C. A. Preparation and Flammability Properties of Polyethylene-Clay Nanocomposites. *Polymer degradation and stability* **2003**, *80*, 163–169.

(181) Zhao, C.; Qin, H.; Gong, F.; Feng, M.; Zhang, S.; Yang, M. Mechanical, Thermal and Flammability Properties of Polyethylene/clay Nanocomposites. *Polymer Degradation and Stability* **2005**, *87*, 183–189.

(182) Kuilla, T.; Bhadra, S.; Yao, D.; Kim, N. H.; Bose, S.; Lee, J. H. Recent Advances in Graphene Based Polymer Composites. *Progress in polymer science* **2010**, *35*, 1350–1375.

(183) Potts, J. R.; Dreyer, D. R.; Bielawski, C. W.; Ruoff, R. S. Graphene-Based Polymer Nanocomposites. *Polymer* **2011**, *52*, 5–25.

(184) Zhang, F.; Qiu, W.; Yang, L.; Endo, T.; Hirotsu, T. Mechanochemical Preparation and Properties of a Cellulose-Polyethylene Composite. *J. Mater. Chem.* **2002**, *12*, 24–26.

(185) De Menezes, A. J.; Siqueira, G.; Curvelo, A. A.; Dufresne, A. Extrusion and Characterization of Functionalized Cellulose Whiskers Reinforced Polyethylene Nanocomposites. *Polymer* **2009**, *50*, 4552–4563.

(186) www.matweb.com (accessed Sep 23, 2015).

(187) Lee, K.-Y.; Tammelin, T.; Schulfter, K.; Kiiskinen, H.; Samela, J.; Bismarck, A. High Performance Cellulose Nanocomposites: Comparing the Reinforcing Ability of Bacterial Cellulose and Nanofibrillated Cellulose. *ACS applied materials \& interfaces* **2012**, *4*, 4078–4086.

(188) Bledzki, A.; Reihmane, S.; Gassan, J. Thermoplastics Reinforced with Wood Fillers: A Literature Review. *Polym.-Plast. Technol. Eng.* **1998**, *37*, 451–468.

(189) Lewis, T.; Nielsen, L. Dynamic Mechanical Properties of Particulate-Filled Composites. *Journal of Applied Polymer Science* **1970**, *14*, 1449–1471.

(190) Tucker III, C. L.; Liang, E. Stiffness Predictions for Unidirectional Short-Fiber Composites: Review and Evaluation. *Composites science and technology* **1999**, *59*, 655–671.

(191) Lu, Y. Mechanical Properties of Random Discontinuous Fiber Composites Manufactured from Wetlay Process, 2002.

(192) Bataille, P.; Allard, P.; Cousin, P.; Sapieha, S. Interfacial Phenomena in Cellulose/polyethylene Composites. *Polymer Composites* **1990**, *11*, 301–304.

(193) Arboronano Website http://www.arboronano.ca/ (accessed Oct 22, 2015).

(194) OTRANIEMI.Fi Website http://www.otaniemi.fi/ (accessed Oct 22, 2015).

(195) USDF Website http://www.nano.gov/ (accessed Oct 22, 2015).

(196) TAPPI Website http://www.tappi.org/ (accessed Oct 22, 2015).